UNIVERSITÀ DEGLI STUDI DI TRIESTE

UNIVERSITÀ DEGLI STUDI DI TRIESTE

XXXIV CICLO DEL DOTTORATO DI RICERCA IN

INGEGNERIA INDUSTRIALE E DELL'INFORMAZIONE

ENERGY SIMULATION OF BUILDING-PLANT SYSTEMS IN SUPPORT OF ENERGY AND CLIMATE ADAPTATION POLICIES

Settore scientifico-disciplinare: ING-IND/10 FISICA TECNICA INDUSTRIALE

DOTTORANDO
AMEDEO PEZZI

COORDINATORE
PROF. ALBERTO TESSAROLO

SUPERVISORE DI TESI
PROF. MARCO MANZAN

ANNO ACCADEMICO 2020/2021

Acknowledgements

I would like to thank Prof. Marco Manzan for the incessant support before and during my PhD journey and for leading me to new frontiers of knowledge.

I would like to thank Dr. Giorgio Lupato, Prof. Ezio Zandegiacomo De Zorzi, Prof. Enrico Nobile and Mr. Walter Moze from the University of Trieste for their valuable support.

I would like to thank my family and my friends for supporting me in this journey.

The author wish to thank the Italian Thermotechnical Committee (CTI) for the given valuable information used in this study.

The author wish to thank the Regional Agency for Environment Protection of Friuli Venezia Giulia region (ARPA FVG) for the given valuable information used in this study.

The author wish to thank the Interreg ITA-SLO Secap Project for the educational experience and for the opportunity of getting in touch with many different and valuable project partners.

The author wish to thank Edilmaster building school of Trieste for giving access to their experimental chamber.

The author wish to thank the Territorial Company for Public Housing of Trieste (ATER Trieste) for the given valuable information used in this study.

Contents

Chapter 1

Introduction

1.1 Energy consumption overview

Worldwide energy consumption and CO_2 emissions are constantly increasing year by year during the last decades as described in the latest reports of the International Energy Agency [1]. Moreover, forecasts for future show a continuation for this trend, mainly due to the raising energy demand of the emerging economies and to the increase of world population [1]. During year 2020 Green House Gas (GHG) emissions and energy requests were affected by the COVID-19 pandemic, hitting respectively a -4.00% and -6.00% variation compared to the previous year [2]. However, thanks to the recovering economy and to the lessening of the pandemic effects on transport and productive sectors, both parameters started to rise again in 2021, with energy demand surpassing the 2019 levels and GHG emissions being slightly below [2].

The forecast for the next years shows an increase of fossil fules demand, with natural gas request being on course for the greatest rise among them. Also electricity demand is heading for its fastest growth in more than ten years [2]. The positive aspect is that more than half of the electricity demand is espected to be supplied through renewable sources.

Regarding the energy final use, building heating and cooling proved to be one of the most rapidly-increasing components. In fact the building sector energy consumption covers nearly 33% of the total energy [3] and more than 40% of the world primary energy [4]. Regarding the energy sources, it exploits more than half of the electricity and one-third of the global natural gas demand [5].

For what concerns the situation in the European Union, it is again widely assessed that the residential sector accounts for a great part of the total energy usage [6, 7], and of Green House Gas emissions [8], covering a 26-28% percentage for the former and 19% for the latter. In Italy, this feature is even more relevant because of the residential sector accounting for about 36% of the total national energy consumption [9].

The building energy performance however also has a significant potential of investment: in fact in the fourth assessment report of the Intergovernmental Panel on Climate Change (IPCC) it is indicated among the energy sectors as the one with the highest economic mitigation potential [10]. Thanks to refurbishment interventions on both envelope and plants and to the development of cutting-edge technologies regarding plants performances and management, the energy consumption of new and existing buildings can be reduced by about 50% and 30% respectively [11].

1.2 Building energy simulations

Many researches have been carried out to reduce the impact of the residential sector on the natural environment and, at the same time, to make building-plant systems resilient to climate changes. About this scope, it has to be considered that many factors influence the energy performance of a building; the International Energy Agency (IEA) Annex 53 [12] identified the most influential ones [4]:

- Climate;
- Building envelope;
- Building equipment;
- Operation and maintenance;
- Occupant behaviour;
- Indoor environmental conditions.

It is evident that is fundamental to properly assess the correlations and reciprocal influences that all these aspects have on each other. About this matter, it is important to consider that buildings behavior is complicated, non-linear and dynamic [3]. Moreover, a reliable prediction of the long-term energy behavior of the buildings is fundamental to reach good energy performances. To fulfill all these purposes, simulation softwares have been developed and used in the last decades [10, 13]. Through these tools, simulations of building-plant systems can be carried on with different levels of accuracy depending on the type of analysis chosen. About this scope, three main types of energy simulation can be identified based on the timestep considered during the process:

- **Stationary:** it uses annual averages of the climatic parameters values throughout all the year, regardless of the analyzed timeframe. As a consequence it requires little computational power but also has poor precision of the results and therefore is rarely used;
- **Semi-stationary:** this type of analysis uses monthly averages of the climatic parameters values for every month of the year. It requires more computational power than the stationary one but provides good quality of the results. Because of this balance between computational burden and output precision, and of its utility in certificating the compliance with legal regulations, it is widely used in the common design practice;
- **Dynamic:** the dynamic type uses values of the climatic parameters computed on hourly bases. This leads to high-precision results although requiring great computational power; because of this, it is usually carried on only for research purpose.

These tools are valuable methods to predict the future performance of the buildings [3, 14, 15] and can be used to carry on processes like building design or retrofit, overheating risk evaluation, heating and cooling system design, new system installation impact and many more [10]. The simulation codes are also very useful because they take into account solar radiation, thermal mass, air humidity and other important parameters not considered in simplified analysis [10, 16].

1.3 Detecting climatic data

To properly assess the evolution of climate and of buildings-plant systems performances, the availability of extensive and reliable historic climatic data is fundamental. About the former aspect, it becomes easier to calibrate the climate models using the recordings if the historical data have a good quality. Regarding the second issue, having reliable data means being able to impose the correct boundary conditions in which the building-plant systems are working.

Because of this requirements, the climate conditions need to be measured and recorded for as many locations as possible and for the longest timeframes available. This task is fulfilled by the detecting stations, defined as "meteorological stations at which observations are made and trasmitted automatically" [17].

Most of the climatic parameters are reported as 1 to 10 min averages, obtained through a linearisation of the dedicated sensor output. In Table 1.1 are reported the parameters that are usually detected by

the meterological stations with the associated detection ranges and uncertainties due to the instruments used. However, it has to be specified that not all the stations detect the same parameters pool or use the same units of measure, thus leading in some cases to less information available or to the need to convert data to the appropriate units of measure.

Table 1.1: Climatic parameters usually detected by meteorological stations.

Variable	**Range**	**Uncertainty**
Atmospheric pressure	500 - 1080 hPa	0.15 hPa
Temperature	-80 to 60 °C	0.2 K
Humidity	0 - 100 %	3%
Wind speed	0 - 75 m/s	\
Wind direction	0 - 360 °	5 °
Precipitation	0 - 500 mm	max(5 %, 0.1 mm)
Sunshine	0 - 24 hours	max(2 %, 0.1 hours)
Solar radiation	\	5 - 8 %
Cloud height	0 - 30 km	10 m
Visibility	0.01 - 100 km	max(20 %, 0.02 km)

Tipically the required parameters used in simulations are: temperature, humidity, solar radiation and wind characteristics, being consequently the most detected ones. In the following a brief description of the instruments used to detect these parameters is reported.

- **Temperature:** many established measurement techniques exist, however those usually adopted in meteorological stations are resistance thermometers or thermistors [18]. This measurements usually requires linearisation and the instrument has to be shielded from solar radiation and artificially ventilated, avoiding aerosol and drizzles content in the ventilation air flow rate [18].

- **Humidity:** it is usually detected by using a hygrometer, an instrument that can measure different air properties such as wet-bulb temperature, relative humidity, humidity ratio and dew-point temperature. Among these, the preferred parameter to be detected is the relative humidity, because of the sensors assigned to its detection having a very reduced cost. However, critical aspects may occur when dealing with pollutants in the air or with air temperatures below 0 °C. On the other hand, dew-point temperature measurement is the most promising technique although it presents high sensibility to power failures and, since the detected parameter is a temperature, radiation shields and ventilation are required, as already stated above.

- **Radiation:** the most common measurements performed by meteorological stations regards the global value of the solar radiation, usually recorded on horizontal plane. This is the total irradiation evaluated in a specific point and it is the sum of the direct, diffuse and reflected components. These three elements can be directly measured however, because of the high cost of the required instruments to detect these components, usually only the global value is detected through the use of pyranometers, with the meteorological stations usually having at least two of them installed upon. The pyranometers are characterized by an hemispherical field of view [19] and can also measure diffuse horizontal radiation, if installed with a shadowing ring. Regarding the direct horizontal radiation it can be obtained, assuming the absence of the reflected component, by subtraction between the global and the diffuse values. The direct normal radiation or DNI is defined as the direct irradiance received on a plane normal to the sun [20] and it is measured through the use of the pyrheliometer, an instrument characterized by a narrow field of view [19] and by the need of being installed on a solar tracker to measure the DNI during the day because of the solar apparent path.

- **Wind:** two wind characteristics are recorded: speed and direction. Regarding the former, the instrument most widely used to detect it is the anemometer, composed by three or four hemispherical cups, radially displaced from a vertical support and stimulated to rotate by the wind [21]. The main issue regarding this tool is related to the risk of mechanical parts freezing

during cold periods; however this issue can be solved by using electric heating resistances [18]. Wind velocity values are reported as 2 to 10 minutes averages, while wind gusts are usually based on 3-second measurements. Regarding the wind direction, it is detected through wind-vane devices with digital encoders [18].

It has to be noted that, among the climatic parameters used in the energy simulations, the solar radiation, fundamental to carry on these analysis, has been disregarded for a long time in the climatic datasets. Nowadays it has been included in nearly all the meteorological stations but it remains the most problematic parameter to deal with [5].

It is then evident that climatic data must be carefully checked and, if necessary, treated before being used in energy simulations.

1.4 Climate evolution and its impact on building-plant systems

As already stated, climate is one of the most influential factors for the building energy simulation and, among the required inputs in simulation tools, the climatic data are one of the highest source of uncertainty [5]. In fact the simulation codes need several data like the hygrometric air conditions, the solar and wind data, affecting both the building energy behaviour [4] and the HVAC sizing outcomes [3]. Therefore, deepening the analysis of the mutual interactions between building energy performance and climate is fundamental.

However, only in the last decades the analysis of climate and of its changes has surged to a global attention. Today, the world scientific community has recognized the impact of the human activities on global warming and climate in general [22]. In literature, several authors focused their studies on the global warming effects on building energy performances, showing that climate change has significant impacts on building energy consumption [3, 16, 23, 24, 25] and that has become crucial for both mitigation and adaptation purposes [26, 27]. In fact, even if sometimes the projections show a reduced impact of climate change in the short term for many aspects, significant variations are forecasted for long term scenarios and should be taken into account into the design procedures. Generally, depending on the climate type, a decrease of the heating energy consumption and an increase of the cooling one is forecasted [10]. The overall energy consumption trend is also strongly influenced by the climate typology [25, 28]: in fact an energy reduction is estimated for cold climates [29], whereas an increase may occur for warm areas [10, 29].

Due to the recent climatic changes recorded around the globe, with an increasing trend of temperatures [30], the importance of the cooling performance of the buildings has considerably grown. In fact, if in the recent past the main trend was to insulate the buildings envelope to decrease winter heating energy usage [31], nowadays the designers are more concerned about cooling related problems.

1.5 Adapting to climate change: from worldwide to local projects

1.5.1 The Paris Agreement

Climate change is becoming more and more a difficult task to deal with, causing frequent extreme events, altering the balance of the ecosystems, affecting the availability of natural sources for large parts of human population. As a consequence it is greatly influencing many aspects of human life like food and water availability, energy consumption rates, health issues, damages to vital infrastructures. It has then become of the utmost importance for the public institutions to be able to prevent and adapt to these phenomena, thus minimizing the effects and damages on human society. Within this context, many initiatives have already been developed, both on worldwide and local scales. About the former, the most notorius initiative developed is the Paris Agreement on Climate, adopted in 2015 and aiming to limit global warming compared to the pre industrial age below 2 °C and pursuing efforts to limit it to 1.5 °C. It also aims to improve the capacity of countries and local governments to deal

with the inevitable effects of climate change and support them in their efforts [32].

Regarding this last aspect the Paris Agreement is coupled with the Covenant of Mayors, launched in 2008 in Europe, and with the development of local plans to adapt to and mitigate climate change effects. This interconnection allows to develop action plans and strategies on both worldwide and local scales to obtain the greatest benefit for both people and environment.

1.5.2 Glasgow COP26

In November 2021 the COP26, the twenty-sixth United Nations Climate Change Conference, has been held in Glasgow. The Climate Change Conferences were established in 1994 and are held annually in order to analyze the progresses in tackling climate change and establish legally binding actions for developed countries to reduce GHG emissions.

The expectation for the COP26 was that the parties would commit themselves to more ambitious goals than those set by COP21. At the end of the conference an agreement was reached, signed by the 197 countries participating, and known as the Glasgow Climate Pact. The Pact aims to limit the increase in global temperature to 1.5 °C, already foreseen by the Paris Agreement, and therefore points out to the necessity to halve GHG emissions in the next decade and to reach zero net carbon emissions by the middle of the century. The countries that have already signed the Paris Agreement have also committed in updating the Nationally Determined Contributions (NDCs).

The Glasgow Climate Pact strongly encourages the signing countries to develop mitigation and adaptation policies; the first ones to reduce the impact of human activities on the environment and the second ones to adapt to the changing climate and reducing its effects on human life. Moreover, great attention is posed also on the financial aspect of the topic, encouraging the governments to invest much more in the transition to a green economy and also to involve private investors in the process.

1.5.3 The European Covenant of Mayors

The European Covenant of Mayors aims to bring together local governments (mainly on city scale) to implement measures to tackle and adapt to climate change. It was launched in 2008 with the aim to reach and if possible exceed the European climate and energy standard targets. The project had and it's still having great success, counting nowadays more than 10,000 local and regional partners scattered across 53 different countries. Within this context, Italy plays the main part with 4,891 signatories, accounting for almost half of the total. The main objectives of the Covenant of Mayors can then be summarized as:

- Increasing the decarbonisation of the territories;
- Grant to the citizens a secured access to renewable and sustainable fonts of energy;
- Implementing adaptation strategies for climate change effects.

In order to achieve such results, the signatories pledge action to support the European objective of 40% Green House Gas emissions reduction within 2030 and to develope an approach to draft both mitigation and adaptation strategies to tackle climate change. This political goal have to be translated into practical measures and projects, therefore the signatories commit to submitting, within two years following the date of the local council decision, a Sustainable Energy and Climate Action Plan (SECAP), highlighting the key actions they plan to develop [33].

An important aspect of this process is the tracking of the progresses made by the municipalities towards their objectives. To do so the signatories are requested to submit a Monitoring Report every second year after the adoption of the SECAP plan; moreover every four years the emission inventory of the plan has to be updated in order to highlight the progress related to Green House Gas emissions and energy consumption reduction.

Figure 1.1: Covenant of Mayors statistics [https://www.eumayors.eu/about/covenant-initiative/covenant-in-figures.html].

Another fundamental characteristic of the Covenant is the sharing of key actions between the municipalities in order to provide to all the participants good practice measures as sources of inspiration to develop their own SECAPs.

1.5.4 The Interreg ITA-SLO Secap Project

Within the broader context of the Covenant of Mayors, many fellow projects have been developed on a regional scale to sustain this kind of initiative; the Interreg ITA-SLO Secap Project is one of them. The purpose of this project is to stimulate the sustainable development of human activities within the cross-border territory composed by the metropolitan city of Venice, the Friuli Venezia Giulia region and the western part of Slovenia, as it can be seen in Figure 1.2.

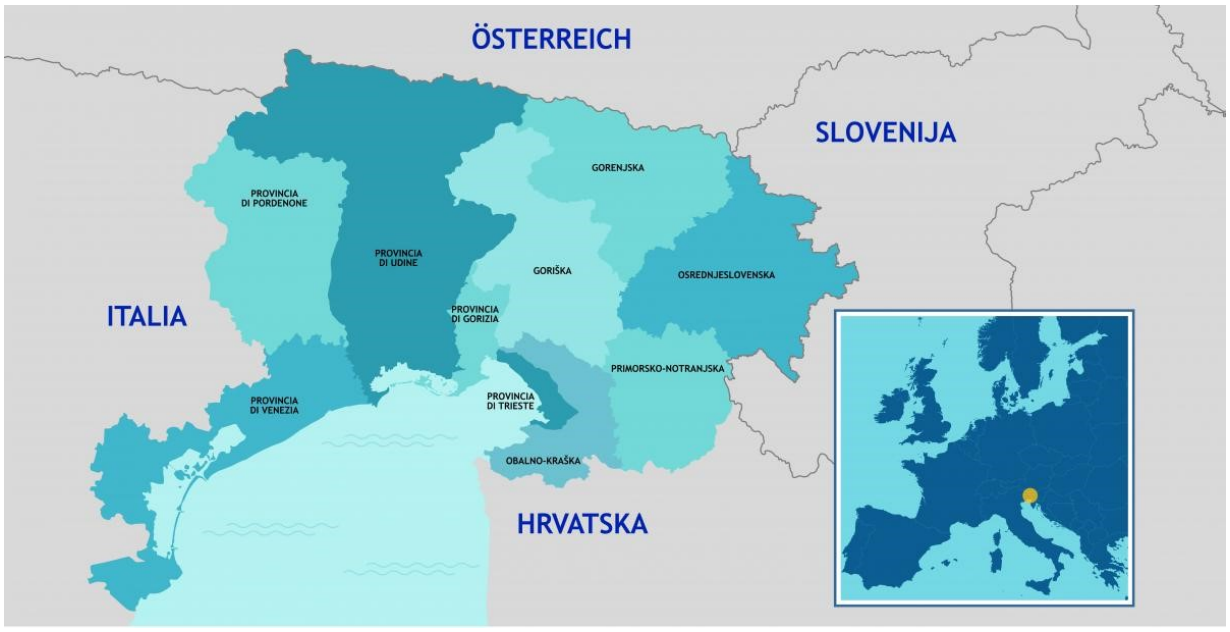

Figure 1.2: Interreg ITA-SLO Secap Project program area. [https://www.ita-slo.eu/sites/default/files/progetti/SECAP%20POSTER%20approved_0.pdf].

The project aims to develop, as already stated in the Covenant, adaptation and mitigation measures to tackle climate change. This have been done also by sharing instruments, methodologies and datasets between the cross-border entities, thus generating positive effects on the local pianification for all the program area.

The transition towards a low-emission society will be carried on also by evolving the current SEAPs (Sustainable Energy Action Plans) into SECAPs (Sustainable Energy and Climate Action Plans) for some municipalities located in the program area [34]. In Figure 1.3 the progress state of the adaptation and mitigation policies for Friuli Venezia Giulia region is reported.

The main objectives of the Project can then be resumed as follows:

- Developing scenarios illustrating the possible impact of climate change on the territory and laying the foundations for the cross-border strategy;
- Developing a single cross-border strategy for climate change mitigation and adaptation;
- Guiding and accompanying municipalities in drawing up plans that combine mitigation/adaptation, with a view to integrated, low-carbon planning, typical of the Mayor Adapt model.

Many important actors are included like the Universities of Trieste and Venice, the Friuli Venezia Giulia, Veneto and Ljubljana Regions, Area Science Park, Italian and Slovenian regional agencies for energy and others. This compound of both institutional and research partners made it possible to generate innovative methodologies easily applicable in the future by public institutions on a local scale.

Important results have already been achieved within the Project like the study on the impact of climate change on the program area with methodological reports for the involved municipalities or the creation of an inventory of strategies, measures and projects, which can be used to increase settlements resilience to climate change. Another important achievement is the development of a bilingual online database regarding energy, climate and environment informations and of an Italo-Slovenian atlas of territorial vulnerability for both present and future climate phenomena. All of this will be used as a basis to evolve the SEAPs of the program area into SECAPs, promoting at the same time the entry of the municipalities still outside of the SEAP-SECAP process.

The Project however does not aim to fully develop the adaptation and mitigation strategies, but rather to provide reliable bases and experiences that could help, both directly and indirectly, the cities to reduce their energy use in public and private buildings [34].

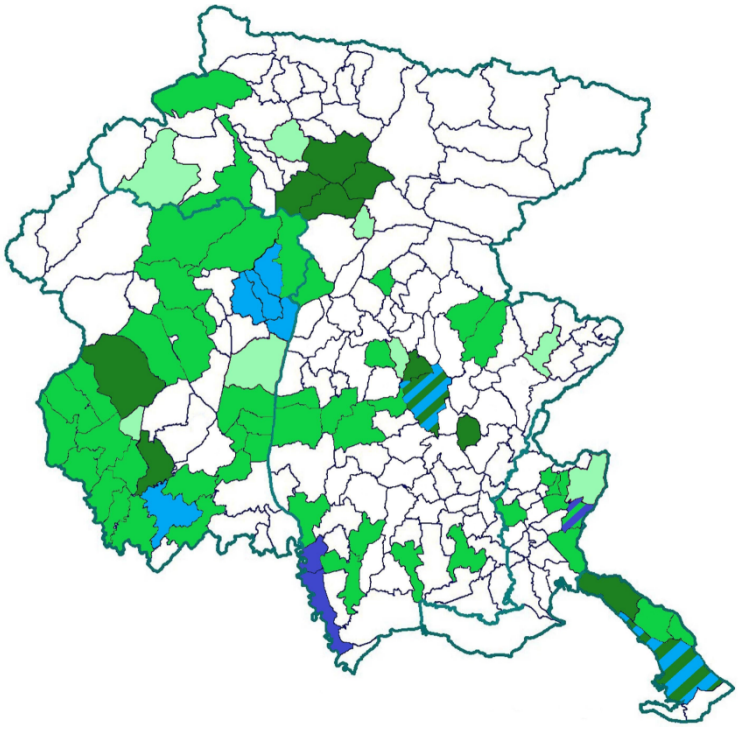

Figure 1.3: FVG municipalities that signed the Covenant of Mayors 2020 (light green), SEAP presented to the Covenant of Mayors but not monitored (green), SEAP approved by the Covenant of Mayors and monitored (dark green), municipalities that signed the Covenant of Mayors 2030 (light blue), SECAP presented to the Covenant of Mayors 2030 (dark blue)

1.6 Research objectives

This research falls within the Interreg ITA-SLO Secap Project, being the author included in it as a research fellow for all the duration of the PhD cycle. Therefore, the main objective of this work is to develop a workflow that could be used as a starting point by the municipalities of the program area for drafting part of their energy and climate adaptation policies, focusing on the energetic aspect of the topic. The other partners treated many other aspects of the project for which they were more suited. Dynamic simulations of building-plant systems have been carried on and applied to the different topics of this research in order to provide support for the presented methodologies and results.

Being this research included in the Interreg ITA-SLO Secap Project, the performed studies mainly focus on Italy and on the Project's program area, aiming to tackle some of the principal topics that the municipalities should take care of when developing their SEAPs and SECAPs by proposing practical approaches, and their results, regarding important arguments like:

- **The main issues regarding actual climatic data and their treatment.** When developing climate mitigation policies, the base material to work with is climatic data. A workflow was then developed in this research to perform climatic data quality assessment to obtain usable data for every required simulation. Moreover, given the increasing importance of buildings cooling performance, as already stated in Section 1.4, a review of the European standard to compute climatic data used in cooling plants sizing has been carried on. Finally, a process to properly represent actual climate was developed and applied to a sample location included in the Project's program area;
- **The modeling of climate change.** To support the development of mitigation measures that have to consider the evolution of energy consumption patterns in the future, an analysis of climate change has been carried on in this research. This led to a standard procedure that municipalities could follow when dealing with this kind of analysis, starting from the correction of climate models results, all the way to the analysis of extreme events evolution and to the projection of actual climatic data into the future;
- **The assessment of the real performances of insulating systems.** Being the improvement of thermal characteristics of buildings one of the main tools municipalities could exploit to reduce human cities impact on climate, it is of the utmost importance to correctly assess the performances of the technologies used in this field. In this research an analysis of internal insulating systems performance has been carried on to highlight how much a wrong evaluation of its behavior could affect the final result of a refurbishment and giving the municipalities an approach to exploit to properly assess insulating packages performances;
- **The optimization of building-plant systems energy refurbishments.** The real performance of a building-plant system is affected by many variables and it is important to consider this aspect when dealing with refurbishment practices. Being climate change one of these variables, it is essential for municipalities to develop refurbishment measures that could deal well with various climatic boundary conditions; this research then proposes an approach to tackle such problem.

Although many researches are already present in literature on how to tackle the single topics presented here, a comprehensive approach to address all of them together with the specific aim to develop mitigation and adaptation policies has not been developed yet. Being these policies a crucial part of the process to counter climate change, this research aims to be a valuable basic tool to be exploited, extended and improved to help countering climate change.

Chapter 2

Climatic data treatment

2.1 Problem definition

As already described above, dynamic energy simulations are heavily influenced by climate and are usually carried on by using climatic datasets collected on hourly bases. The sets mainly include parameters like dry-bulb temperature, solar radiation, relative humidity and wind speed.

The availability of extensive and reliable climatic data is crucial and this necessity could often be a problem because of both poor quantity and/or quality of available material. In fact, usable data for different locations always vary in length, with some sites having long timeframes of detected material and others having only few years of recording. This could be an important limitation when choosing a location to analyze because of the international standards recommending minimum amounts of detected data to be used [35]. Moreover, it is essential to have usable material to work with, implying high quality of raw information, however the datasets often present unusable, unreadable, or poor data.

These issues are caused by the operation of meteorological stations, which are subject to many potential problems like, for example, black outs, severe working conditions and storage software failures. Furthermore, it sometimes happens that during the data collection and the subsequent post-processing, human and software errors may cause the loss or corruption of some information. Finally, as stated before, the solar radiation parameter proved to be the most problematic parameter to deal with [5].

Considered all these critical issues, it is of particular importance to carry out a qualitative analysis of the available raw data in order to assess which one can be used for energy simulations and which one to discard because of their low quality. In fact, the use of unchecked climatic data could lead to large discrepancies between the predicted and measured performance of the building systems [36, 37].

Many authors have faced these issues using different approaches. Regarding the importance of data availability on energy simulations, Murano et al. [38] compared three official climatic databases to highlight the main differences between them. Datasets were obtained from the national standard UNI 10349-1:1994 [39], from the ENEA database [40] and from the EPW files of EnergyPlus climatic data [41]. A quasi-steady-state analysis was then performed for an NZEB building case study, showing relevant differences in energy performances for both heating and cooling due to the different datasets used.

In order to tackle the common scarcity of climatic data, Cannistraro et al. [42] approached the problem in a particular way; instead of selecting the widest dataset available and filling the possible gaps with interpolation-like methods, they decided to reduce the amount of data to be used. In fact, through the methodology proposed by Erbs et al. [43], they calculated the hourly values of temperature for 29 European locations starting from the mean monthly temperatures and from the amplitude of diurnal variations leaving unchanged all other climatic parameters. By using the original and modified climatic data they carried on energy simulations of three sample modules, showing differences of the final energy consumption below 9% between the results obtained by applying the two climatic datasets to the three modules.

Another approach was carried on by Yang et al. [44] that developed an automated system for climatic data scraping, filtering and displaying, originally created for climatic analysis applied to agricultural prediction. The tool checks for erroneous information (like relative humidity over 100%), removes them and treats them as missing and fills the gaps in the dataset using methods like Linear Interpolation, Adjusted Historic Average, Spatial Interpolation, Functional Estimation or Weather Data Generator on the bases of gaps length and parameter to be treated.

2.2 Analysis scope

In order to support the development of the Interreg ITA-SLO Secap Project, a quality check of the available Italian climatic data has been carried on in order to evaluate the overall status of the material detected by the meteorological stations located in the Italian territory. This work should give an overview of the stations functioning and of their eventual failures in order to address the main issues in detecting climatic data. Moreover, another aim is to create a standard review process of the climatic data to exploit when dealing with this procedure.

Moreover, given the increasing importance of the cooling component for building energy consumption, a review of the EN ISO 15927-2 standard method for selecting Cooling Design Days has been developed, leading to a sensitivity analysis of its results and to the development of an alternative selection method in order to make the process clearer for the users and easier to automate.

Finally a procedure for representing actual climate through the generation of a Test Reference Year has been developed.

2.3 Italian raw data quality analysis

Raw climatic data were obtained from local meteorological stations operated by Italian regional agencies for climate. The stations are placed in 108 sites throughout Italian territory and record the values of dry-bulb temperature, total solar global radiation, relative humidity and wind speed on hourly bases. Raw climatic data have been measured according to the methods specified in the World Meteorological Organization Guide.

As previously stated, this material cannot be directly used for energy simulations because of the common issues affecting this kind of data, like having many missing values in the datasets. In fact days in which there are too many data gaps cannot be used as reliable inputs for whatever analysis because they cannot precisely represent the real climate of that timeframe. Moreover, writing and syntax errors are also detected in the climatic sets. Therefore, in order to obtain a solid and computable data pool for energy analysis, a data quality treatment is necessary.

2.3.1 Quality filters

After a preliminary correcting action on syntax and writing errors, every dataset has been treated through the imposition of four quality rules, described below, in order to obtain a database of days valid for energy analysis. The four rules that are to be fulfilled for a day to be considered valid are:

- **Rule A:** *Every climatic parameter has to be valid in at least 18 hours during the day.* This condition has to be satisfied in order to have consistent data to be used in the computation and avoids the presence of too many gaps to be filled with interpolation in the following steps [45];
- **Rule B:** *The first and last values of the whole dataset have to be valid for all parameters, if not the first and/or last day of the set have to be considered invalid.* This requirement is necessary because, if interpolation of values is to be taken in the first/last day, a valid data may be required in the first/last hour to compute the interpolated values;

- **Rule C:** *For every climatic parameter, a maximum of 6 consecutive hours of invalid data is acceptable across two contiguous days.* This limitation aims to avoid the problem of interpolating data across too long time intervals as, for example, near stocks of 5+5 hours of invalid values [45];
- **Rule D**: *Solar radiation values have to be valid in all the hours comprised between sunrise and sunset.* This rule is the most restrictive one because if solar radiation is invalid in just one hour, the whole day is to be considered unacceptable. This is due to the fact that data gaps are filled through linear interpolation and, if this approach is consistent for parameters like temperature and relative humidity, it cannot be extended to solar radiation because the latter does not vary on linear bases.

Through the application of these rules on the 108 Italian stations, the pool of valid data for each one has been obtained. In first instance, it has been noted that the number of detected days varies greatly between the sets, depending on the recording time of the station itself. This fact is an additional aspect to be carefully considered when dealing with climatic data, since a minimum amount of recorded days, ten years to be precise, is recommended to obtain reliable datasets in representing the actual climatic situation [21]. In Figure 2.1 the total amount of detected data is reported for each station.

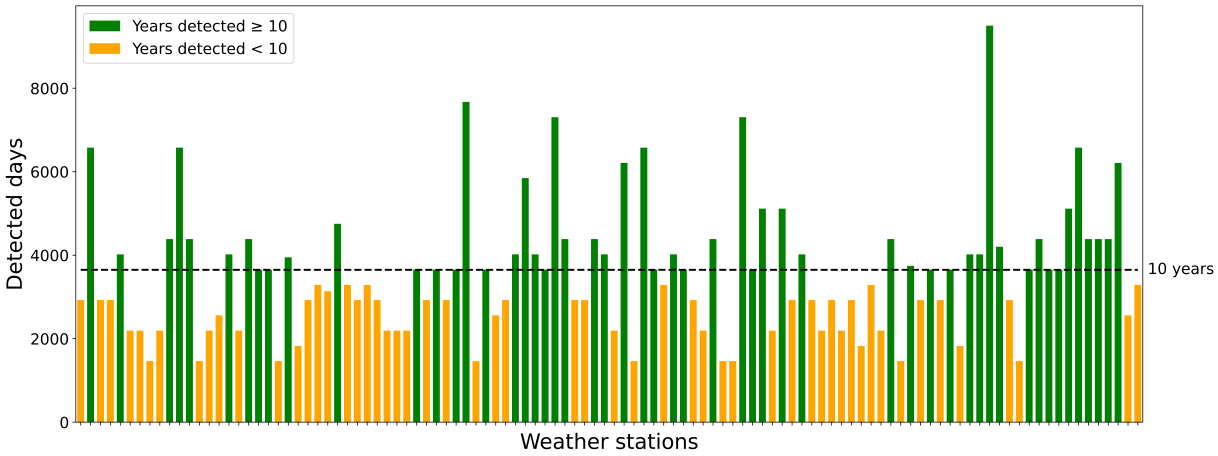

Figure 2.1: Italian meteorological stations detected data amount.

As it can be seen, approximately half of the stations (55) don't reach ten years of recorded data. Most of these stations (35) are located in the southern part of Italy, thus highlighting major problems in having long timeframes of recording in this part of the nation.

2.3.2 Results

The percentage of days rejected because of the quality rules greatly varies between the Italian stations, however data quality have been discretized in three main categories: a good one displaying less than 25% of rejected days, the acceptable one that shows an amount between 25 and 50% of rejected days, and the bad one, characterized by more than 50% of rejected days. Figure 2.2a presents the percentage of locations falling in each category. It can be noted that the majority of sites presents a good data quality, a quarter of them an acceptable behavior and only 5% of locations falls into the bad category.

The influence of the four quality rules on the rejection process can be observed by the inspection of Figure 2.2b, which reports the relative occurrence of each rule considering the total number of not respected rules in the various datasets. The first notable feature is that Rule B, applied to the first and last days of a dataset only, obviously has the lowest effect on the quality check. Generally, rules A, C and D show a similar impact in rejecting values from each dataset, with the latter having a slightly minor impact than the other two. This last one is an interesting feature because Rule D, regarding the solar radiation, is the most restrictive one but does not demonstrate a predominance over the others. This reflects an overall good quality of the instruments devoted to the detection of this climatic parameter.

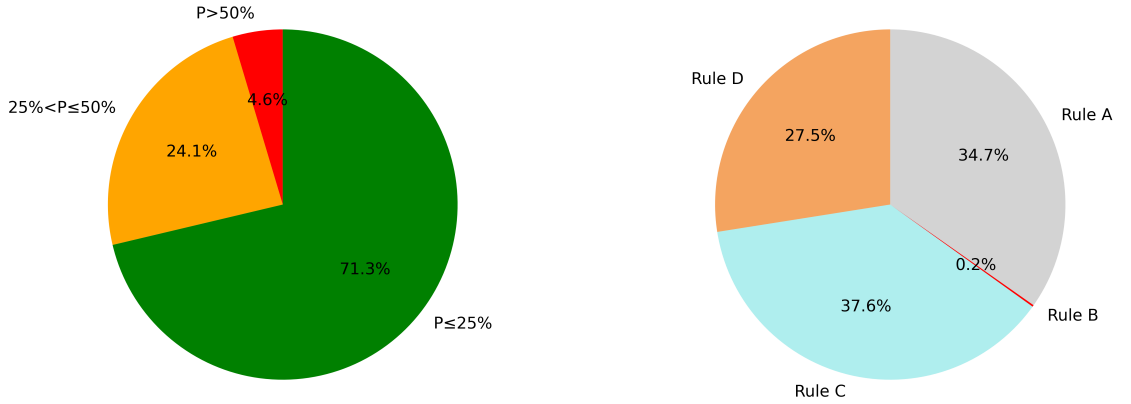

(a) *Percentages of locations having good (green), acceptable (orange) and bad (red) data quality.*

(b) *Average quality rules influence on the rejection of days among all the locations.*

Figure 2.2: Quality check results for 108 Italian meteorological stations.

Once having defined the days that can be used for simulations, there are still gaps in the pool to be filled to obtain continuous sets. This is done through the linear interpolation of values; the number of interpolated hours for each parameter, solar radiation excluded, are reported in Figure 2.3.

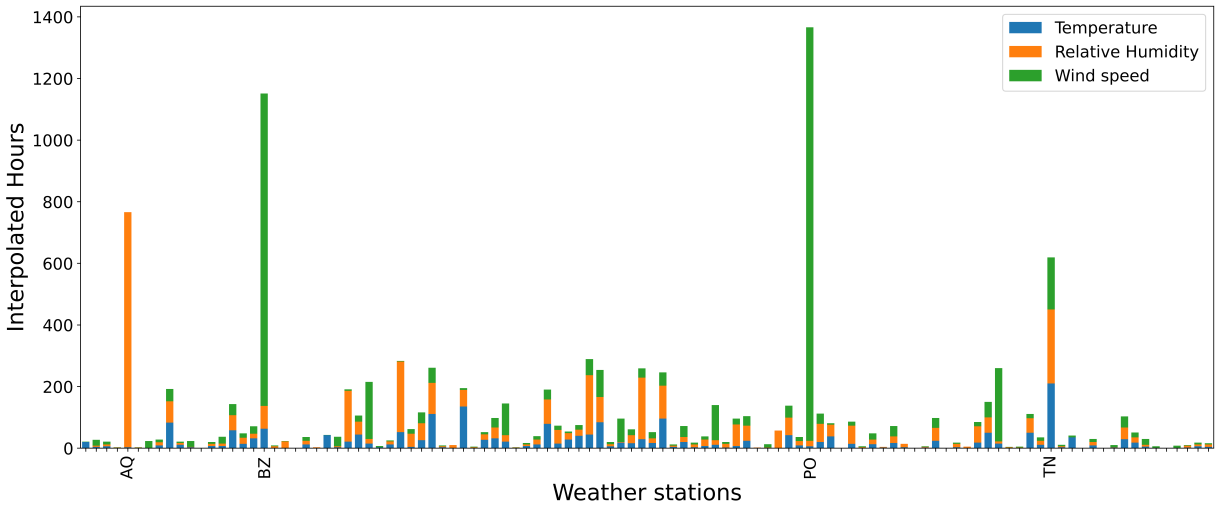

Figure 2.3: Hours of interpolated data for temperature (blue), relative humidity (orange) and wind speed (green) after the application of the quality filters.

At a first glance it is evident that four locations, highlighted in Figure 2.3, Aquila (AQ), Bolzano (BZ), Prato (PO) and Trento (TN), have a relevant amount of hours being interpolated, reaching peaks of over one thousand hours in Bolzano and Prato. All the other locations, however, show a much smaller amount of interpolated hours, with, at worst, three hundred filled gaps. It can then be deduced that, once the invalid days are removed from the dataset, the quality of the remaining ones is fairly high.

An interesting feature is that all the four worst stations mentioned above are located in hilly or mountain environment, thus highlighting the possibility of a correlation between this kind of environment and the major issues in detecting climatic parameters. It can also be noted that the majority of the gaps to be filled regards relative humidity and wind speed data, while air temperature needs only minor adjustments.

The qualitative analysis of raw climatic data highlighted a heterogeneous behavior throughout the 108 Italian locations. One problem highlighted by this research is the amount of data available, with many locations presenting less than ten years of data recorded, the minimum time length recommended by the standards to have reliable data. On the other hand, more than 70% of the stations present a good data quality, with less than 25% of days rejected, showing a good detection and storage capacity of

the meteorological station system. Finally, the interpolated hours display that major number of gaps are present in relative humidity and wind speed values, then highlighting the presence of diffuse and recursive criticalities concerning the instrumentation dedicated to the detection of these parameters.

2.4 Heading to warmer temperatures: the importance of cooling plants sizing

As already stated, the recent climatic changes leading to increasing temperatures in all seasons have heavily enhanced the importance of the cooling performance of the buildings. Because of this pattern, it becomes more and more important to correctly size the cooling systems, even more in refurbished buildings, where overheating risk due to major envelope insulation is higher [46, 47].

In order to determine the cooling load the definition of the external boundary conditions, that are a series of data defining the solar and thermo-hygrometric parameters of the external climate, is obviously fundamental. They affect the heat gain terms and the cooling load results: as a consequence, climatic data is a fundamental factor when sizing an HVAC system [3].

The climate parameters used in the sizing process can be obtained with different statistical methodologies and they represent extreme conditions assessed with confidence levels or percentiles. Regarding the hourly data for design cooling load, the reference method for European users is the one proposed by the EN ISO 15927-2 standard [35]. For every calendar month the standard aims to identify real days within the analyzed dataset that impose a cooling load likely to be exceeded for very low percentages of cases. These days are named Cooling Design Days and their selection process is here described, analyzed and formally reformulated.

This study supports the updating of the national technical standard on climate data for the design of technical building systems. The Italian Thermotechnical Committee Energy & Environment (CTI) [48], a not-for-profit organization which is part of UNI (Italian Certification Body), is currently working on updating the UNI/TR 10349-2 [49] technical report which represents the national reference document which provides climatic input data for the application of technical standards that support the EPBD Directive. Due to this aspect and to the Cooling Design Days being the main method to size cooling plants in European practice, the analysis were centered on this particular sizing method, leaving out other approaches like the one focusing on the Cooling Degree Hours.

2.4.1 The EN ISO 15927-2 Cooling Design Days selection method

Despite being the reference method for Europe, the process described in the EN ISO standard is difficult to interpret and is based on a cyclical process challenging to implement. The methodology to extract monthly Design Days for cooling systems from measured data proceeds as follow.

It first defines a set of parameters to be used in each calendar month (i.e. all the January data taken together, all the February data taken together, etc.) to obtain individual days of hourly data that impose three different risk levels, RL_5, RL_2 and RL_1, defined through a cooling load likely to be exceeded by 5%, 2% and 1% of cases respectively. To select the monthly Design Day, two parameters are strictly required: daily mean dry-bulb temperature and daily total global solar radiation. Other parameters can be optionally used, like daily mean dew-point temperature, daily dry-bulb temperature swing and daily mean wind speed or any other parameters the designer considers relevant for the case study analyzed.

The first step is to calculate the daily values of the considered parameters for each day of the dataset. Then, for each calendar month and for each one of the three risk levels RL, the percentiles of the used parameters and reported in Table 2.1 must be computed. The method then defines for each parameter an initial neighborhood of the aforementioned percentiles using the ranges listed in Table 2.1.

Table 2.1: EN ISO 15927-2 order (i), parameters, ranges, steps and percentiles.

i	Parameter	EN ISO range (R_i)	EN ISO steps(s_i)	Percentiles P_i [%]		
				RL_1	RL_2	RL_5
1	Daily mean dry-bulb temperature	± 0.5 °C	± 0.1 °C	99	98	95
2	Daily total global solar radiation	± 0.05 kWh/(m^2 day)	± 0.01 kWh/(m^2 day)	99	98	95
3	Daily mean dew-point temperature	± 0.5 °C	± 0.1 °C	99	98	95
4	Daily dry-bulb temperature swing	± 0.5 K	± 0.1 K	1	2	5
5	Daily mean wind speed	± 0.5 m/s	± 0.1 m/s	1	2	5

For each calendar month, once defined the percentiles and relative ranges, the days for which all parameters fall within the ranges of Table 2.1 are identified. Following this scheme, three events could happen:

1. Exactly one day is identified;
2. No day is identified;
3. Two or more days are found with all the parameters within the ranges.

In the first case scenario, the identified day can be directly used as monthly Cooling Design Day with no further selection work. If no day is identified, the initial range for each variable is increased using the steps defined in Table 2.1 and following the parameter order there reported, until one day is found. On the other hand, if two or more days are initially found, the ranges are reduced using the same steps and order of Table 2.1, until only one day remains.

Such method presents two main issues: the first is the iterative nature of the process that leads to an unpredictable number of cycles to be completed to achieve the goal; the second is the trouble to interpret the method itself following the explanation given in the standard. Moreover, it does not define the reference precentiles and the steps to use for other parameters considered in the analysis. In order to resolve some of these issues a new process is here proposed: the Coordinates Method. This process maintains the theoretical principles established by the standard, but tries to reformulate them in a clearer and more direct way to give users a more friendly and straightforward selection method, also easier to implement in numerical codes.

2.4.2 Proposal of an alternative process: the Coordinates Method

A new Cooling Design Day selection process, called Coordinates Method, has been developed during this research. The coordinates are an alternative description of the range enlargement/shrinkage modification process. In fact the new method keeps the calculation of the daily climatic parameters and of the monthly reference percentiles as presented in the standard but replaces the concept of ranges and steps with the one of coordinates. Therefore coordinates represent, for each daily climatic parameter, the difference between its value and the reference percentile, normalized using the step values reported in Table 2.1. The greater the coordinate, the greater the difference between the daily parameter value and the monthly percentile.

All the parameters and the reference percentiles described by the standard for all risk levels have already been reported in Table 2.1. The standard gives the opportunity to use less or more than five parameters, with a minimum of two: dry-bulb temperature and total global solar radiation. In this case, the Coordinates Method here described still holds; it is simply applied to the required number of parameters. As reported in the following procedure, the monthly Design Day refers to each calendar month and each risk level RL.

The first step of the procedure is to compute the five daily coordinates $C_{i,d}$, referred to the five climatic parameters of Table 2.1 and identified by the i-index having values 1 to 5, computed for every day d of the analyzed calendar month of the dataset using Eqn. 2.1:

$$C_{i,d} = \frac{|V_{i,d} - P_i|}{s_i} \qquad d = 1, \ldots, n_m \tag{2.1}$$

Where $V_{i,d}$ is the i-th parameter value in the analyzed day, P_i is the monthly reference percentile of the parameter, s_i is the step defined by the standard and reported in Table 2.1, and n_m the total number of days of the dataset included in the analyzed calendar month. The coordinate $C_{i,d}$ represent the number of enlargement steps required by the standard method to include the i-th variable of day d, but starting from a null initial neighborhood of the reference percentile. A practical example of the application of this step of the process is reported below in Example 1.

Once having computed the coordinates, the selection method proceeds as follows: first a Reference Coordinate is extracted for every day of the dataset following Eqn. 2.2:

$$C_{ref,d} = max[C_{i,d}] \qquad d = 1, \ldots, n_m \tag{2.2}$$

Then a Selection Coordinate is computed as reported in Eqn. 2.3:

$$C_{sel} = min[C_{ref,d}] \qquad d = 1, \ldots, n_m \tag{2.3}$$

The Selection Coordinate represents the minimum number of steps required to have at least one day discovered by the iterative enlargement method of the standard assuring that all the i-th variables of Table 2.1 fall inside the selection ranges of the standard. Therefore, only the days that have the Reference Coordinate equal to the Selection Coordinate, i.e. satisfying Eqn. 2.4, are suitable as Cooling Design Days for that month:

$$C_{ref,d} = C_{sel} \qquad d = 1, \ldots, n_m \tag{2.4}$$

However, the standard method also introduces a precedence in the enlargement of the ranges, following the i-index order of Table 2.1. To take into account this imposition the following steps are therefore needed. The first one is to determine for every day selected through Eqn. 2.4 the maximum positional index of the Reference Coordinate, here named as Reference Index, as stated in Eqn. 2.5. This index represents the i-th variable to be selected last during the final iteration of the enlargement loop of the standard. This passage accounts also for the possibility of different variables sharing the same Reference Coordinate.

$$I_{ref,d} = max(i) : C_{i,d} = C_{ref,d} \qquad d = 1, \ldots, s \tag{2.5}$$

Where s represents the total number of days selected through the imposition of Eqn. 2.4. Similarly to the Selection Coordinate, a Selection Index is then computed, as reported in Eqn. 2.6:

$$I_{sel} = min[I_{ref,d}] \qquad d = 1, \ldots, s \tag{2.6}$$

As stated in the standard, the monthly Design Days are the ones that first satisfy the selection ranges for all the parameters and in the order imposed by the standard, i.e. the ones for which Eqn. 2.7 apply:

$$I_{ref,d} = I_{sel} \qquad d = 1, \ldots, s \tag{2.7}$$

One or more monthly Cooling Design Days are obtained and can be used to size the cooling systems.

Figure 2.4 shows a comparison between the Coordinate and original method workflows. The presented process follows exactly the iterative approach of the standard, but can be easily automated and modified as needed. A practical sample of the complete application of the Coordinates Method is reported below in Example 2.

The new selection method was applied to the 108 Italian datasets and, as expected, gave exactly the same results as the ones obtained using the EN ISO 15927-2 method, demonstrating the complete equivalence of the two processes.

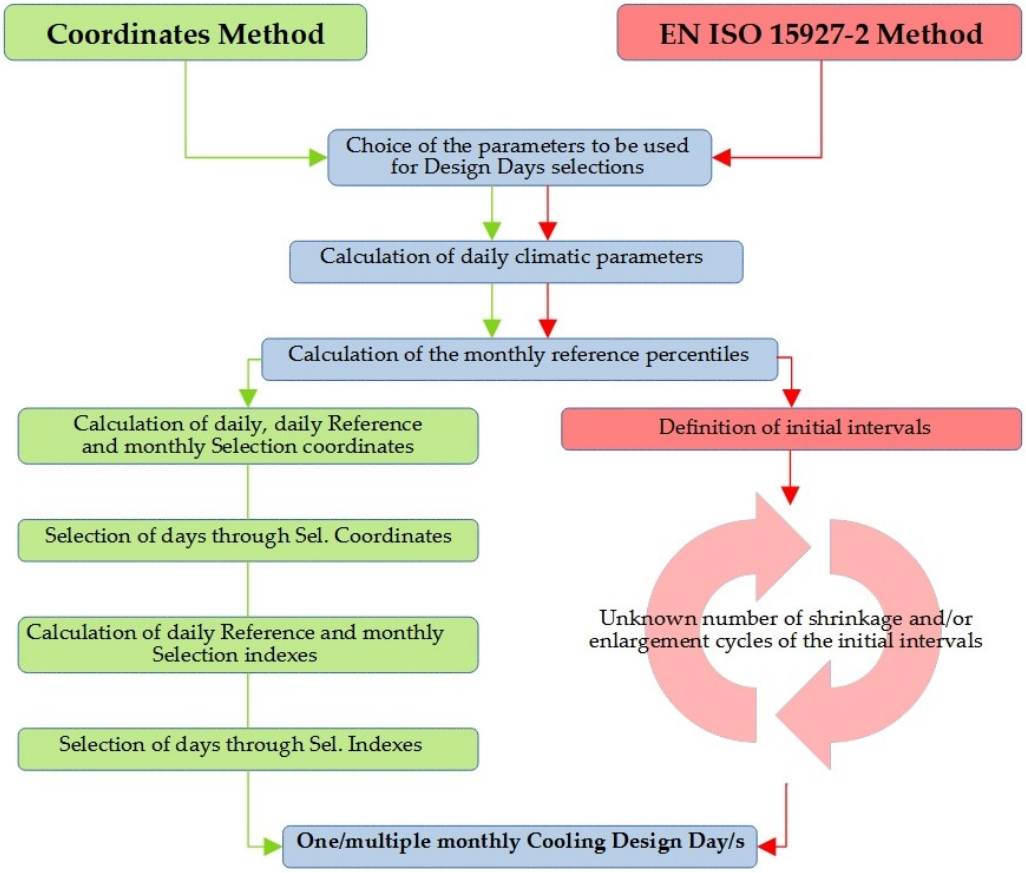

Figure 2.4: Workflow of the Coordinates and EN ISO methods.

2.4.2.1 Coordinates Method: Applicative Example 1

Applicative example of the Coordinates Method for the calculation of the coordinates for a sample day. The climatic parameters for the analyzed day and the reference percentiles for the analyzed month are computed according to paragraph 4.2.2 and 4.2.3 of EN ISO 15927-2 standard respectively and are reported in Table 2.2.

Dataset timeframe: 01/01/2004 – 31/12/2009
Sample Day: 15 July 2005

Table 2.2: Daily parameters and reference percentiles for 15 July 2005.

i	Parameter	V_i	P_i			U.M.
			RL_1	RL_2	RL_5	
1	Daily mean dry-bulb temperature	25.39	29.32	28.82	28.04	°C
2	Daily total global solar radiation	7.89	8.26	8.25	8.12	$kWh/(m^2day)$
3	Daily mean dew-point temperature	11.13	18.45	17.68	15.97	°C
4	Daily dry-bulb temperature swing	12.3	5.27	5.94	6.6	K
5	Daily mean wind speed	2.37	1.75	1.82	1.95	m/s

By applying Eqn. 2.1 the coordinates of the analyzed day are computed and reported in Table 2.3. By analyzing Table 2.3, a clearer explanation of the coordinates concept can be given. Considering for example risk level RL_1, the first coordinate states that 40 steps of 0.1 °C are needed to reach P_1 starting from V_1, as reported in Table 2.2, and so on for the other parameters. This means that the maximum coordinate, $C_3 = 74$, represents the parameter that is last included in the selection range defined by the standard and, consequently, is the most influential coordinate for the identification of a day suitable as monthly Cooling Design Day.

Table 2.3: Coordinates for 15 July 2005.

i	Parameter	C_i RL_1	RL_2	RL_5
1	Daily mean dry-bulb temperature	40	35	27
2	Daily total global solar radiation	37	36	24
3	Daily mean dew-point temperature	74	66	49
4	Daily swing in dry-bulb temperature	71	64	58
5	Daily mean wind speed	7	6	5

2.4.2.2 Coordinates Method: Applicative Example 2

Applicative example of the whole Coordinates Method for the identification of the monthly Cooling Design Day for July for risk level RL_1. The procedure for the other percentiles is identical.

Dataset timeframe: 01/01/2004 – 31/12/2009
Month: July –> m = 7 (number of months in the dataset)
n_m = 186 (total number of days of July in the whole dataset)
RL_1 = risk level where the cooling load is likely to be exceeded in 1% of cases

After having calculated the coordinates $C_{i,d}$ of every July day in the dataset following the procedure reported in Example 1, the determination of the Reference Coordinate for every day is carried on by applying equation 2.2:

$$C_{ref,d} = max[C_1; C_2; C_3; C_4; C_5]_d \qquad d = 1, ..., 186$$

After this, it is then possible to compute the Selection Coordinate for July using equation 2.3:

$$C_{sel} = min[C_{ref,d}] = 58 \qquad d = 1, ...186$$

The Selection Coordinate value for July for RL_1 is 58. The first selection of days is now carried on applying the condition reported in equation 2.4:

$$C_{ref,d} = C_{sel} \qquad d = 1, ..., 186$$

There are three days that meet the aforementioned condition, as reported in Table 2.4, where the Reference Coordinate is higlighted in green.

Table 2.4: Days selected through the Selection Coordinate condition.

d	ID	Day	C_1	C_2	C_3	C_4	C_5
1	566	20/07/2005	**58**	**58**	30	36	1
2	921	10/07/2006	47	**58**	50	49	13
3	1277	01/07/2007	**58**	57	54	44	5

As it can be seen in Table 2.4, the three selected days all have a Reference Coordinate equal to 58, meaning that fifty-eight enlargement cycles would be required to find these days if the method of the standard were used starting from a null neighborhood.

The final step is to choose, between these selected days, the one that displays the Reference Coordinate at the minimum i-index, thus representing the first day to satisfy all the parameters ranges following the modification order given by the standard. The Reference Index for every remaining day is then obtained using Eqn. 2.5:

$$I_{ref,d} = max(i) : C_{i,d} = C_{ref,d} \qquad d = 1, ...3$$

The result of the application of the equation is also evident by looking at Table 2.4, leading to Reference Index equal to 2 for the days with ID 566 and 921 and to 1 for the day with ID 1277. Subsequently, the Selection Index is obtained using Eqn. 2.6:

$$I_{sel} = min[I_{ref,d}] = 1 \qquad d = 1, ..., 3$$

By imposing the condition of Eqn. 2.7 the second and last selection is carried on, leading to the final result of day 1277, 01 July 2007, as the Cooling Design Day for July.

$$I_{ref,d} = I_{sel}$$

In the following table the daily climatic parameters of the selected Cooling Design Day are reported.

Table 2.5: Daily climatic parameters of the Cooling Design Day for July month.

Parameter	**Value**	**U.M.**
Daily mean dry-bulb temperature	23.55	°C
Daily total global solar radiation	7.69	$kWh/(m^2day)$
Daily mean dewpoint temperature	13.14	°C
Daily dry-bulb temperature swing	9.6	K
Daily mean wind speed	2.16	m/s

An interesting output of this example is that the selected Design Day, ID 1277, is characterized by coordinates values that are generally higher than the ones of the other two days, ID 566 and 921, that made it to the final stage of selection, as it can be seen in Table 2.4. This means that generally the selected Design Day is more distant from the reference percentiles than the other two days are. However, because of it having the same Reference Coordinate of the other two and having the minimum Reference Index, it has been the one finally selected. This demonstrates how the method proposed by the EN ISO standard does not assure that the selected Design Day is the one that best fit the reference percentiles and therefore it is also not sure that the risk levels RL defined by the standard are respected. This aspect will be further analyzed in the next section.

2.4.3 Review of the Cooling Design Day selection process results

2.4.3.1 EN ISO results sensitivity analysis

Because of the standard giving the possibility to use different climatic parameters when searching the monthly Cooling Design Days, the improved flexibility of the new selection method has been exploited to carry on a sensitivity analysis of the whole process to assess how the use of different climatic parameters could influence the results of the selection workflow.

Different Cooling Design Days selections have been carried on for the 108 Italian locations, already analyzed in terms of data quality, by considering all the possible combinations of parameters. As a consequence, eight different sets of results have been compared and the percentages of Design Days shared by the different sets across all the locations have been computed. The sets with the parameters involved in the analysis are defined in Table 2.6.

Table 2.6: Parameters included (V) in the possible combination sets.

Set	**Dry-bulb temperature**	**Solar radiation**	**Dew-point temperature**	**Temperature swing**	**Wind velocity**
Tmp_rad	V	V			
Tmp_rad_tdp	V	V	V		
Tmp_rad_tsw	V	V		V	
Tmp_rad_vel	V	V			V
Tmp_rad_tdp_tsw	V	V	V	V	
Tmp_rad_tdp_vel	V	V	V		V
Tmp_rad_tsw_vel	V	V		V	V
Tmp_rad_tdp_tsw_vel	V	V	V	V	V

The analysis of the results highlighted some interesting characteristics as it can be deduced by inspecting Figure 2.5 which reports the matching percentage for each combination of sets, defined as the number of Cooling Design Days selected from both sets compared to the total amount of selected days.

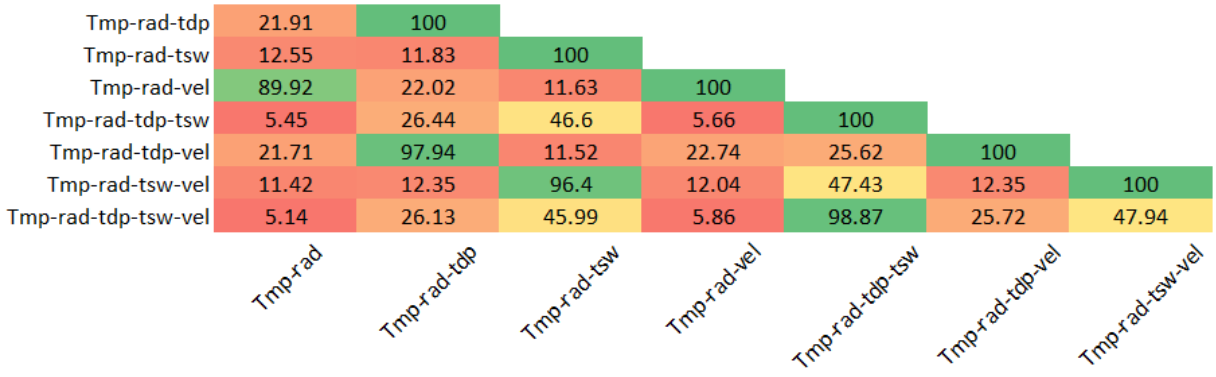

Figure 2.5: Cooling Design Days matching percentage between all combinations of parameter sets across 108 Italian locations.

The first feature to note is the low number of coincident Design Days between each set, with some notable exceptions. Analyzing for instance the case with only two parameters, *Tmp-rad*, including dry-bulb temperature and solar radiation, it shares very few Design Days with every other set, with the exception of the case *Tmp-rad-vel*, where the wind speed is added to the analysis. This consideration leads to another interesting behavior: the wind speed parameter, *vel*, has very reduced effects on the choice of Design Days. This is demonstrated by the high matching percentages, generally over 90%, between the sets where the unique difference is the presence of this parameter. An explanation to this behavior is that generally the wind speed presents values very near to the reference percentiles, with very low coordinate values, as it can be seen in the example reported below in Table 2.7.

Another interesting behavior is that when adding the dew-point temperature, *tdp*, to an analysis that already includes the dry-bulb temperature swing, *tsw*, the matching rate tends to be higher than in other cases, generally amounting to around 45%. This is predictable because the dew-point temperature is physically related to dry-bulb temperature and relative humidity. Regarding their coordinates, *tsw* and *tdp* parameters often have values that are close to each other as it can be seen in the example shown below in Table 2.7.

To further highlight the effects of different parameter sets on the selection of Cooling Design Days, a case study is reported as an example. It considers the location of Rome, risk level RL_1, and identifies for every parameter set the Design Day for July month. The process results, i.e. the Design Days and their coordinates, are reported in Table 2.7.

Table 2.7: Rome Cooling Design Days coordinates values for every parameter set for July and risk level RL_1.

Parameter set	**Cooling Design Day**	C_1	C_2	C_3	C_4	C_5
Tmp-rad	18/07/2003	19	25	\	\	\
Tmp-rad-vel		19	25	\	\	13
Tmp-rad-tdp	21/07/2006	15	45	47	\	\
Tmp-rad-tdp-vel		15	45	47	\	1
Tmp-rad-tsw	02/07/2003	31	2	\	57	\
Tmp-rad-tsw-vel		31	2	\	57	11
Tmp-rad-tdp-tsw	04/07/2006	44	13	63	61	\
Tmp-rad-tdp-tsw-vel		44	13	63	61	14

As it can be noted, the chosen Design Day is the same for the parameter sets where the only difference

is the presence of the wind speed in the analysis. This further highlights that wind velocity has a very low impact on the choice of the Design Day, confirmed by the low coordinate values for every set. Table 2.7 moreover highlights that the coordinates C_3 and C_4, related to dew-point temperature and temperature swing respectively, show the highest values. Therefore, if considered in the analysis, these are the most influential parameters in the selection of the Design Days for this particular case.

The hourly values of the climatic parameters of the Cooling Design Days of the case study, with the exception of the temperature swing, are graphically reported in Figure 2.6. For dry-bulb, dew-point temperature and wind speed the reference percentiles are also reported. As already stated, the results are coincident for the couples of sets where the only difference is the presence of the wind speed in the selection process so only four distributions are presented for the eight sets.

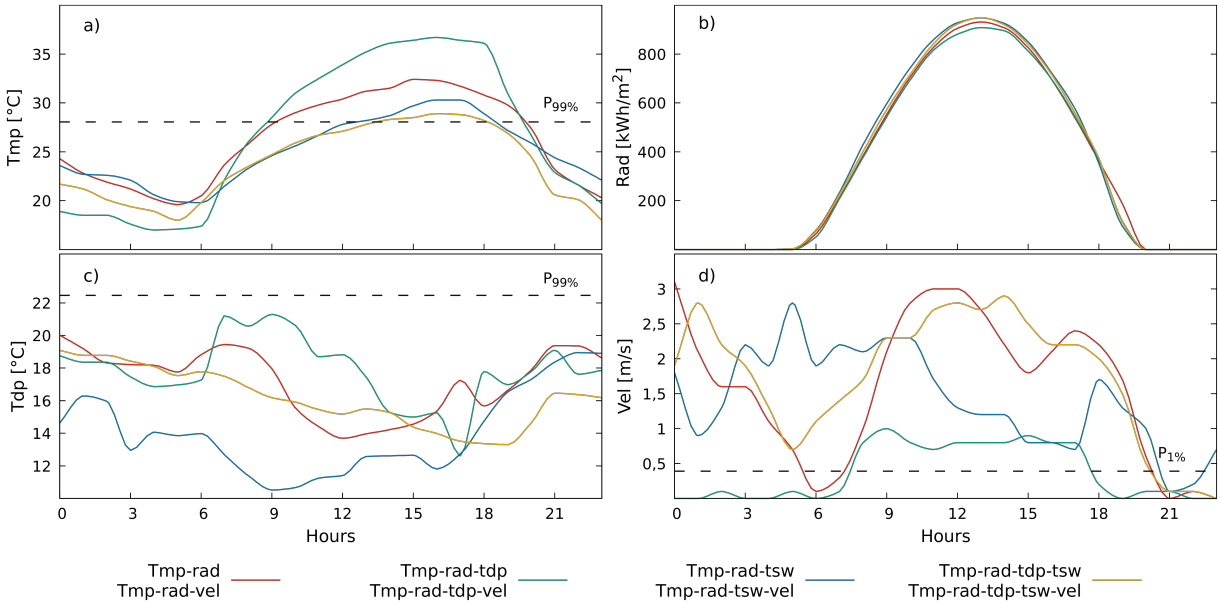

Figure 2.6: Hourly values of climatic parameters of Rome Cooling Design Days for every parameter set for July and risk level RL_1.

As it can be seen in Figure 2.6, the selected Design Days regarding the four couples of sets show different distributions of the parameters, solar radiation excluded. The dry-bulb temperature displays differences up to almost 8 °C between the *Tmp-rad-tdp* and *Tmp-rad-tdp-tsw* sets at 3 p.m. as it can be noted in Figure 2.6a). The dew-point temperature also shows remarkable variability, with differences of up to almost 11 K between the *Tmp-rad-tsw* and *Tmp-rad-tdp* cases, as highlighted in Figure 2.6c).

2.4.3.2 Output sizing powers: a case study

To further study the behavior of the Cooling Design Days an analysis of the computed sizing powers for a test building applied to three sample locations, Milan, Rome and Palermo, has been carried on. According to ISTAT data [50], the 1961 - 1975 period includes the majority of the existing Italian buildings. Therefore two versions of the test building, representative of the insulated and uninsulated configurations of buildings related to this period was analyzed in this case-study.

The main characteristics of the test building for both cases were obtained from the Tabula Web Tool of the Tabula Project [51]. The floor area of the building is of 934 m^2, leading to a heated/cooled air volume of 3,074 m^3, while the Heat Loss Surface (HLS) accounts for 1,667 m^2, leading to a Surface Area to Volume Ratio (SV) of 0.54. Finally, the Window-Wall Ratio (WWR) is 9.33%. The model was not divided into zones to speed up the calculation, instead a fixed space distribution was set: 50% bedrooms, 35% kitchen and living room and 15% other areas with no internal gains. No shadings were modeled during simulations to avoid human behavior influences. Opaque constructions and windows characteristics are illustrated in Table 2.8.

Table 2.8: Opaque construction and windows characteristics for uninsulated and insulated models.

Case	U			M			SHGC	Uw
	Wall	Roof	Floor	Wall	Roof	Floor		
	$[W/(m^2K)]$			$[kg/m^2]$			\	$[W/(m^2K)]$
Uninsulated	1.15	1.1	0.94	194	406	478	0.7	2.2
Insulated	0.23	0.21	0.21				0.398	0.8

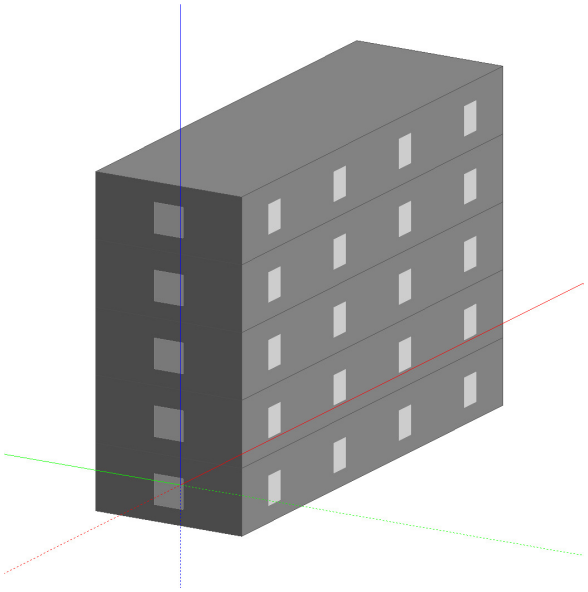

Figure 2.7: Test building geometry model.

Time-varying heat gains were modeled. Electric heat gains can be summarized into a maximum design power of 4.6 W/m^2. Occupancy was set to a maximum of 0.04 $people/m^2$ between 05:00 p.m. and 08:00 a.m. and to 0.01 $people/m^2$ between 08:00 a.m. and 05:00 p.m. Cooling system availability was modeled as always-on during the whole year. Heating and cooling systems types were modeled as ideal with 100% convective effects, therefore air temperature was preferred over the operative one to fix the cooling set-points. These were fixed to 26 °C from 8 a.m. to 10 p.m. and to 28 °C for the remaining time.

In order to model an ideal system, EnergyPlus object ZoneHVAC:IdealLoadsAirSystem was used. It provides a model for an ideal HVAC system and it supplies cooling or heating air to a zone in sufficient quantity to meet the zone load. Cooling design supply conditions were modeled with 12°C air temperature and 8 gw/kgda humidity ratio. Since cooling supply air conditions are far below zone internal air saturation conditions, latent gains were considered: the cooling system provides dehumidification even if there is no dehumidification set-point. The ZoneHVAC:IdealLoadsAirSystem object is modeled as an ideal VAV terminal unit with variable supply air temperature and humidity. The supply air flow rate varies between zero and the maximum in order to satisfy the zone cooling load. Outdoor air flow rate, intended as intentionally or inadvertently introduced into the building, was set to 0.3 ACH.

Using the climatic data available for the three locations, sizing simulations were run for every day of the dataset included in June, July and August months using EnergyPlus software. Subsequently, the 99_{th}, 95_{th} and 91_{th} monthly percentiles of the sizing outputs were computed for the three months analyzed, to identify the reference values for the three risk levels *RL*. Then the Cooling Design Days were identified for the three months using the Coordinates (i.e. the EN ISO) method.

The sizing powers obtained through the Design Days were then confronted with the percentiles to evaluate how the CDDs really work within a dataset for both uninsulated and insulated configurations of the test building. The results are reported in Table 2.9 and 2.10 respectively.

Table 2.9: Test building cooling sizing powers [W] for three sample locations. Uninsulated configuration

MILAN

	RL_1		RL_2		RL_5	
Month	%ile	CDD	%ile	CDD	%ile	CDD
June	52378	50195	51542	*47758*	48363	*47758*
July	50901	*40923*	49423	*40923*	46104	**42464**
August	45790	*44326*	44574	*44326*	41789	*44326*

ROME

	RL_1		RL_2		RL_5	
Month	%ile	CDD	%ile	CDD	%ile	CDD
June	49894	*43474*	47801	*43474*	45889	*43474*
July	50296	37648	49669	**41538**	47848	**41538**
August	47791	*36441*	47171	*36441*	43949	*36441*

PALERMO

	RL_1		RL_2		RL_5	
Month	%ile	CDD	%ile	CDD	%ile	CDD
June	48212	*40981*	47164	*40981*	43349	39382
July	47570	42910	45234	*41037*	42538	*41037*
August	45093	*41850*	44604	*41850*	43556	*41850*

Table 2.10: Test building cooling sizing powers [W] for three sample locations. Insulated configuration.

MILAN

	RL_1		RL_2		RL_5	
Month	%ile	CDD	%ile	CDD	%ile	CDD
June	25020	25027	24567	*25006*	23813	*25006*
July	23569	*20576*	23469	*20576*	22968	**21105**
August	23472	*22507*	22728	*22507*	22250	*22507*

ROME

	RL_1		RL_2		RL_5	
Month	%ile	CDD	%ile	CDD	%ile	CDD
June	25623	*22380*	25320	*22380*	24688	*22380*
July	27135	18821	26649	**21643**	25406	**21643**
August	25122	*19116*	24860	*19116*	23911	*19116*

PALERMO

	RL_1		RL_2		RL_5	
Month	%ile	CDD	%ile	CDD	%ile	CDD
June	29771	*21607*	27568	*21607*	24756	20320
July	26605	*22868*	26079	*22855*	24546	*22855*
August	25924	*23910*	25520	*23910*	24699	*23910*

As it can be seen in Tables 2.9 and 2.10 the sizing powers are different from the reference percentiles of the three risk levels *RL*. Moreover in many cases, highlighted in orange in the tables, CDD computed for different risk levels lead to the same sizing power, thus indicating that the same CDD was selected for different risk levels. This aspect highlights the difficulty of the EN ISO method to effectively appreciate the differences between the risk levels and to subsequently differentiate the CDD.

However, this is not even the worst problem that emerges from this analysis. In fact, in some cases, highlighted in red in the tables, the sizing power computed for risk levels that refer to lower percentiles are greater than the ones computed for risk levels referring to higher percentiles. This is the exact opposite of the expected behavior, meaning that the EN ISO method could sometimes give unreliable results in terms of sizing power.

2.4.3.3 Conclusions

The sensitivity analysis highlighted large differences in terms of chosen Design Days when using different sets of parameters in the selection process, thus assessing the importance for the users to carefully evaluate the effects that different choices about the parameters to be analyzed could have on the results and, consequently, on the sizing of a cooling system.

The analysis of the computed sizing powers for a case study highlighted important issues about the results obtained through the application of the EN ISO method. This leads to the conclusion that a major review of the standard should be carried on in the near future to properly address this criticalities and to give users a more reliable selection method for Cooling Design Days.

2.5 Representing actual climate: a case study for Trieste

Simulations actually used to assess building energy [52, 53], solar systems performances and other aspects of building-plant systems need accurate climatic data to be accomplished. According to Keeble [54], regarding building energy simulation weather files, three typologies can be identified:

- Multi-year weather data AMY;
- Representative days;
- Typical or reference years like TRY, TMY or DRY, 8760 hours long.

Actual meteorological years, or AMY, are single-year series of wheather data for a specific location. Typical years gained great consensus compared to multi-year weather data mainly because of the lower computational work needed; a crucial aspect to consider when dealing with the limited computational power available in the past. Today, multi-core processors are common, therefore parallel simulations and single-simulation times have greatly decreased, allowing to perform multi-year simulations when analysing building energy behavior. Regarding these ones, several authors studied and compared multi-year and TRY simulations outcomes [3, 36, 55]. Cui [3] performed an analysis related to the Chinese territory, writing a deep introduction, first highlighting reference years' critical aspects which can be summarized as follows:

- Typical year is derived from actual months that are selected using weighting factors that enhance some climate aspects over others. The factors' choice is related to a specific building or system typology that is somehow "an average building";
- Typical years are expected to represent long-term climate conditions; while several authors confirmed this aspect [56, 57], others found significant variations [55];
- Reference years represent typical conditions, therefore they are not suitable to study buildings response to extreme conditions.

Regarding the latter issue, a solution has been proposed by Nik et al. [58, 59] when trying to properly represent climatic data generated by Regional Circulation Models (RCMs). The method consisted in representing climate using three distinct TRYs: the typical one describing the mean behavior of the analyzed period, the Extreme Cold Year (ECY) and the Extreme Warm Year (EWY), representative of the extreme situations of the dataset. Nik showed that by considering TRY, ECY and EWY together (which is called Triple), it is possible to achieve a probability distribution of climatic conditions which is very similar to the full set of 30 years RCMs data.

Cui [3] highlighted the multi-year simulations benefits as well, emphasizing that studying a longer period leads to a more comprehensive and thorough analysis and that building designers and policy makers can employ result-based regulations. Barnaby and Crawley [60, 61] highlighted that using single-year simulations doesn't allow to show the long-term variations and the peak energy consumption. However, when dealing with a multi-year approach, the wrong or missing data represent an issue [55] that needs to be treated with interpolation methods [62].

According to Skeiker [63], reference years consist of 8670 hourly values made of single-month climate data selected from different years within a reasonably long [64] dataset. There are several versions with major or minor differences in the statistical methods used to generate them. They include: TRY, TMY, DRY and others. Even though these datasets sometime contain synthetic solar data, they share a common feature: the selected months that compose the reference year are obtained from actual recordings [65, 63]. Although a multi-year approach shows undeniable benefits [3], at the state of the art, reference years are generally preferred [61, 66]. Several authors studied the variability between single-year and multi-year energy consumption [67, 68, 69], generally finding differences around 10% for U.S. and Hong Kong climates. Therefore, single-year simulations can be used to obtain typical building energy performances [55] and are reasonably accurate [60].

2.5.1 Test Reference Year generation

According to UNI EN ISO 15927-4 [64], a reference year is an artificial year suitable to determine the average annual energy for heating and cooling. It is a representative database that is usually known as typical meteorological year (TMY) in the U.S.A. and test reference year (TRY) in Europe [63].

In literature, several methodologies were proposed; one of the first was released in 1976 by National Climate Data Center: these weather files are called TRY-US. Unlike more modern methods, the outcome does not consist of a collection of months, but rather of an entire year that actually occurred, that is not an artificial year. In this case, the selected year is identified gradually removing the years that ones containing months with outliers mean temperatures. Since they are obtained from totally different approaches, the TRYs and TRY-US are not comparable.

Another widely used approach was developed in the same years, based on Filkenstein–Schafer statistic [70] and on the selection of single months from different years of the dataset [63]. The outcome was an artificial year that collected the most representative months of the dataset [55]. According to Lund [71], the approach allowed to maintain the cross-correlation between the variables.

Other methods present a roughly equivalent procedure, but they differ for several aspects like the weighting factors, used to select reference year months [3, 55] or the number of parameters to consider [3]. Another difference could be the statistic used; many of the methods use the Finkelstein-Schafer, while others [72] use the Kolmogorov–Smirnov [55]. Essentially all these methodologies are intended to identify hourly data, from a much wider dataset, that are representative of a specific location climate.

In this research a Test Reference Year is generated for the location of Trieste, the regional capital of Friuli Venezia Giulia region, through the following steps:

- Raw data quality check;

- Additional quality check on monthly bases and removal of unsuitable months if the following two conditions are not met;
  1. Less than 15% of gaps in the raw data [73];
  2. Absence of invalid days in the treated data.
- Computation of the daily means of the analyzed parameters;
- Creation of the TRY through the selection of real months within the dataset using the Finkelstein-Schafer statistic;
- Smoothing of data at the interface between TRY months;
- Calculation of derived parameters like dew-point temperature, etc.

The analyzed period spans from 1995 to 2019. The raw data quality check was performed using the rules described in Section 2.3. In the additional quality check the imposition of having less than 15% of gaps for every month inside the original raw data aims to avoid too many interpolated values in the treated dataset and therefore a not so good representation of the real climate of that month. This is the same reason for the condition of not having invalid days within the treated data.

2.5.2 The Finkelstein-Schafer statistic

The Finkelstein-Schafer statistic compares for every calendar month m the yearly and the long-term CDFs of the daily means of the analyzed parameter.

$$FS_m = \sum_{i=1}^{n} \delta_i \tag{2.8}$$

Where FS is the value of the Finkelstein-Schafer statistic, m is the calendar month (January, February,...,December), n is the number of daily readings for that month (e.g. for January, n=31) and δ is the absolute difference between the long-term and the yearly CDF at i value of parameter x (T_i in the example reported in Figure 2.8).

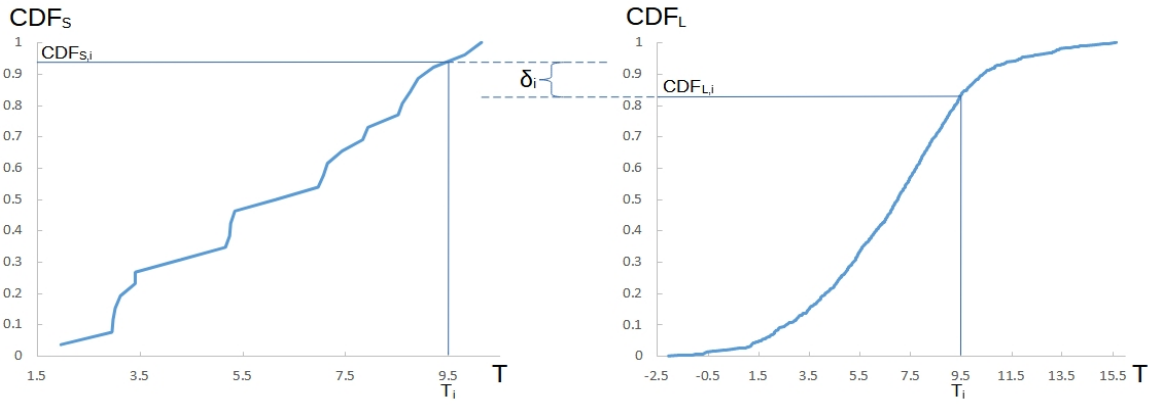

Figure 2.8: Example of delta computing by comparing yearly (CDF_s) and long (CDF_l) cumulative distribution functions for temperature T.

The FS scores were computed for dry-bulb temperature, solar radiation and relative humidity. In Table 2.11 the FS scores for the former are reported as an example; the missing values are from months considered not suitable for the analysis. For every calendar month and parameter analyzed, the FS scores are then used to rank the yearly months of the dataset in order to search for the ones that best fit to the overall behavior for said parameter. The lower the FS score, the better (lower) the ranking, the better the fitting of the analyzed month. Three distinct rankings were computed for temperature, solar radiation and relative humidity. In Table 2.12 the FS ranking for dry-bulb temperature is reported as an example.

Table 2.11: Dry-bulb temperature Finkelstein-Schafer scores.

	Gen	**Feb**	**Mar**	**Apr**	**May**	**Jun**	**Jul**	**Aug**	**Sep**	**Oct**	**Nov**	**Dec**
1995	/	/	/	/	/	/	6.32	/	9.49	13.85	/	/
1996	/	8.36	9.1	5.09	5.78	13.28	10.07	10.19	/	13.13	15.98	11.8
1997	/	5.65	12.35	11.95	8.66	7.15	7.71	8.88	15.26	18.56	13.19	10.87
1998	13.33	/	11.73	/	9.7	7.86	/	/	13.95	13.08	15.72	8.22
1999	13.36	9.34	/	9.5	/	11.56	9.45	11.21	9.31	10.52	16.12	14
2000	11.5	7.4	6.88	3.63	/	9.56	14.3	9.16	10.24	/	/	/
2001	/	/	7.48	7.56	6.57	/	6.1	/	13.17	13.73	/	14.43
2002	7.1	/	11.65	5.72	5.39	/	/	9.05	14.21	9.02	8.46	9.33
2003	9.67	8.76	/	5.88	8.38	9.81	7.53	/	8.84	/	8.23	10.84
2004	11.07	9.21	6.23	/	/	/	/	/	/	10.85	/	13.24
2005	/	/	/	6.5	5.46	/	/	11.92	15.08	/	/	13.82
2006	11.57	9.47	9.01	5.01	7.09	3.48	7.21	11.34	9.75	11.83	6.8	14.65
2007	13.81	7.62	13.55	7.45	9.15	5.77	7.5	8.33	10.56	16.38	12.17	13.06
2008	9.81	/	9.71	7.61	4.68	5.88	10.52	12.09	19.91	10.95	15.95	12.91
2009	5.8	12.03	7.71	9.65	/	/	8.48	10.97	/	/	5.6	13.64
2010	13.12	5.5	/	/	6.39	8.32	13.97	8.57	11.5	14.12	12.59	12.28
2011	12.55	10.76	4.47	7.59	6.06	6.18	13.37	8.41	12.07	15.8	14.13	14.51
2012	13.75	/	5.93	6.86	10.74	5.17	12.01	11.81	12.47	/	/	7.83
2013	12.49	9.25	/	4.49	12.18	/	/	16.29	/	5.41	14.25	7.13
2014	15.06	9.72	10.27	/	5.83	9.17	10.41	14.44	11.94	17.3	14.24	13.8
2015	11.61	3.97	4.72	/	10.35	12.97	12.98	16.07	13.18	13.05	/	/
2016	/	8.8	5.99	10.68	6.51	5.7	8.73	9.5	14.95	10.82	9.73	8.56
2017	13.02	7.16	6.29	11.09	3.7	7.03	9.72	13.16	12.77	11.24	/	10.14
2018	10.18	11.66	/	6.29	9.54	10.72	/	/	/	12.83	16.33	12.57
2019	10.24	/	7.5	7.41	11.5	6.63	/	/	/	/	/	/

Table 2.12: Dry-bulb temperature Finkelstein-Schafer ranking.

	Gen	**Feb**	**Mar**	**Apr**	**May**	**Jun**	**Jul**	**Aug**	**Sep**	**Oct**	**Nov**	**Dec**
1995	/	/	/	/	/	/	1	/	2	13	/	/
1996	/	6	11	3	4	17	10	7	/	11	13	8
1997	/	2	16	18	12	8	5	3	17	18	7	7
1998	14	/	15	/	15	9	/	/	13	10	11	2
1999	15	11	/	14	/	15	8	9	1	2	14	17
2000	7	4	6	0	/	12	17	5	4	/	/	/
2001	/	/	7	11	9	/	0	/	11	12	/	18
2002	1	/	14	4	2	/	/	4	14	1	3	4
2003	2	7	/	5	11	13	4	/	0	/	2	6
2004	6	9	4	/	/	/	/	/	/	4	/	13
2005	/	/	/	7	3	/	/	12	16	/	/	16
2006	8	12	10	2	10	0	2	10	3	7	1	20
2007	17	5	17	10	13	3	3	0	5	16	5	12
2008	3	/	12	13	1	4	12	13	18	5	12	11
2009	0	16	9	15	/	/	6	8	/	/	0	14
2010	13	1	/	/	7	10	16	2	6	14	6	9
2011	11	14	0	12	6	5	15	1	8	15	8	19
2012	16	/	2	8	17	1	13	11	9	/	/	1
2013	10	10	/	1	19	/	/	17	/	0	10	0
2014	18	13	13	/	5	11	11	15	7	17	9	15
2015	9	0	1	/	16	16	14	16	12	9	/	/
2016	/	8	3	16	8	2	7	6	15	3	4	3
2017	12	3	5	17	0	7	9	14	10	6	/	5
2018	4	15	/	6	14	14	/	/	/	8	15	10
2019	5	/	8	9	18	6	/	/	/	/	/	/

An overall ranking was then obtained by summing up the three distinct rankings, thus identifying the months that best fit to the overall behavior for all three parameters as reported in Table 2.13. For every calendar month the three best ranked yearly months are selected as suitable for the TRY generation and are reported in green in Table 2.13.

Table 2.13: Overall Finkelstein-Schafer ranking. In green the three best ranked years for every calendar month. In bold, underlined green the years chosen for TRY generation.

	Gen	Feb	Mar	Apr	May	Jun	Jul	Aug	Sep	Oct	Nov	Dec
1995							22		25	31		
1996		22	25	19	23	38	27	21		**18**	26	25
1997		16	34	39	21	27	15	18	38	37	22	25
1998	33		31		37	34			26	33	33	**15**
1999	24	22		26		32	34	32	13	19	23	38
2000	28	21	26	16		30	25	24	20			
2001			31	25	29		8		22	30		50
2002	19		32	11	29			18	34	10	**16**	22
2003	10	17		14	38	26	**18**		**4**		20	30
2004	23	34	**13**							26		38
2005				23	23			23	37			33
2006	31	29	30	28	32	**4**	23	23	34	27	13	33
2007	44	22	44	26	32	12	19	15	23	43	24	27
2008	26		29	31	**15**	17	33	30	50	22	36	33
2009	19	33	29	44			20	**13**			15	34
2010	27	**16**			27	23	28	26	22	33	22	30
2011	30	39	18	36	25	19	32	17	29	39	19	40
2012	40		16	19	47	18	36	32	22			20
2013	24	24		**13**	40			42		10	23	21
2014	41	24	18		20	29	30	45	18	35	17	31
2015	28	13	18		32	35	35	33	40	21		
2016		34	15	41	22	23	25	21	28	22	19	28
2017	31	13	21	46	18	23	29	26	28	33		28
2018	17	29		27	18	44				24	32	29
2019	**18**		29	29	42	25						

The final step for each calendar month is to choose, among the three best ranked yearly months, which one best represent the long-term behavior of wind speed. This means choosing the one having the monthly mean value of wind speed that is closest to the mean value of wind speed computed over all the dataset for that particular calendar month.

It is worth noting that wind was not included in the Finkelstein-Schafer statistic because of its extreme variability, thus probably leading to relevant differencies between short and long-term CDFs. This characteristic could have led to an alteration of the statistic results, worsening the quality of the finished TRY. Because of this, it has been chosen to disregard wind speed evaluation in the first step of the procedure and applying it only to the best three ranked yearly months, already showing high performances in representing the climate of the overall period.

2.5.3 TRY smoothing

Because of the TRY creation method, based on the selection of real months from various years, discrepancies could emerge at the interface between months, like for example unphysical temperature leaps around the midnight between the last and first days of contiguous months.

To avoid this type of situation a smoothing procedure was conducted at the interfaces of the TRY months. This operation included the removal of the data located in the first and last eight hours of every month e their substitution through second degree spline interpolation methods. Through this process the discrepancies between months were reduced and brought back to values more appropriate for a real physical behavior of climatic parameters.

The smoothing procedure was conducted for temperature and relative humidity values; it was not

applied to wind speed because of the latter parameter not being affected by this kind of problems, nor to solar radiation having null values during the hours object of the correcting operation.

The effects of the smoothing procedure can be observed in Figure 2.9 where the original and smoothed values for temperature are reported for the interface between November and December months of the TRY generated for Trieste. As it can be seen, near the midnight of November 30th temperature values present a nearly immediate drop of almost 7 °C, highlighting then an unphysical pattern. Through the smoothing procedure this drop is modified and brought back to more appropriate, and more physical, values.

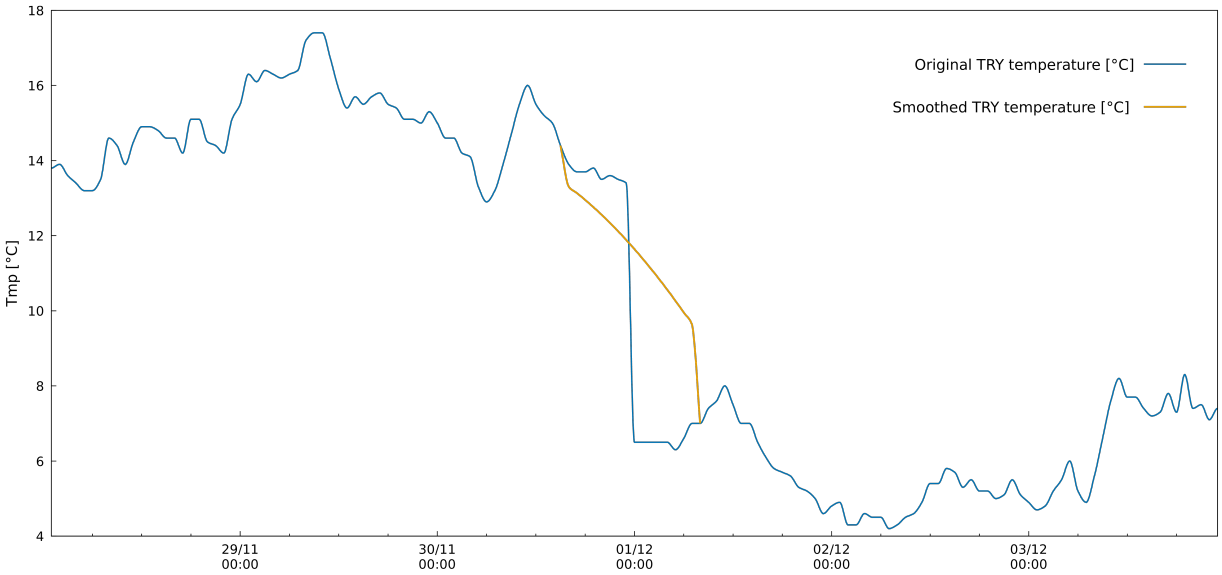

Figure 2.9: Temperature smoothing at the interface between November and December months of Trieste's TRY.

Chapter 3

Climate change

3.1 Modeling climate evolution

Climate change is becoming more and more a concerning problem for many aspects of human life and activities. The growing trend of temperature has been widely assessed throughout many studies in the latest years and a valuable summary of these researches can be found in the 2014 Fifth [30] and in the newly published 2021 Sixth [74] Assessment Reports of the Intergovernmental Panel on Climate Change. These documents report that Earth surface temperature has increased on average 0.85 °C since 1880, speeding up in the last three decades. This strong increase is said to be due to the anthropogenic Green House Gas emissions that trap the solar radiation in the atmosphere causing excessive warming. In fact, many aspects related to human presence like the continuous growth of global population, the economic activities, the energy consumption and land use patterns heavily influence the concentration of GHG in the atmosphere. However, some actions like technology evolution and the drafting of climate and adaptation policies could be developed to counterbalance this effect.

In order to properly assess the future effects of human actions on the atmosphere, the IPCC considers all the GHG emissions human-related drivers to create Representative Concentration Pathways (RCPs) to make projections of future GHG emissions, air pollution and land use. The RCPs are divided into a mitigation scenario (RCP2.6), two intermediate ones (RCP4.5 and RCP6.0) and a high emission one (RCP8.5) also defined as "business as usual". These scenarios are then applied to General Circulation Models, or GCM, developed by exploiting numerical codes, to carry on forecasts about global climate evolution. The GCMs are in fact defined as "numerical models representing physical processes in the atmosphere, ocean, cryosphere and land surface, for simulating the response of the global climate system to increasing greenhouse gas concentrations" [75]. They divide the planet in a three-dimensional grid having a horizontal resolution between 250 and 600 km and 10 to 20 vertical layers for air and to 30 for oceans. For every block of the grid they compute all the climatic parameters that represent the climatic situation of that particular location. The four primary GCMs are [10]:

- HadCM3 (United Kingdom);
- CSIRO2 (Australia);
- CGCM2 (Canada);
- PCM (USA).

These GCMs, applied to the RCPs scenarios, are exploited to make predictions about the future surface temperature variations to year 2100 as it can be seen in Figure 3.1. The IPCC predicts an increase in surface temperature by the end of the century (2081-2100) of 0.3 °C to 1.7 °C (RCP2.6) and 2.6 °C to 4.8 °C (RCP8.5) in comparison to the reference 1986-2005 period. These evolution will lead to several collateral effects like fewer cold and more frequent and longer hot extremes, including intense heat waves [76]. The oceans will continue to warm and could double in acidity. Global glacier volume (excluding Greenland and Antarctic ice sheets) could decrease by 85%, near surface permafrost by 81% and the Arctic Ocean could be ice free by mid-century. RCP8.5 scenario estimates a rise in sea

water level of more than 0,8 m [30].

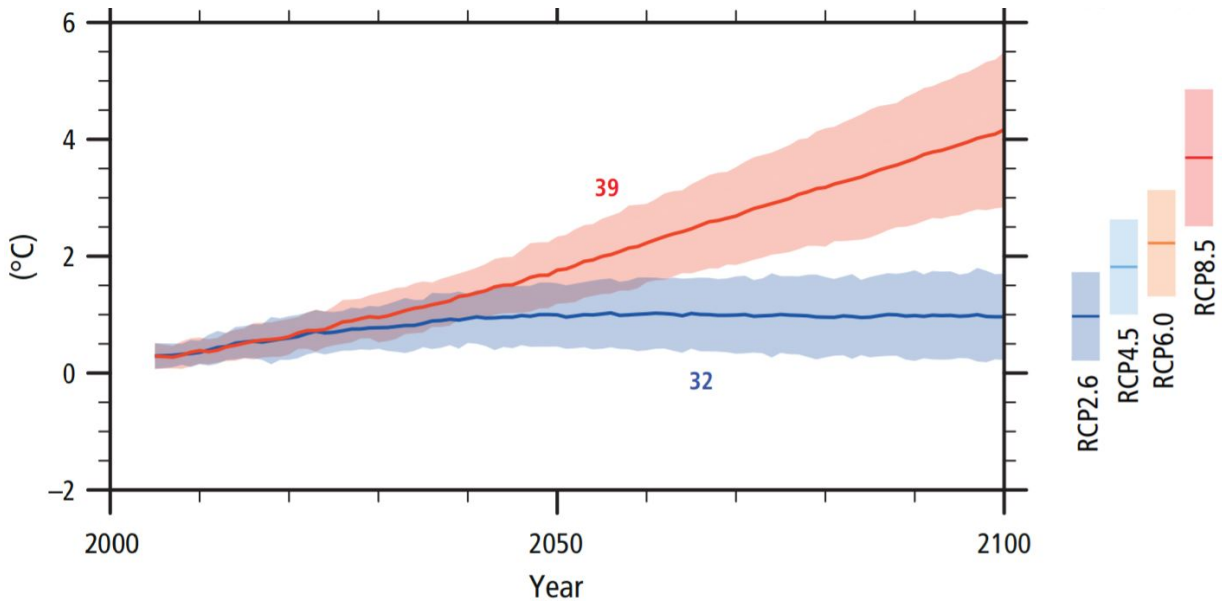

Figure 3.1: Global average surface temperature change from 2006 to 2100 for all RCP senarios. All changes are relative to 1986–2005 period. Time series of projections and a measure of uncertainty (shading) are shown for scenarios RCP2.6 (blue) and RCP8.5 (red). The mean and associated uncertainties averaged over 2081–2100 period are given for all RCP scenarios as coloured vertical bars at the right hand side of the panel. [*IPCC: Climate Change 2014: Synthesis Report.* `https://ar5-syr.ipcc.ch/ipcc/ipcc/resources/pdf/IPCC_SynthesisReport.pdf`]

When dealing with climate forecasts, the most used RCP scenarios are the 2.6 and 8.5. This because the first one represents the target situation of all the mitigation measures to be developed by the governments, aiming to keep the increase in global temperature under 1.5 °C at the end of the century. The latter instead represents the future evolution of climate if no mitigation measure is developed at all in the next decades, approximately representing the actual global situation.

Regarding the Global Circulation Models, they are characterized by a coarse resolution of the computational grid, not fit to properly represent many local climate phenomena, happening on a much smaller scale. Therefore, when applied to studies on local climates, they are downscaled into Regional Circulation Models, or RCMs. A regional climate model is generated from a GCM by imposing specific working conditions and simulates atmospheric and land surface processes to make a detailed forecast for a given limited area of interest by focusing resolution over it and accounting for high-resolution topographical data, land-sea contrasts, surface characteristics, and other components. RCMs thus downscale global GCM runs to simulate climate variability with regional refinements. It should however be noted that solutions from the RCM may be inconsistent with those from the global model, which could be problematic in some applications.

3.2 Analysis scope

The aim of this research is to provide to the municipalities included in the Interreg ITA-SLO Secap Project a general overview of the situation of climate change in this region and a procedure to exploit when studying climate change and its effects. To do this, a literature review of the studies developed for this topic has been carried on in collaboration with other actors of the Interreg Project like Area Science Park, Metropolitan City of Venice, ARPA FVG and others. Within the program area of the project, the research here presented focused on the analysis of Friuli Venezia Giulia region itself, leaving to the other actors the analysis for their target territories. The overall review led to the creation of the "Preliminary Context Analysis" document [77] of the Secap project.

Furthermore, because of the possibility of the climate models to provide considerable errors in projecting climatic data, a procedure to calibrate them is here proposed. This will give on municipalities the possibility to exploit a calibration method before using the models to project climatic data and therefore obtain more reliable results.

Moreover, in continuity with the procedure for the generation of the Test Reference Year presented in Section 2.5.1 a process to project the TRY into the future is here developed. This aims to couple the two methods to give the municipalities a complete methodology to properly consider both present and future climate in their analysis for the development of mitigation policies.

Finally, an analysis of climatic extreme events has been carried on within the Secap project, considering phenomena like heavy precipitations, floods, sea level rise, droughts, wild fires, extreme heat and cold. The research here presented focused on heat waves and cold spells, for both actual and future timeframes, leaving the other hazards to the project actors more suited to study that particular phenomena. This analysis also led to a methodology that municipalities could exploit to compile the Risk & Vulnerabilities Assessment within their Secap plans.

3.3 Climate change in Friuli Venezia Giulia

The main study on past and future climate changes in this region has been carried on by the Regional Agency for Environment Protection of Friuli Venezia Giulia region, ARPA FVG, leading to the creation of the "Studio conoscitivo dei cambiamenti climatici e di alcuni loro impatti in Friuli Venezia Giulia" [78]. This document first displays a report of the climate changes detected during the 1961 – 2016 period then, through the analysis of Regional Climate Models (RCM), provides future climate change projections for the investigated region.

Friuli Venezia Giulia (FVG) region has peculiar geographic position and orography that influence its meteorology. The region is situated at mid latitudes where a strong contrast between polar and tropical air masses is present, thus causing strong atmospheric perturbations. In addition, the northern mountain reefs significantly influence the atmospheric circulation, with wide effects on both temperature and rain. The Alps impede the flux of particularly cold air masses thus mitigating the temperature and retaining the fluxes of humid air from south-west and south-east. Very important is also the presence of the Adriatic Sea which also mitigates the temperature (particularly in the coastal area), allowing for cooler summers and warmer winters.

Similarly to the national scale, in FVG an increasing trend of temperature has been detected and reached almost +1.5 °C since 1960. The yearly mean temperature increased 0.3 °C per decade over the last fifty years with a significant trend to accelerate in the last decades. This tendency is even more remarkable in the Alps, where the mean temperature at 2,200 m of altitude grew up to +1.7 °C if compared to the 1851 values, showing almost a double increase compared to the global values [78].

In the analysis of the heat waves, compared with the mean temperatures of 1961-1990 period, there is a significant evidence of an increasing trend. In particular, during the summer season the number of days where the maximum temperature is over 30 °C increased from 30 to 50, while the number of "tropical nights", defined as the ones when the minimum temperature is above 20 °C, increased from 5 to 15. Moreover, during winter season frost days, having temperature below 0 °C, diminished from 60 to 40 [78].

As regards climate change projections in FVG, since many coupled Global-Regional circulation models are available, ARPA FVG chose the most representative ones that featured data availability for all RCP scenarios, availability of models having high, medium and low climate sensitivity, and good performance while reproducing climatology during the chosen reference period (1970 – 2005). Because of these prerequisites, five different GCM-RCM couplings in the CORTEX database were selected:

1. HadGEM2-ES_RACMO22E;

2. MPI-ESM-LR_REMO2009;
3. EC-EARTH_CCLM4-8-17;
4. EC-EARTH_RACMO22E;
5. EC-EARTH_RCA4.

The models reference period covers the years between 1976 and 2005 while the projections cover the years 2006 to 2100. The scenarios used are the RCP2.6, RCP4.5 and RCP8.5. The future projections were compared with the reference period data in order to obtain the predicted changes. The future anomalies of the relevant climatic parameters are then computed for every RCP scenario using every model listed above. The different RCP scenarios for FVG show that in winter, the mean value of the investigated models for what concern temperature is predicted to increase from 1.3 °C (RCP2.6) to 5.3 °C (RCP8.5) at the end of the century as it can be seen in Figure 3.2a.

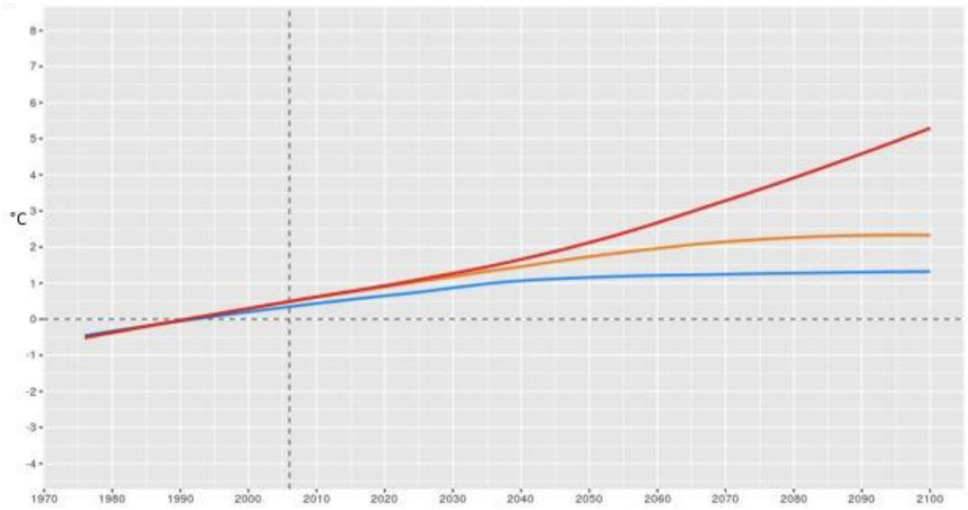

(a) *Winter season.*

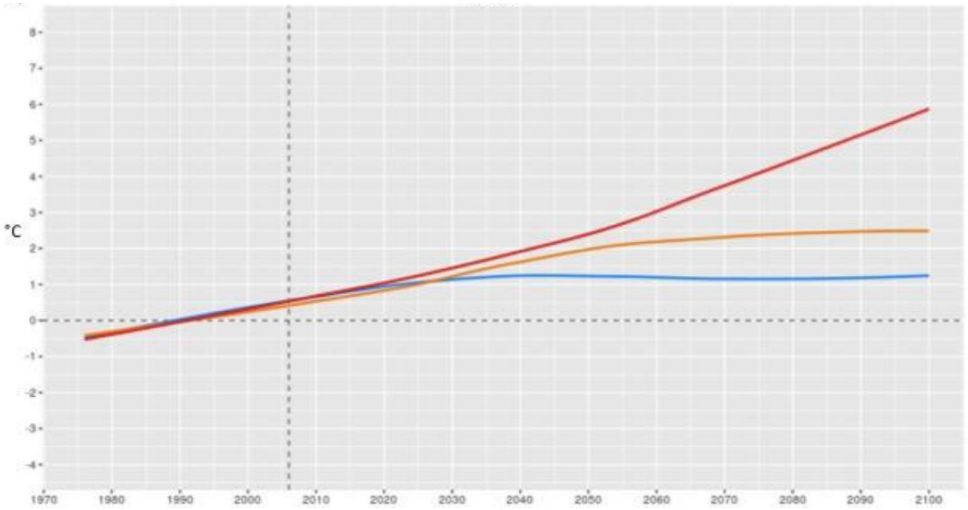

(b) *Summer season.*

Figure 3.2: Temperature anomalies in FVG to 2100 for RCP2.6 (blue line), RCP4.5 (orange line) and RCP8.5 (red line) scenarios. [*ARPA FVG.* `https://www.meteo.fvg.it/clima/clima_fvg/03_cambiamenti_climatici/01_REPORT_cambiamenti_climatici_e_impatti_per_il_FVG/impattiCCinFVG_marzo2018.pdf`]

Summer temperatures show a similar trend, with a possible increase up to 6 °C for the RCP8.5 as reported in Figure 3.2b. In the RCP8.5, the temperature continues to rise until 2100, while in the other two scenarios it tends to stabilize in the second part of the century. The five models used show a spread around the mean value of about +/- 1.5 °C for winter and of +/- 2 °C for summer temperature

predictions. This is due to the different representation in the models of the investigated processes; moreover, this spread tends to increase in time, especially for summer season projections [78].

The evolution of extreme temperature events was also considered in the analysis by ARPA FVG. Some of the phenomena considered by ARPA were the "hot days" and the "tropical nights", defined before. For these events, five FVG locations were analyzed: the four province capitals (Trieste, Udine, Pordenone, Gorizia) and the town of Tolmezzo, representative of the mountain territory. In the following tables, the number of hot days (Table 3.1) and tropical nights (Table 3.2) for the reference period (1976-2005) are reported, as well as the ones predicted at the end of the century for the three RCP scenarios and the percentage of variation.

Table 3.1: Number of "hot days" in the reference period and predicted with all RCP scenarios and relative percentage of variation.

Location	**Reference**	**RCP2.6**	**RCP4.5**	**RCP8.5**
Trieste	20	30 (+50%)	40 (+100%)	70 (+250%)
Udine	30	50 (+65%)	60 (+100%)	90 (+200%)
Pordenone	30	55 (+85%)	65 (+115%)	95 (+215%)
Gorizia	25	50 (+100%)	60 (+140%)	95 (+280%)
Tolmezzo	15	30 (+100%)	40 (+160%)	70 (+360%)

Table 3.2: Number of "tropical nights" in the reference period and predicted with all RCP scenarios and relative percentage of variation.

Location	**Reference**	**RCP2.6**	**RCP4.5**	**RCP8.5**
Trieste	40	70 (+75%)	90 (+125%)	120 (+200%)
Udine	5	20 (+300%)	35 (+600%)	70 (+1300%)
Pordenone	5	25 (+400%)	35 (+600%)	75 (+1400%)
Gorizia	5	20 (+300%)	35 (+600%)	70 (+1300%)
Tolmezzo	3	5 (+65%)	15 (+200%)	45 (+800%)

Trieste, representative for the coastal area, is the location having the major number of tropical nights, 40, and the minor of hot days, 20, for the reference period. This is also the location affected by the minor percentage changes in the various RCP scenarios for 2100, showing an increase of tropical nights between 75% and 200% and of hot days between 50% and 250%. This is mainly due to the mitigation effect of the sea.

Regarding Udine, Pordenone and Gorizia, representative of the plains environment, in the reference period they display a relevant number of hot days, about 30, but very low values of tropical nights (5). This represents the typical temperature swing that occurs between day and night in the plains environment. Regarding the number of hot days predicted by the RCP scenarios, the three locations show a similar behavior, with an increase of hot days between 65% and 280%. About tropical nights, the behavior is essentially identical in all three locations, showing a huge increment in their number, between 300% and 1400% [78].

Finally Tolmezzo, representative of the mountain environment, shows the lowest number for both hot days, 15, and tropical nights, 3, coupled with the greatest percentage increase of hot days, between 100% and 360%, and an intermediate increase of tropical nights, between 65% and 800%.

Global warming, besides increasing the number of hot days and tropical nights, will also reduce the frost days in which minimum temperature falls below 0 °C. In Trieste, the reference number of frost days is 10 - 20 per year and is predicted to diminish in 2100 to less than 10 for RCP2.6 and 4.5 scenarios, and even to 0 for RCP8.5. Regarding Gorizia, Udine and Pordenone, the reference number of frost days is 60 - 70 per year, predicted to diminish in 2100 to a 30 - 50 range for RCP2.6 and 4.5

scenarios and about 10 for the RCP8.5. Finally, Tolmezzo will see a reduction from 80 days per year (reference value) to 10 for the RCP8.5 scenario in 2100 [78].

3.4 Climate models quantile correction

Simulations from global and regional climate models (GCMs and RCMs) may differ from local measurements generating a bias error, and will therefore influence the expected climatic output [79]. The difference can be more evident for long-term scenarios as highlighted by Grenier [80]. A better explanation of this problem is reported in Figure 3.3, where a sample comparison between hypothetical measured and modeled values distribution is reported.

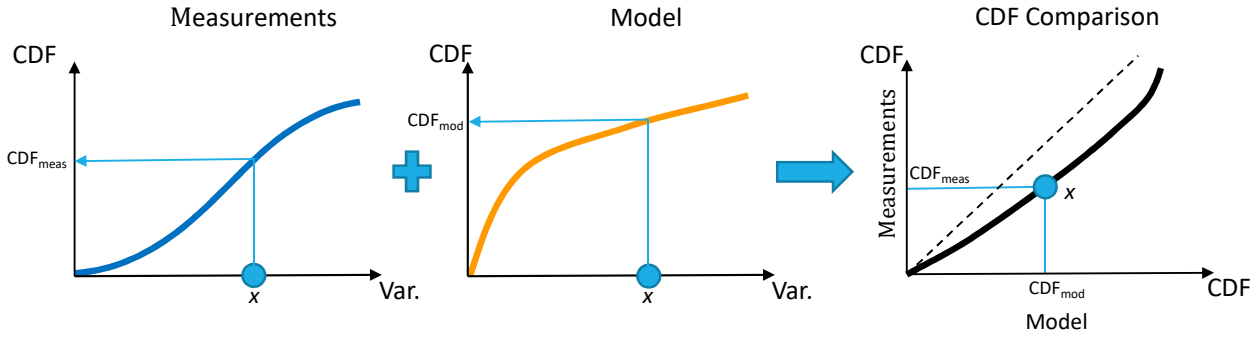

Figure 3.3: A sample comparison between measured and modeled data statistical distributions.

As it can be seen, the two CDFs are not equal, highlighting different statistical distributions of measured and modeled data. In fact the same variable x is associated with different CDF values in measured and modeled situations. This underlines that the model is unable to properly reproduce the statistical pattern of the measured data. The comparison of the two CDFs reported in the right graph would be coincident with the diagonal line if the two statistical distributions would have been equivalent. Instead, because of the bias generated by the model the comparison is shifted, in this case under the diagonal. This highlights that the model generally tends to give lower values than the measured ones (it reaches higher CDF values with the same value x), creating then a systematic bias.

Because of this possible issue regarding the models, also the climate projections for the Friuli Venezia Giulia region could be affected by systematic biases. In order to assess if this problem could emerge, a comparison between measured and modeled temperatures was carried on for Trieste. The timeframe considered was the one comprised between 2006 and 2019, period for which the projected values of the models could be compared with measured data. As it was done in the previous example, the analysis was carried on by confronting for the check period the statistic distributions of measured and modeled data, in this case focusing on minimum, mean and maximum daily temperatures values. The analysis highlighted relevant discrepancies for all models and RCP scenarios, especially pertaining minimum and mean daily temperatures, while the maximum daily one showed no significant issues.

In order to correct the bias in models outputs from simulations, available measurements for typical climatic variables can be used. A common form of bias correction is the quantile mapping which accounts for models errors assuming that biases in historic observations will be repeated during the projections [81]. The method corrects models data so that they match the quantiles obtained from measurements, leading to a projection more adherent to the data detected by meteorological stations. The correction of models data can be done through addittive or multiplicative operations, depending on the parameter analyzed. The quantile correction process can also be used to correct inaccuracies due to different positioning between model grid points and data collection units. The method consists of two parts, a first one of data training and a second one of adjustment, referring to distinct timeframes.

The temperature, relative humidity and atmospheric pressure values for Trieste obtained through the climate models have been bias corrected by using the quantile delta mapping correction [82] which

preserves relative or absolute changes in modeled quantiles while correcting systematic biases. An additional feature of the method is that it automatically deals with projected values outside the range of the historical period. The correction was not performed on the solar radiation, because of this parameter presenting minor issues and of the quantile mapping not performing well in correcting radiation biases. The quantile correction was performed on the daily temperature range through a multiplicative operation and on the daily maximum temperature through an addittive one. The corrected mean and minimum temperatures were subsequently obained by subtracting from the corrected maximum one half and all the corrected temperature range respectively. The mean and minimum temperatures were not directly modified through the quantile correction because that approach proved to sometimes lead to minimum temperatures greater than the maximum ones. Regarding relative humidity and atmospheric pressure, the correction was performed through multiplicative and addittive operations respectively. However, in the following the whole correction process is reported for temperature only to preserve clarity of presentation.

The data training has been performed by comparing models and detected data for 1995-2005 period, while the adjustments were performed on the models for the timeframe between 2006 and 2100 (the projection period of the models). Moreover, to check the performance of the procedure, the corrected and original model values have been compared to the measurements for the period comprised between 2006 and 2019, timespan for which the projected values of the models could be compared with measured data as already stated. All the timeframes are reported in Figure 3.4.

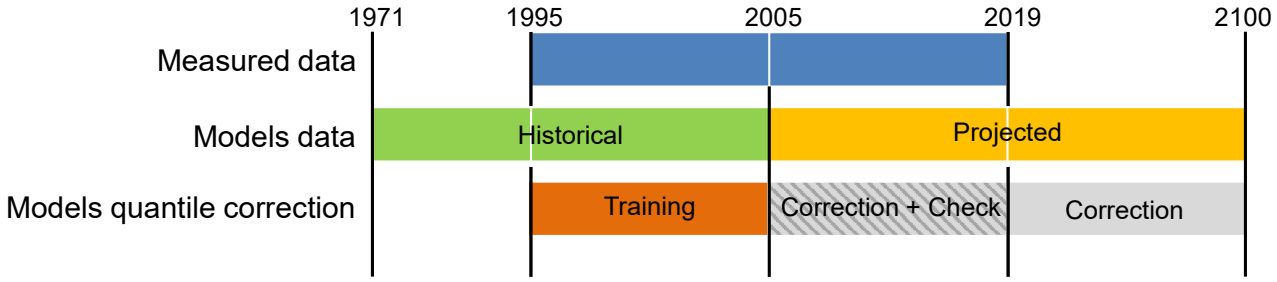

Figure 3.4: Measurements, models data and quantile correction timeframes.

A sample of the correction results for the check period for daily minimum temperature are reported in Figure 3.5, where the quantile-quantile plot (qqplot) of measurements and original (a) or corrected (b) values of HadGEM2-ES_RACMO22E climate model applied to RCP2.6 scenario for Trieste, is reported. The qqplot is another way to represent the measured-modeled data comparison and is essentially the opposite version of the CDF comparison reported in Figure 3.3. Rather than having on the axes the CDFs values of the same variable x, the qqplot reports on the axes the variables sharing the same CDF value. In this way was reported the comparison between measured and modeled daily minimum temperature in Figure 3.5.

As in the example reported in Figure 3.3, a perfect equivalence between model and measured data quantile distributions is represented by the diagonal line reported in Figure 3.5. By observing Figure 3.5a however, it is evident that original model tends to provide lower temperature values than the measured ones, showing a distribution located below the diagonal. Through the quantile correction instead, modeled temperature trend better imitates the measured data behavior, as highlighted by the distribution reported in Figure 3.5b, closely sticking to the diagonal.

To further highlight the effects of the quantile correction, monthly temperature averages have been computed for the observed, original model and corrected model values for the check period, as reported in Figure 3.6, highlighting the beneficial effect of the correction on the projections performances. As it can be seen in Figure 3.6 and as already stated, the most troublesome parameter to deal with was the daily minimum temperature, while mean and maximum ones showed minor issues. It can also be noted that the quantile correction greatly improves the capability of the model to stick to the measured data during the check period.

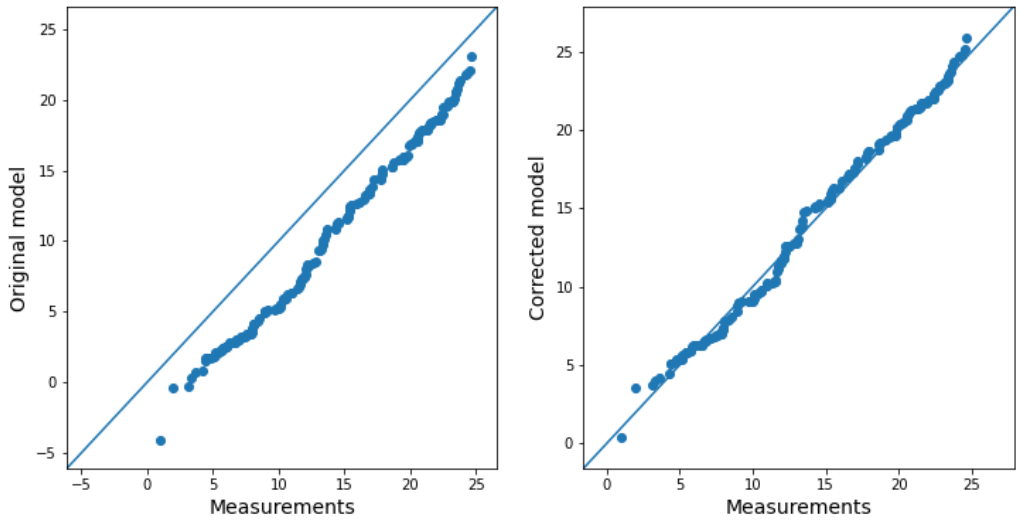

Figure 3.5: Minimum daily temperature quantile distribution comparison between measurements and original (a) or corrected (b) values of HadGEM2-ES_RACMO22E climate model applied to RCP2.6 scenario for Trieste, 2006-2019 period.

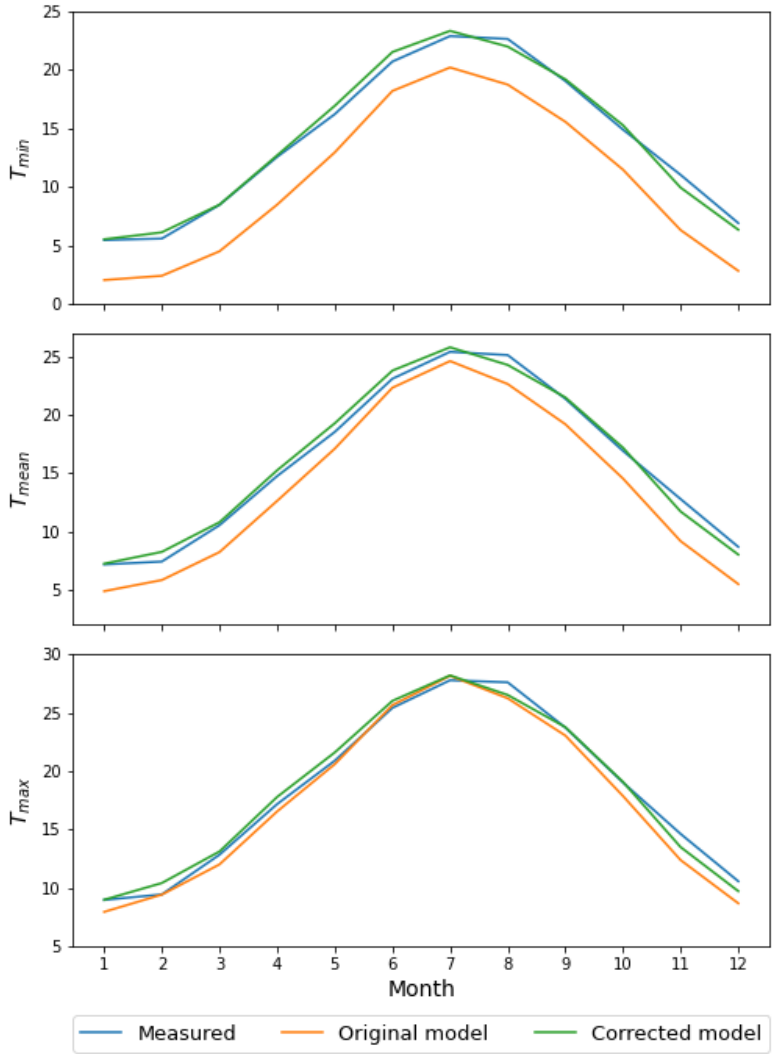

Figure 3.6: Trieste monthly mean values of minimum, mean and maximum daily temperatures computed during 2006-2019 period for measurements, original and corrected data of HadGEM2-ES_RACMO22E climate model applied to RCP2.6 scenario.

Finally, in order to provide a concise description of the quantile correction effect on the prevision of the climate models, the Root Mean Square (RMS) error of monthly values has been computed using the original and corrected models values through Equation 3.1, where the subscript j can be m for the original and q for the corrected models values.

$$RMS_j = \sqrt{\sum \frac{(v_o - v_j)^2}{n}} \tag{3.1}$$

Figure 3.7 reports the distribution of the monthly mean RMS values for minimum, mean and maximum daily temperatures of the HadGEM2-ES_RACMO22E climate model applied to RCP2.6 scenario for Trieste. This figure further highlights the major problems concerning the modeling of minimum and mean temperatures and the better performance in modeling the maximum one. Moreover, it further underlines the effects of the correcting actions of the quantile mapping process. Table 3.3 reports the mean RMS values for every model for mean, minimum and maximum temperature. From the table it can be seen that the correction reduces the bias error for every model and variable considered.

The corrected models where then used to perform all the analysis reported in the following sections.

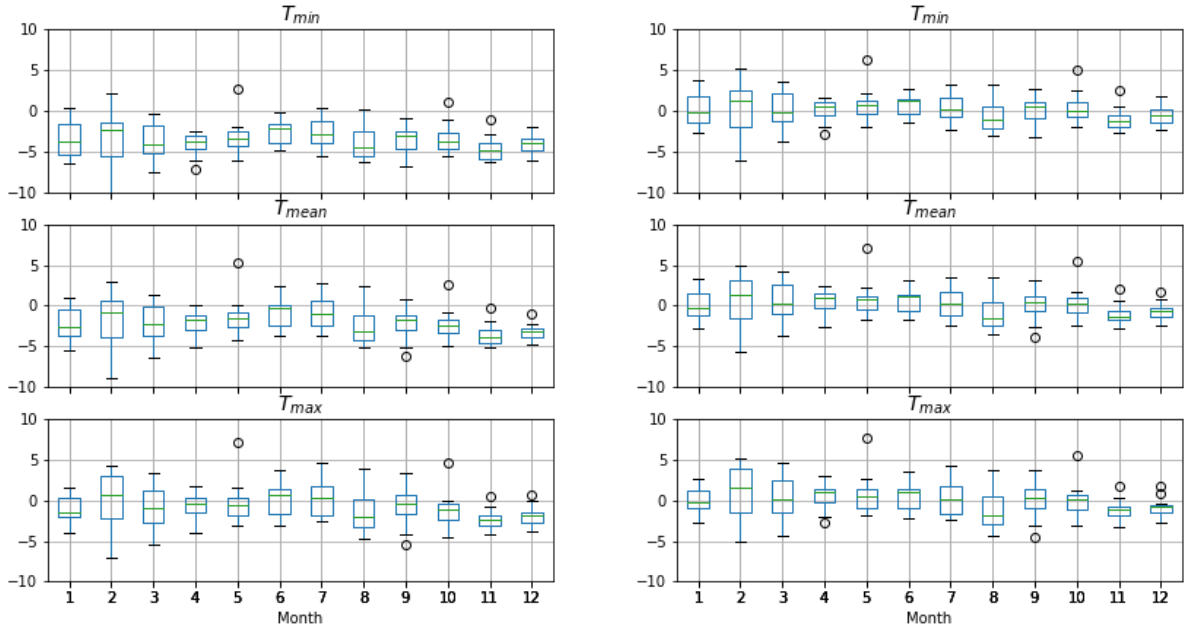

(a) *Original model data.* (b) *Quantile corrected model data.*

Figure 3.7: Distributions of the mean monthly RMS errors for minimum, mean and maximum daily temperatures of HadGEM2-ES_RACMO22E climate model applied to RCP2.6 scenario for Trieste, 2006-2019 period.

Table 3.3: RMS of the five models, original (m) and corrected (q), for the check period (2006-2019).

RCM	$\mathbf{T_{min}}$		$\mathbf{T_{mean}}$		$\mathbf{T_{max}}$	
	$\mathbf{RMS_m}$	$\mathbf{RMS_q}$	$\mathbf{RMS_m}$	$\mathbf{RMS_q}$	$\mathbf{RMS_m}$	$\mathbf{RMS_q}$
HadGEM2-ES_RACMO22E	4.03	2.08	2.93	2.12	2.36	2.24
MPI-ESM-LR_REMO2009	2.56	2.06	2.35	2.09	2.31	2.2
EC-EARTH_CCLM4-8-17	2.56	2.07	2.35	2.07	2.31	2.13
EC-EARTH_RACMO22E	6.00	2.03	4.63	2.02	3.58	2.08
EC-EARTH_RCA4	5.66	1.98	4.51	1.96	3.4	2.02

3.5 Analysis of extreme thermal events for Trieste

As already stated in Section 3.2, an analysis of climatic extreme events was carried on within the Interreg Secap Project, regarding many different aspects like heavy precipitations, floods, sea level rise, droughts, wild fires, extreme heat and cold. In this work the research is focused on the last two phenomena, for both actual and future situations.

There is not a unique definition for heat waves and cold spells in literature, in fact many works present different representations for these phenomena. In this research were selected the definitions proposed by Casati et al. [83] and Robinson [84]. The heat wave is described as an event where the minimum and maximum daily temperature exceed a given threshold for a consecutive number of days. In this work the threshold were defined as follows:

- Minimum temperature: 22 °C;
- Maximum temperature: 30 °C;
- Number of consecutive days: 3.

Obviously different thresholds values could lead to different results. Heat waves frequency, HW_{freq}, given by the number of events in a determined period, heat waves maximum, $HW_{len,max}$, and total, $HW_{len,tot}$, length were also considered in this research.

Alongside with the high temperatures, an analysis regarding low temperatures was also carried on, probably of little interest for Trieste, being located at sea level, but which could become important for the settlements located on the Karst plateau. The cold spells are then defined as events where the mean daily temperature is lower than a given threshold for a consecutive number of days. In this work the threshold used is -5 °C and the number of consecutive days is set to 3. In addition, also the pattern of the frost days, defined as the ones where the minimum daily temperature falls below 0 °C, have been studied.

3.5.1 Actual heat waves and extreme colds phenomena

Through the imposition of the aforementioned thresholds, an assessment of the actual situation of extreme thermal events in Trieste was carried on. Figure 3.8 shows the trend of heat waves, as defined previously, using the climatic data collected by the Trieste meteorological station between 1995 and 2019.

By analyzing the graph, it can be immediately noted the intense heat event of 2003, presenting a great number of days included in heat waves, 25, and also a remarkable maximum length of a single event, 14 days. A slightly smaller event is present in 2015 and is also immediately noticeable, as well as the 2006 and 2018 events, while in the other years these phenomena have very reduced occurrence, nearly always presenting only one heat wave per year.

The pattern of extreme cold events is described in Figure 3.9 where the cold spells frequency, CS_{freq}, is reported alongside with the maximum number of consecutive frost days, $FD_{cons,max}$, and their total number, FD_{tot}, all computed year by year.

It can be quickly noticed that there are no cold spells in the analyzed period although frost days were recorded, in particular is evident the event of 2012 counting fourteen consecutive frost days. It can be noted however that this was an extraordinary event, never replicated in the analyzed timeframe. This results then highlight the behavior of a climate heavily influenced by the sea presence, not allowing to reach very cold mean temperatures for relevant amount of days, although displaying some days having minimum temperature below zero.

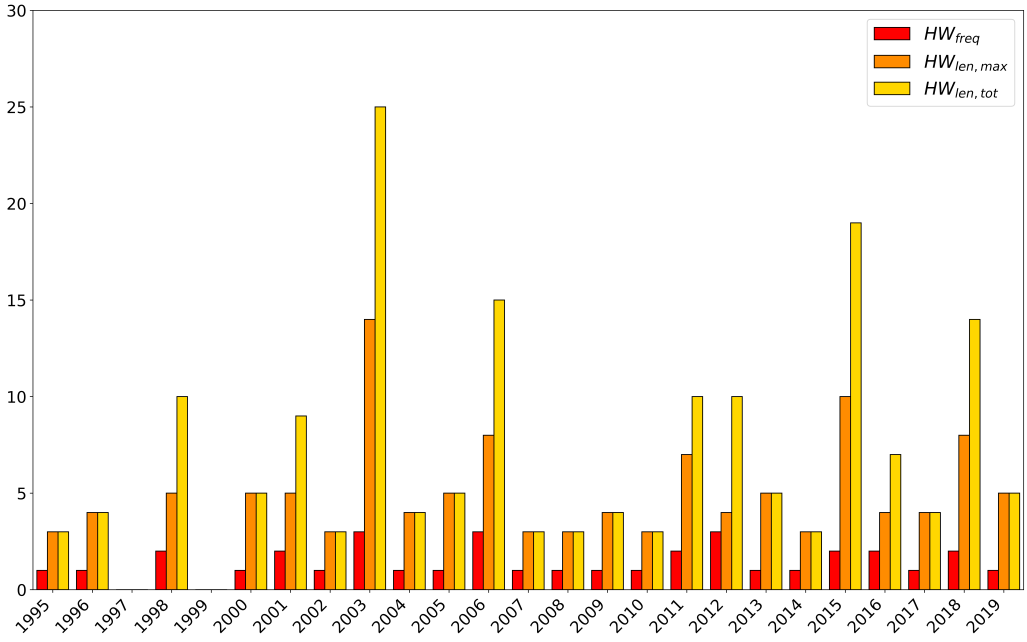

Figure 3.8: Heat waves phenomena in Trieste during 1995-2019 timeframe.

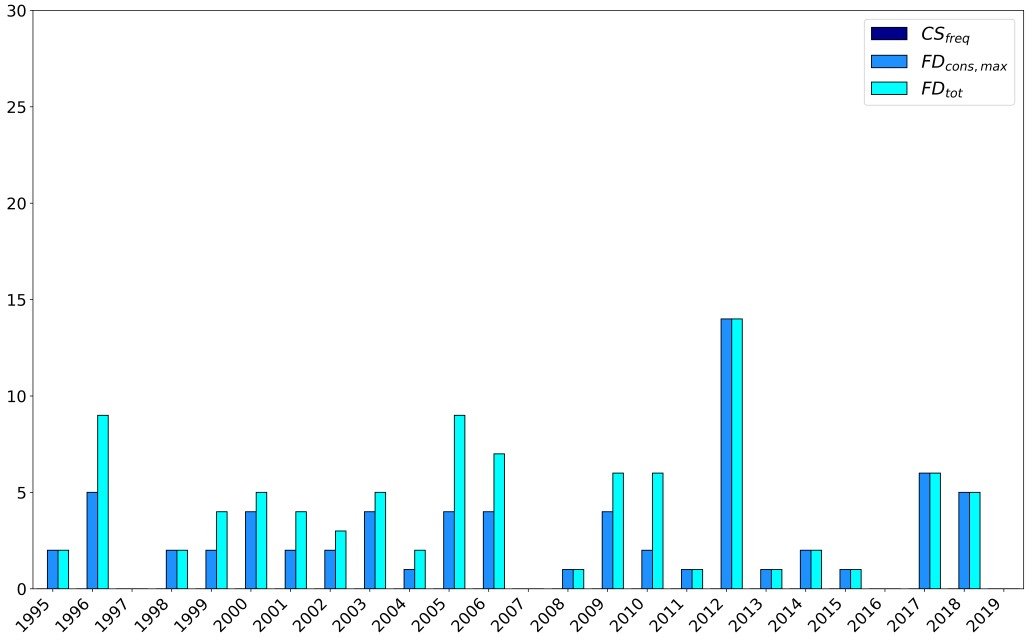

Figure 3.9: Cold spells and frost days phenomena in Trieste during 1995-2019 timeframe.

In order to better highlight the particular configuration of the environment in which Trieste is placed, an analysis of the extreme cold events was carried on also for Sgonico municipality, located on the Karst plateau. Although being distant only 9 kilometers as the crow flies from Trieste, Sgonico is located 278 meters above sea level and it is much less influenced by the sea presence. Moreover, this location is more affected by the Bora, a northerly to north-easterly wind, characteristic of Trieste and of its surrounding areas. These effects can be appreciated by analyzing Figure 3.10, where cold spells and frost days behavior is reported as it was done in Figure 3.9 for Trieste.

It can be immediately noticed that cold spells were detected, although in reduced numbers, in years 1996, 2012 and 2018, highlighting a mean daily temperature well below 0 °C for a considerable number of days. Moreover, also the frost days display totally different occurrencies than in Trieste case study, often reaching a total yearly number near 50 with an extreme peak of 70 in 2005. This kind of behavior then describes a more continental climate, characterized by minimum temperatures frequently below

0 °C but relatively low amount of cold spells, this is due to a great daily temperature range, typical of continental climates, despite the analyzed location being so near to the seashore.

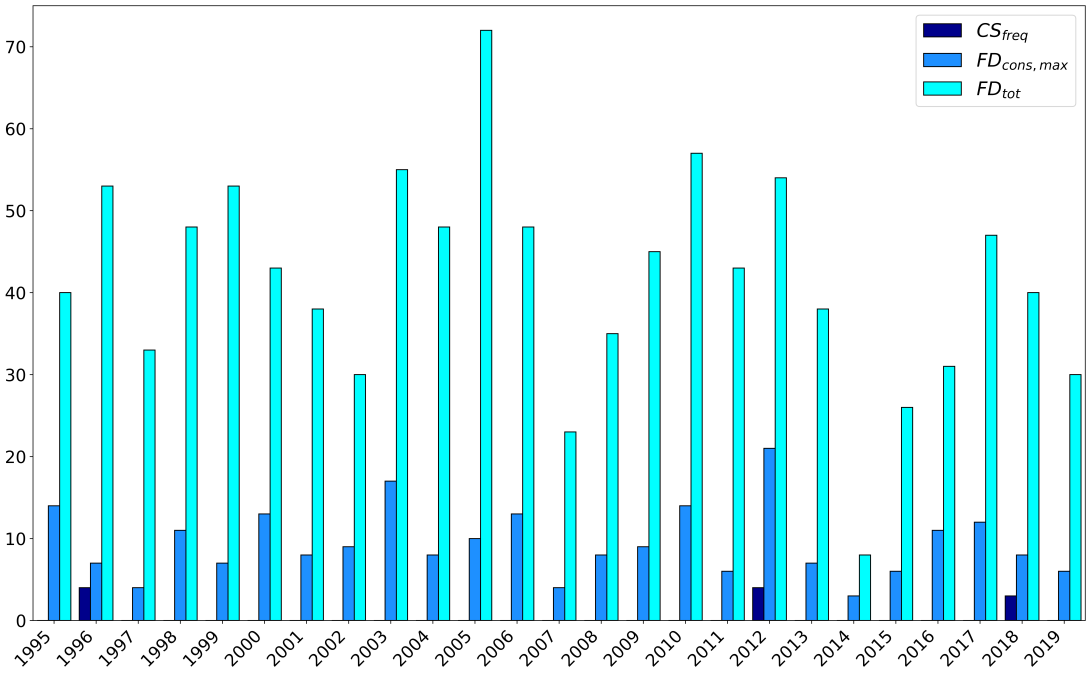

Figure 3.10: Cold spells and frost days phenomena in Sgonico during 1995-2019 timeframe.

3.5.2 Analysis of extreme events future evolution

By exploiting the projections of the climate models a study of the future evolution of extreme thermal events for Trieste was carried on. Because of the great number of configuration considered, fifteen cases, due to the five models applied to the three RCP scenarios, in order to keep the exposition clear and easy to understand boxplot graphs were used.

A boxplot is a standardized way of displaying the distribution of data based on five reference values of the distribution itself: minimum, first quartile, median, third quartile, and maximum. By analyzing a boxplot the outliers values can be immediately identified and the data distribution characteristics can be quickly guessed, like data symmetry, or how tightly the data is grouped, and so on.

In the analysis of the heat waves only the yearly frequency, HW_{freq}, was reported to simplify the exposition. Figure 3.11 reports the boxplots describing the distribution of heat waves frequency for RCP2.6 (a), 4.5 (b) and 8.5 (c) scenarios. The HW_{freq} yearly distributions for 2006 - 2100 timeframe are given by the five climatic models considered in the analysis applied to the reference scenario. Moreover, also the distribution of HW_{freq} for the historical timeframe, 1995-2019, is reported on the left of each graph to highlight the differences between the two periods.

As it can be seen by analyzing Figure 3.11a, for RCP2.6 scenario the number of events will increase but will keep relatively low values, with only some isolated peaks. Moreover, a well defined increasing trend is not present within the century. Finally, the five models seem to give results near to each other, as it can be appreciated through the vertical extension of the boxplots.

Regarding RCP4.5 scenario, presented in Figure 3.11b, an increasing trend across the century is well established. HW_{freq} will reach high values more often than in the RCP2.6 case and the overall situation will get worse in the second part of the century, where all the climate models tend more to higher values, in contrast with the first part of the period. Finally, through the analysis of the boxplots it can be appreciated that the dispersion between models results is greater than in RCP2.6 case.

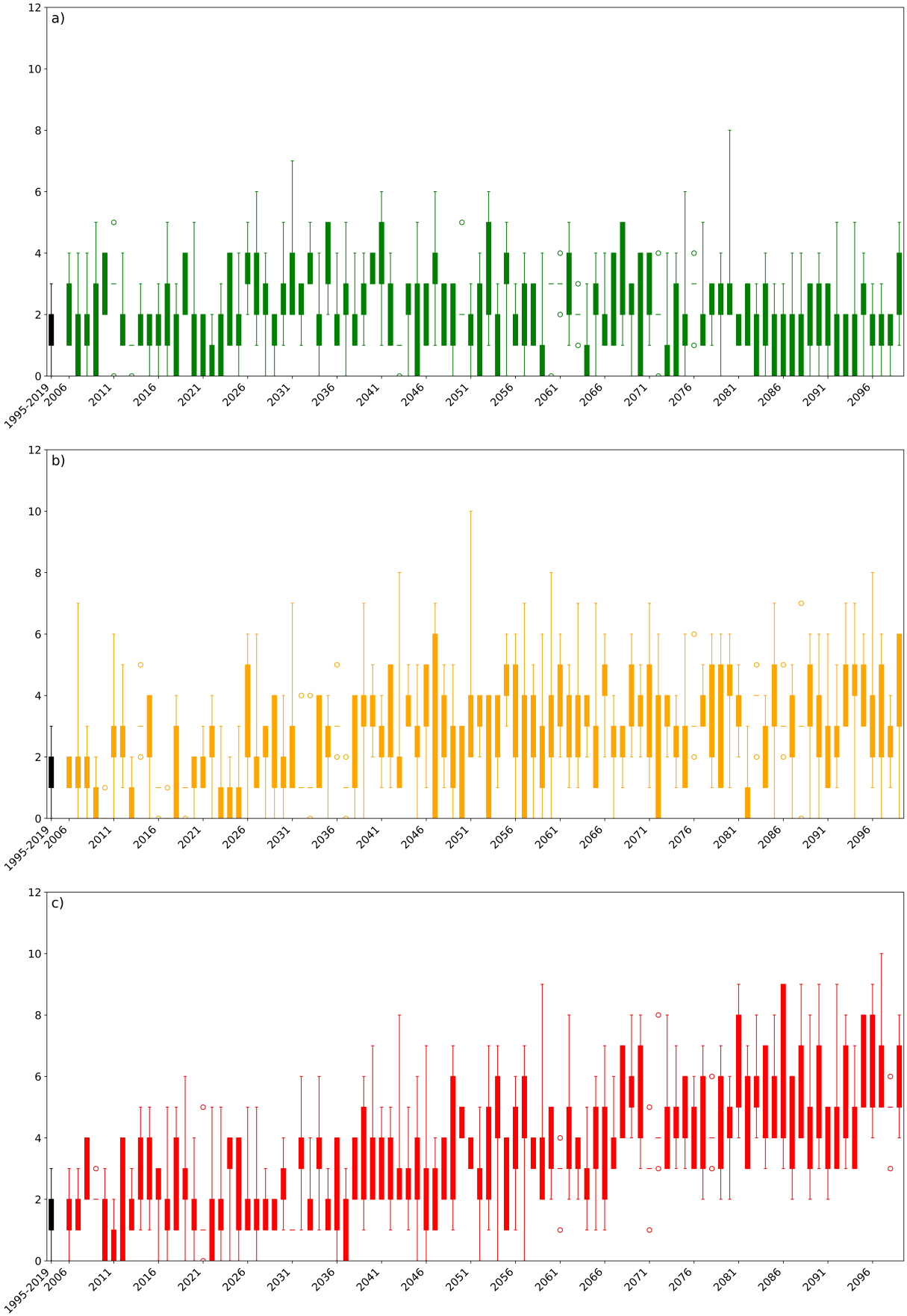

Figure 3.11: Heat waves yearly frequency distribution for Trieste for RCP2.6 (a), 4.5 (b) and 8.5 (c) scenarios. Distributions for 2006-2100 timeframe were obtained through the five climatic models. Distribution for historical timeframe, 1995-2019, is also reported.

Finally, the extension of whiskers in RCP8.5 scenario represented in Figure 3.11c, shows a relevant increasing trend for heat waves frequency, strengthening in the second part of the century. HW_{freq} values will be definitely higher than in the historical period, reaching frequent peaks during the future timeframe.

For what concerns cold spells the analysis highlighted that no significative variations are forecasted in any combination of climate models and RCP scenarios. As an example, within all future projections the maximum number of days included in cold spells for Trieste between 2006 and 2100 is 26 for climate model EC-EARTH_RACMO22E applied to RCP2.6 scenario. It is evident that such a small number cannot be considered a significant variation compared to the historical situation; since all the other cases have numbers lower than this it is evident that in no situation there are significant variations.

3.5.3 Methodology for compiling the SECAPs Risk & Vulnerability Assessment

The process to define heat waves and cold spells described above was exploited to determine the Risk & Vulnerability Assessment (RVA) for such events for Trieste.

First of all, the actual risk of danger due to these events has been determined, following what is stated in the Reporting Guidelines of the Covenant of Mayors [85], defining two parameters that represent the actual level of risk:

- Probability of hazard;
- Impact of hazard.

Both parameters have four different levels of importance that could be associated to, High, Moderate, Low and Not Known. To determine these levels for the probability of hazard the instructions proposed by the Guidelines [85] have been exploited, defining the different levels as follow:

- **High:** extremely likely to happen, having occurence possibility greater than 5%;
- **Moderate:** likely to happen, having occurence possibility between 0.5% and 5%;
- **Low:** unlikely to happen, having occurence possibility between 0.05% and 0.5%;
- **Not Known:** the analyzed location has not observed such phenomena in the past or does not have the possibility to accurately report these informations based on reliable data.

In order to obtain values to compare with the limits defined by the Guidelines, the total amount of days included in heat waves have been compared with the total number of days included in the summer months, 92 days for June, July and August months. Referring to the data measured at Trieste between 1995 and 2019, 173 days were included in heat waves phenomena. Considering a total of 2,300 summer days for the analyzed timeframe, a percentage of occurrence of 7.52% was obtained, superior to the limit of 5%; therefore the actual probability of these events is **High**.

In the same way the cold spells occurrence has been computed. Because of the total absence of such phenomena in the 1995-2019 timeframe, the occurrence probability is 0%, therefore the actual probability of these events is **Low**.

Regarding instead the impact of actual extreme events the choice of the importance level is delegated to the municipalities, folllowing what is reported in the guidelines of the Covenant of Mayors [85].

To evaluate the future risk of danger due to these events three parameters are used in the Risk & Vulnerability Assessment:

- Expected change in hazard frequency;

- Expected change in hazard intensity;
- Timeframe(s).

For what concerns the first two parameters, the guidelines of the Covenant of Mayors provide a choice between three options: Increase, Decrease and Not Known. However, no instructions are reported on how to choose between the proposed options. Regarding the timeframes in which the changes are expected, the guidelines define three periods;

- Short-Term: within 20-30 years from now;
- Mid-Term: after 2050;
- Long-Term: within 2100.

To determine the future evolution of heat waves and cold spells, the Modified Mann-Kendall Trend Test (MMKT) was used, in the version proposed by Hamed et al. [86] derived from the modification of the original Mann-Kendall Test [87, 88]. The Modified Mann-Kendall is a non-parametric test used to analyze data collected over time presenting constant monotonous trends of the analyzed variable. It is based on the concept of "ranking", i.e. on the sorting characteristics of the analyzed series. As an example, a time series that presents a "perfect" upward trend is characterized by the fact that given any observation $x(\bar{t})$, carried out at time $\bar{t}$, all observations made for $t > \bar{t}$ will have values greater than $x(\bar{t})$ and all observations made for $t < \bar{t}$ will have values less than $x(\bar{t})$. The test is then constructed to quantify how close the analyzed historical series can be to a series characterized by a "perfect" ascending (or descending) trend.

This test was first conducted on the frequency of extreme events, defined before as the total number of days included in the extreme heat (cold) events compared to the total days of the summer (winter) months. The evolution of the frequency was studied in relation to the five climatic models defined in Section 3.3 for each RCP scenario for 2020-2045, 2046-2070 and 2071-2100 periods, representative of the Short, Mid and Long Term respectively. In addition to identifying the trend, the Theil-Sen (T.S.) indicator, representative of the change in magnitude of the analyzed event, was also computed. Only the test results having a statistical significance value p less than 0.05 were considered significant.

As regards the heat waves, the test revealed statistically significant changes already in the 2020-2045 period for all cases except for the EC-EARTH_RACMO22E model in the RCP4.5 scenario, having $p = 0.095$. As reported in Table 3.4, all cases except the latter show an increase in the frequency of events, as it can also be deduced from the values of the Theil-Sen indicator. Consequently, for heat waves the choice for the expected frequency variation is the **Increase** option, while for the Timeframe the choice falls on **Short-Term**.

As regards the cold spells, the test did not identify any statistically significant variation in the frequency of the phenomena in any of the periods analyzed for every combination of climate models and RCP scenarios. Consequently, for cold spells the choice regarding the frequency variation is the **No Change** option, while for the Timeframe choice falls on **Long-Term**. Table 3.5 shows the results of the MMKT for the frequency of cold spells.

Subsequently, the MMKT was also applied to the trend of events intensity, defined in this research as the maximum duration of the single extreme event detected in each season. This step has been applied only to heat waves since cold spells did not show any significant variation in terms of frequency if compared to the current situation, characterized by null phenomena. Consequently the options chosen for the cold spells frequency variation can also be applied to the intensity variation, i.e. **No Change** and **Long-Term**.

The results of the MMKT for heat waves instead denote an increase in the intensity of the phenomena already in 2020-2045 period, for almost all the climate scenarios and models analyzed, as reported in

Table 3.6. As a consequence of these analysis, the choice for the variation of intensity of heat waves is seto to **Increase**, while for the timeframe the choice falls on **Short-Term**.

The future behavior of both heat waves and cold spells was already highlighted in the analysis conducted in Section 3.5.2, by studying different parameters.

Finally, it has to be specified that the methodology here described exploits the total amount of days included in heat and cold extreme phenomena instead of the frequency of such events in order to have a usable parameter to compute the percentages of occurence defined by the guidelines of the Covenant of Mayors [85]. Then, having used these parameters to assess the current level of risk, in order to keep a coherent method, they were also used to assess the future situations.

Table 3.4: Modified Mann-Kendall Test results for heat waves frequency for 2020-2045 timeframe.

Model/Scenario	**RCP2.6**		**RCP4.5**		**RCP8.5**	
	Trend	**T.S.**	**Trend**	**T.S.**	**Trend**	**T.S.**
HadGEM2-ES_RACMO22E	Increase	0.18	Increase	0.18	Increase	0.18
MPI-ESM-LR_REMO2009	Increase	0.32	Increase	0.57	Increase	0.58
EC-EARTH_CCLM4-8-17	Increase	0.18	Increase	0.19	Increase	0.17
EC-EARTH_RACMO22E	Increase	0.17	No Change	0.06	Increase	0.28
EC-EARTH_RCA4	Increase	0.35	Increase	0.26	Increase	0.37

Table 3.5: Modified Mann-Kendall Test results for cold spells frequency for all the considered timeframes.

Model/Scenario	**RCP2.6**		**RCP4.5**		**RCP8.5**	
	Trend	**T.S.**	**Trend**	**T.S.**	**Trend**	**T.S.**
HadGEM2-ES_RACMO22E	No Change	0.00	No Change	0.00	No Change	0.00
MPI-ESM-LR_REMO2009	No Change	0.00	No Change	0.00	No Change	0.00
EC-EARTH_CCLM4-8-17	No Change	0.00	No Change	0.00	No Change	0.00
EC-EARTH_RACMO22E	No Change	0.00	No Change	0.00	No Change	0.00
EC-EARTH_RCA4	No Change	0.00	No Change	0.00	No Change	0.00

Table 3.6: Modified Mann-Kendall Test results for heat waves intensity for 2020-2045 timeframe.

Model/Scenario	**RCP2.6**		**RCP4.5**		**RCP8.5**	
	Trend	**T.S.**	**Trend**	**T.S.**	**Trend**	**T.S.**
HadGEM2-ES_RACMO22E	Increase	0.09	Increase	0.11	Increase	0.08
MPI-ESM-LR_REMO2009	Increase	0.10	Increase	0.21	Increase	0.20
EC-EARTH_CCLM4-8-17	Increase	0.07	Increase	0.07	Increase	0.05
EC-EARTH_RACMO22E	Increase	0.08	No Change	0.00	Increase	0.12
EC-EARTH_RCA4	Increase	0.16	Increase	0.11	No Change	0.19

3.6 Test Reference Year projection

As already stated in Section 2.5.1, the Test Reference Year is a valuable way to compactly represent climate for a location, and it is also the main source of climatic data for the softwares that carry on the energy simulation of building-plant systems. Therefore, if building simulation has to consider also incoming evolutions of climate, a TRY representing the future situation is needed to perform the analysis. In this section the process to obtain a TRY for future climatic data is reported.

Two main methods are commonly used to create future weather files: the first one combines climate projections with a weather generator to allow the creation of typical future weather years data. The second one applies a mathematical transformation, i.e. morphing, to the actual climatic data using climate change scenarios. Weather generators use algorithms that produce long time-series of climatic variables with statistical properties comparable to existing historical records. The morphing process instead uses high-resolution climatic data for a specific site and transforms them using the projections from a GCM or RCM. Another possible approach is to apply the Finkelstein-Schafer statistic, described in Section 2.5.2, to the projected data of the climatic models to generate future TRYs [89]; however, this approach tends to be more troublesome to implement. In this research the morphing process was used to project into the future the Test Reference Year for Trieste.

3.6.1 The Morphing process

The morphing process adjust the current climatic data through the method developed by Belcher et al. [90]: once having obtained high-quality climatic data for a specific location, they are morphed using the projections of a Global-Regional Circulation Model (GCM-RCM). The main benefit from using this method is that it maintains the consistency of the historic data. On the other hand, one of its limitations is that some climatic variables are produced individually and then the relationship between them in the projected data could not be the same as in the historic series [91]. Once having chosen the reference and future timeframes of the climate model to be considered, the first step is to compute the monthly mean values of the required climatic parameters for the selected model timeframes. Every observed hourly climatic variable (x_0) is then projected into the future (x) through one of the following operations:

- Shift;
- Linear stretch;
- Shift + Linear stretch.

The shift is used for variables for which an absolute monthly variation (Δx_m) to the mean between future and reference timeframes is computed from the climate model, as in the case of atmospheric pressure and relative humidity and is defined as:

$$x = x_0 + \Delta x_m \tag{3.2}$$

The linear stretch is used when the projections are obtained as a fractional monthly change between future and reference timeframe, as in the case of the solar radiation and wind speed. A scaling factor for the m-month, $\alpha_{x,m}$, is obtained through the following equation:

$$\alpha_{x,m} = 1 + \frac{\Delta x_m}{\overline{x}_{0,m}} \tag{3.3}$$

Where $\overline{x}_{0,m}$ is the monthly mean of the climatic parameter from the observed historic timeframe. The scaling factor is then applied to all the hourly data to be projected using the following equation:

$$x = \alpha_{x,m} \cdot x_0 \tag{3.4}$$

The combination of a shift and a linear stretch is used for variables where it is important to highlight changes in both mean, maximum and minimum daily values, as in the case of dry-bulb temperature. Therefore, in addition to the monthly variation to the mean Δx_m, also the monthly variation to the daily maximum, $\Delta x_{max,m}$, and the monthly variation to the daily minimum, $\Delta x_{min,m}$, are computed. The scaling factor, $\alpha_{x,m}$, is then obtained through the following equation:

$$\alpha_{x,m} = \frac{\Delta x_{max,m} - \Delta x_{min,m}}{\overline{x}_{0,max,m} - \overline{x}_{0,min,m}} \tag{3.5}$$

Where $\overline{x}_{0,max,m}$ and $\overline{x}_{0,min,m}$ are the monthly mean of the observed daily maximum and minimum values respectively. Afterwards, the projected parameter can be computed as:

$$x = x_0 + \Delta x_m + \alpha_{x,m} \cdot (x_0 - \overline{x}_{0,m}) \tag{3.6}$$

Where $\overline{x}_{0,m}$ is the monthly mean value for the m-month of the observed variable. In Figure 3.12 the workflow of the morphing process is reported.

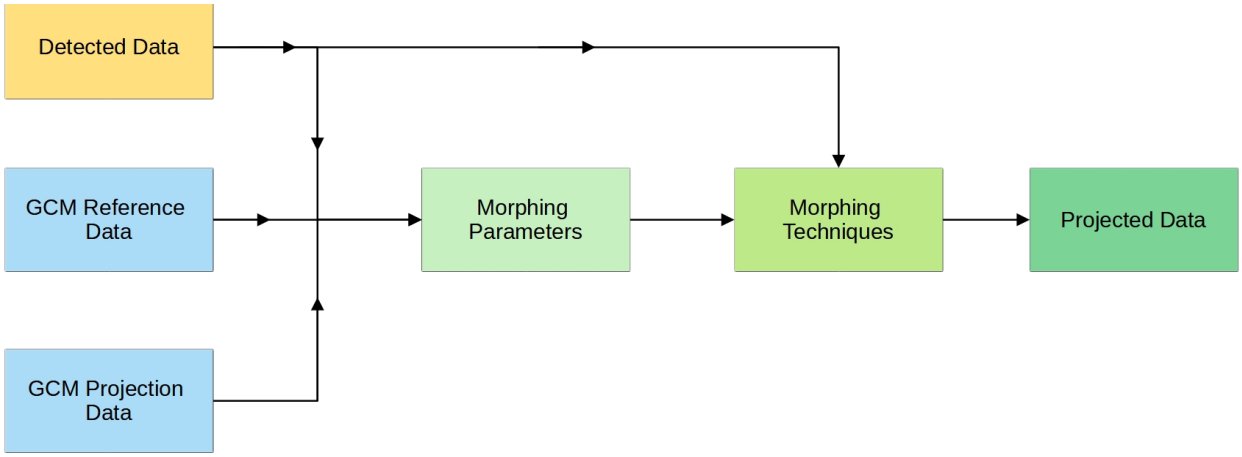

Figure 3.12: Morphing process workflow.

In order to assess the possible climatic evolutions, the models described above were used to project the current TRY for Trieste into the future. The five models referred to the RCP8.5 scenario were used as baseline to obtain the morphing parameters for all the considered climatic variables. The RCP8.5 scenario was chosen in order to reflect the actual situation where no relevant worldwide mitigation measures have been developed yet. In this work the chosen reference period for every climate model is 1995-2005. For the future two timeframes, 2021-2035 and 2036-2050, were chosen to further highlight the climatic evolution in the near term, therefore two different future TRYs were generated for every model disregarding the long-term projection for this case study. This choice has been done to better focus on the timeframe considered by the SECAPs projects, centered on the first half of the century. Table 3.7 summarizes how the climatic parameters of the future TRYs were obtained.

Table 3.7: Methods used to obtain future TRY climatic parameters.

Climatic parameter	**Methodology**
Dry-bulb temperature	Shift + Linear stretch
Relative humidity	Shift
Dew-point temperature	Recalculated from morphed dry-bulb temperature and morphed relative humidity
Atmospheric pressure	Shift
Global radiation	Stretch
Direct radiation	Recalculated from morphed global radiation using split methods
Diffuse radiation	Recalculated from morphed global and recomputed direct radiation
Wind speed	Stretch

3.6.2 Results for Trieste case study

A quick method to evaluate the overall behavior of a Test Reference Year is to compute its Degree Days. These are measures of how cold or warm a location is. A Degree Day compares the mean outdoor temperatures recorded for a location to a standard one. The more extreme the outside temperature, the higher the number of Degree Days. A greater value of Degree Days generally results in higher levels of energy use for space heating or cooling. In this case the Heating (HDD) and Cooling (CDD)

Degree Days were computed for all the TRYs generated for Trieste, using a reference temperature of 20 °C. The results are reported in Figure 3.13.

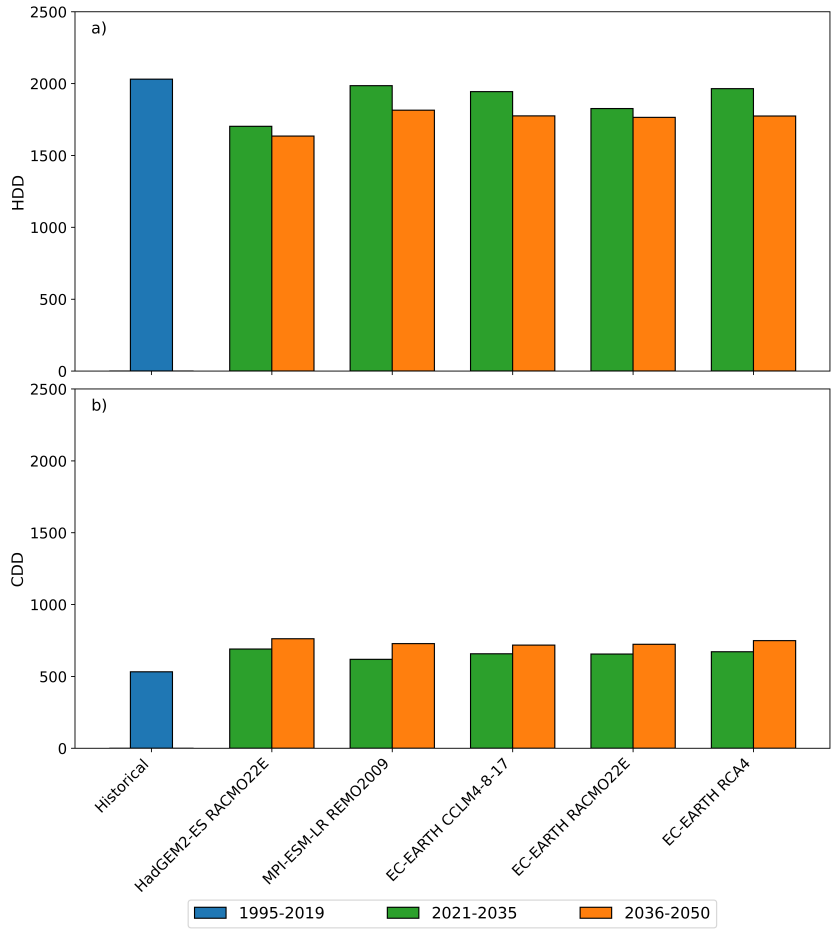

Figure 3.13: Heating (a) and Cooling (b) Degree Days of the historical and projected TRYs for Trieste.

As it can be seen the TRY referring to the historical timeframe, 1995-2019, proved to be the coldest among all, as expected. In fact, it had the highest amount of HDD and the lowest of CDD. Regarding the future TRYs generated through the five circulation models the Degree Days values are reported for the two future timeframes previously described, 2021-2035 and 2036-2050. As it can be seen in Figure 3.13, in all the projections the temperature will rise, leading to lower values of HDD and higher ones of CDD. An interesting feature is that the increase in temperature will not be constant in time, being greater in the first period, 2021-2035, for some models and in the second one, 2036-2050, for others.

Finally, it can be seen that the TRY generated through HadGEM2-ES_RACMO22E model is the hottest among all for all timeframes, while the one created using the MPI-ESM-LR_REMO2009 model proved to be the coldest among the projected TRYs.

In Figures 3.14 and 3.15 the mean daily patterns for dry-bulb temperature for all months are reported using data from the original TRY, the hottest and coldest future ones, considered for both the future timeframes defined before. As already stated, the overall climate will be warmer in the future however, the pattern will not be constant across the months and the timeframes considered in the analysis. In fact, through the inspection of Figures 3.14 and 3.15, different behaviors can be highlighted.

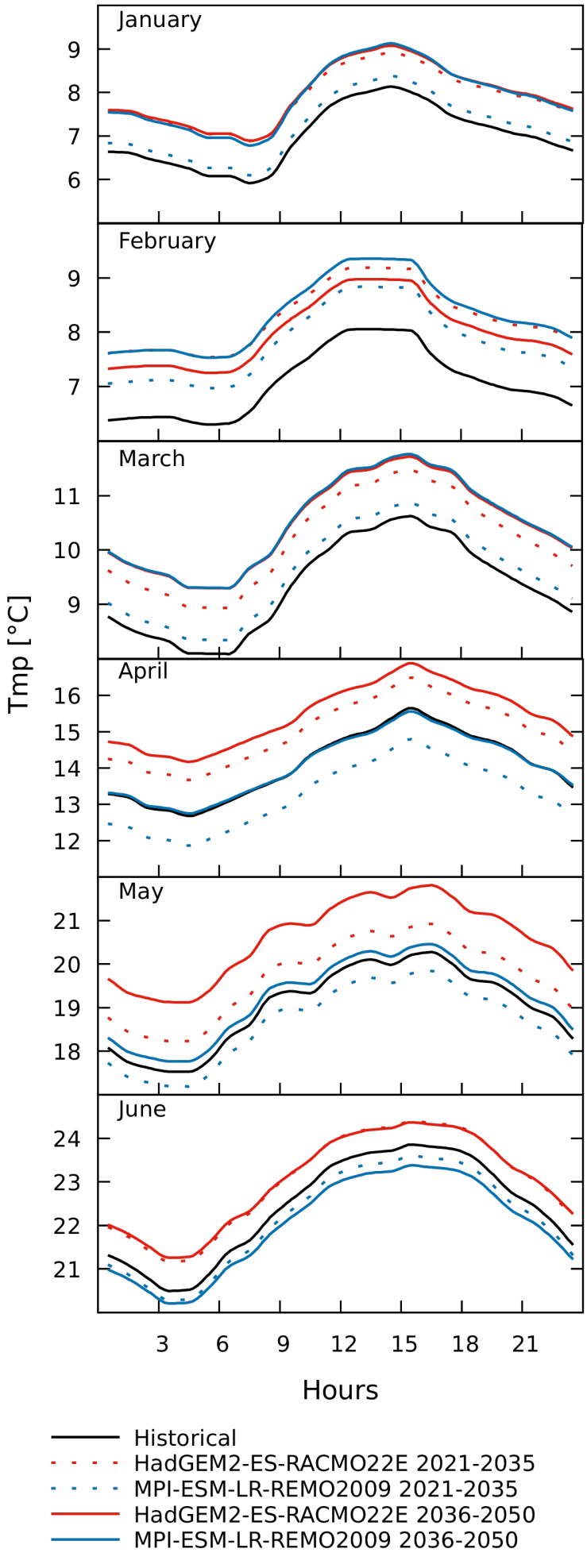

Figure 3.14: Historical, hottest and coldest future TRYs mean daily temperature patterns for January - June months.

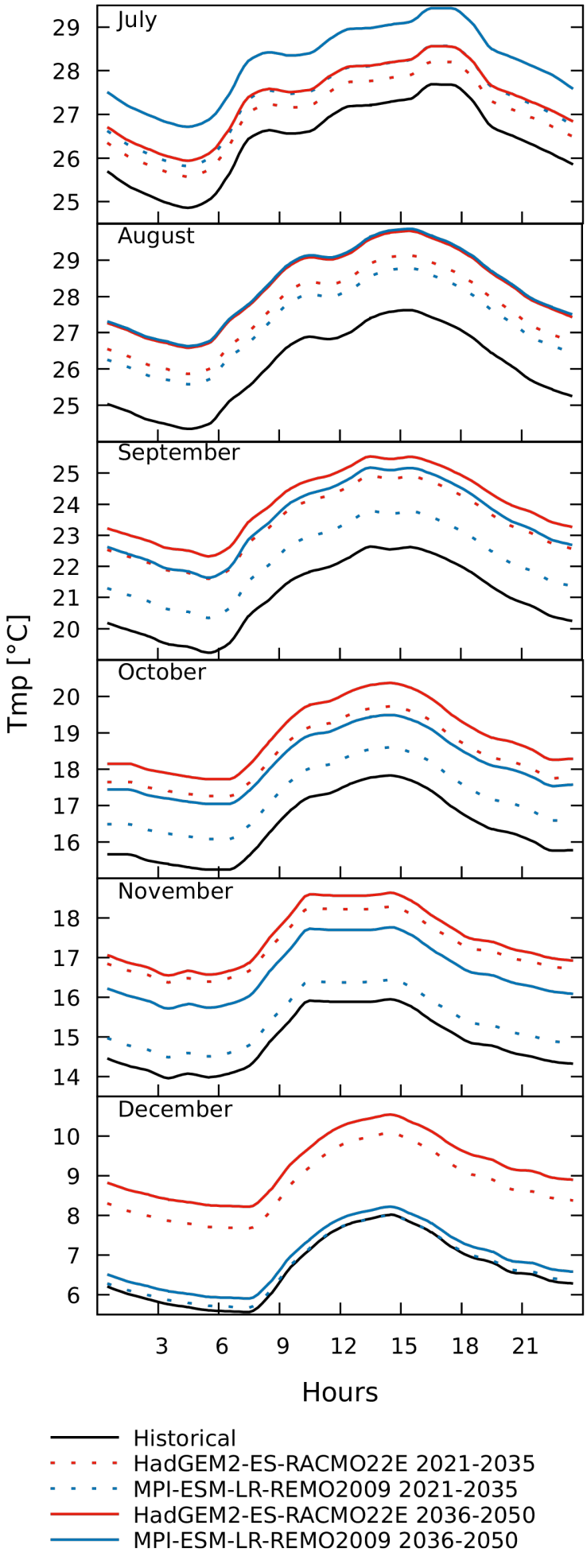

Figure 3.15: Historical, hottest and coldest future TRYs mean daily temperature patterns for July - December months.

First of all, as already highlighted through the analysis of the Degree Days, the temperature rise will not be constant in time. The case analyzed in Figure 3.14 and 3.15, shows that the temperature increase will be greater in the first period for HadGEM2-ES_RACMO22E, slowing down in the second one; an opposite behavior is instead highlighted for MPI-ESM-LR_REMO2009 model. This can be noted by comparing the patterns of the future TRYs for 2021-2035 period (dotted lines), where the values for HadGEM2-ES_RACMO22E model are always higher than the MPI-ESM-LR_REMO2009 ones, with the exception of July month. By comparing the 2036-2050 values it can be immediatly noted that the gap between the two models nearly always decreases, and in some months it is even canceled.

Another interesting feature is that sometimes the temperature computed for the two timeframes is nearly coincident, thus locating all its variations in the first period analyzed. Sometimes it even decreases in the second timeframe, like in February and June months for HadGEM2-ES_RACMO22E and MPI-ESM-LR_REMO2009 models respectively.

Moreover, the MPI-ESM-LR_REMO2009 model forecast a decrease of temperature for the period from April to June for 2021-2035 period and a slight to no increase for 2036-2050 timeframe, thus highlighting a discontinuous trend across the year.

Finally, the variations between the historical and projected TRYs are more evident in the second part of the year, where the forecasts always give higher temperatures than in the historical case, while in the first part of the year the projections tend to stick more to the measured data.

3.6.3 Approach limitations and future improvements

The approach here described presents some important limitations. First of all the projections are carried on by exploiting the morphing process, characterized by the issues described in Section 3.6.1; moreover the climatic data are projected only until 2050, disregarding the second half of the century. Finally the intrinsic nature of the TRY leads to a representation of the mean behavior of climate, leaving out the analysis of its possible extremes.

Further improvements for this method will then focus on resolving these issues; other projection methods will be used and their results will be compared to assess the quality of the various methods to project climatic data into the future. Moreover the projections will be extended to year 2100 and for more locations included in the Interreg ITA-SLO Secap Project program area. Finally the approach developed by Nik et al. [58, 59] will be exploited to create different TRYs, representative of the mean and extremes behaviors of climate for the analyzed periods.

Chapter 4

Analysis of buildings internal insulation system performance

4.1 Problem definition

Within the SECAP projects a fundamental practice to carry on when developing climate adaptation and mitigation measures is the improvement of the building stock energy performance. Regarding this, the municipalities developing their SECAPs normally focus on the building stock of their own property, as it was found in the work of Palermo et al. [92], where they analyzed the plans of 315 signatories of the Covenant of Mayors classifying their policies according to the fields of action. They highlighted that the municipalities mostly concentrate their efforts on their own building sector, accounting for a remarkable 46 % of the total of implemented policies. In fact this is the sector where they can intervene through a more systematic approach, having a full knowledge and control of their own buildings and equipment. Therefore, they can directly implement measures and monitor the results accurately; all without having to involve private actors in the process. This process can be carried out by refurbishing old buildings or by replacing them with new ones. In the second case, where new buildings are involved, the fabric and system plants can be accordingly designed, also exploiting renewable energy resources. The approach is quite more difficult for existing buildings where the interventions can be limited by technical reasons and national regulations. However, because of the building stocks owned by the municipalities being predominantly composed by historical buildings, the focus is often placed on this category.

As stated before, for existing buildings the design choice among the available interventions is usually restricted because of the working boundary conditions. This is the case, for example, of buildings where plant and envelope modifications are troublesome because they conflict with the bearing structure. Another major issue could emerge when dealing with the refurbishment of historical or old buildings featuring particular facades, where attention is required as described in a guideline by De Santoli [93]. In fact is often impossible to modify the facades due to the national regulations usually imposed for the preservation of fine arts. Sometimes this also applies to the substitution of windows, thus limiting the possible interventions on a great part of the envelope.

This last case is very common for Italian municipalities, characterized by a huge number of historical buildings within their stocks, thus leading to major issues when tackling refurbishment practices. Due to the impossibility of using external insulations, often prohibited by regulations, the internal ones assume great relevance in this context, despite being characterized by some criticalities. The main issues regard the possibility of mold formation at the interface between the insulating panels and the structural layer of the wall and the loss of livable space due to the presence of the additional internal insulating layer.

Given the wide applicability of this refurbishment practice in Italy, it should be carefully analyzed how reliable this intervention could be, that is, to assess whether the characteristics shown in the technical data sheets are correct or if they provide values that do not properly reflect the real performance of this

technology. In fact, a common mistake about the thermal losses computation in buildings refurbished through internal insulating systems is to evaluate the envelope thermal resistance omitting the effect of the structural studs used to build the insulating structure, as described in [94] for light steel frame structures. This aspect is of particular importance because if a discrepancy between design and real values is present, the performance of the real refurbished building could be very different from the design one, therefore leading to major energy consumption and economic losses.

4.2 Literary review

Being the internal insulation of walls one of the main refurbishment practice, an extensive literature has been developed about this topic, often focusing on the possibility of increasing the thermal properties of the solution through the insertion of low emissivity sheets. In fact, in many cases, this insulation system presents air gaps, therefore one way to increase its thermal performance is to reduce the radiative heat exchange in the air cavity by applying low-e thin layers to one or both air gap surfaces.

A laboratory setup conducted by Johansson et al. [95] demonstrated the suitability of Vacuum Insulation Panels applications. They analyzed four brick and six mortar wall typologies by using numerical simulations. Moreover, they tested the material impact in a climatic chamber comparing wall performances with and without interior Vacuum Insulation Panels, they measured relative humidity in thermal bridges and performed hygro-thermal numerical simulation and measurements. The results showed that interior insulation significantly reduced the wall temperature, while increasing its thermal resistance of a range between 60% and 100%, but causing at the same time condensing phenomena.

Eben Saleh [96] used the NBSLD numerical tool to investigate the effect of different insulation configurations on the daily cooling and heating demand of a typical 125 m^2 residence in Saudi Arabia. In all the 10 different wall configurations studied, the external insulation of walls was found to outperform the internal insulation configuration. However it was also noticed that, during the summer period, thermal comfort conditions could be achieved faster using the internal insulating systems.

Galatioto et al. [97] reviewed some technologies for retrofitting historical buildings emphasizing the difficulties in adopting renewable energy sources in historical city centers and the particular attention required to preserve the cultural heritage.

Ibrahim et al. [98] demonstrated, through a numerical simulation, the correlation between different insulation thicknesses and surfaces emissivity in determining the energy savings in a building, highlighting that with high levels of insulation the influence of surfaces emissivities becomes nearly negligible.

Saber [99] conducted a parametric study to investigate the effects of inclination angle, foil emissivity and heat flow direction for an isolated air cavity inside a shell structure. He evidenced that by decreasing the foil emissivity from 0.90 to 0.05 in a horizontal building component with downward heat flow, representative of a typical summer season roof case, the structure's thermal resistance, R, increased by 26.10%. Considering the same solution with an upward heat flow, i.e. winter season roof case, the R-value increased by 8.90%. Instead, with an inclination of 30°, the decrease in emissivity led to a R-value increment of 17.65% and 10.50% for downward and upward heat flux respectively.

Despite the great amount of studies dealing with walls internal insulation systems, no extensive information is available in literature about the overestimation of the thermal performance of the internal insulation packages applied to massive constructions. As already stated, this issue happens because the presence of the structural steel studs is neglected when computing the thermal performance of the structure, despite the possibility of them leading to the formation of thermal bridges. However, this problem is well known in light frame and light steel frame constructions. Kosny et al. [100] numerically analyzed various metal frame walls configurations highlighting the difference between clear

wall and frame R-values. In another study, De Angelis et al. [101] displayed the necessity of using numerical methods to obtain the correct U-value of light frame walls and discouraged the application of simplified calculation methods. Another work [102] explained the problem related to heat exchange in such structures and how thermal bridges created by metal studs affect the whole system.

Regarding massive constructions, Manzan et al. [103] studied the effect of structural elements with internal compact insulation without air gaps. They used simplified methods to compute the overall conductance of the insulated wall; the results showed that the conductance of the system was 6.60% higher for wooden studs and 32.80% higher for metal studs if compared with the clear wall values.

In another work [104] the metal studs case was studied by using numerical techniques, highlighting the influence of the steel studs on the total performance of an internal insulation wall package. It was proved that the correct evaluation of the whole insulation system displayed a mean conductance 20% higher than the one computed using the one-dimensional clear wall values.

4.3 Analysis scope

Energy refurbishment of buildings is one of the most important mitigation and adaptation measures to tackle climate change and in Italy one of the most widely applicable interventions to improve buildings thermal performance is the application of internal insulating packages. Because of the importance of this insulation technique for the Italian municipalities drafting their SECAPs, in this research an impact assessment of steel studs presence inside the air cavities on the overall system performance is carried on for internally insulated massive structures with variable insulating thicknesses.

Moreover, because of the extended presence of solutions including low emissivity layers applied to the air gaps of the insulation package, the combined effect of steel studs and surfaces with low values of emissivity have been studied.

This study aims to give the municipalities a clue on how to assess the real performances of the insulating techniques used in their refurbishment plans of their building stock, also highlighting the errors that could emerge by taking for granted the performances described in the producers data sheets. It has also to be pointed out that this analysis focuses on the assessment of the discrepancies between the real performance of the package and the one declared in the technical data sheets. Therefore the analysis are carried on in a stationary condition, with fixed boundary conditions, not considering the real climate in which the package will operate in the reality.

4.4 Numerical simulation

In order to assess the effect of the steel studs within a range of possible thicknesses of the insulating layer and their interaction with surfaces having different emissivity, a 3D model has been created to accurately represent the heat transfer phenomenon. The model was developed using ANSYS Fluent, a software that employs a finite volume discretization and has the ability to consider the coupled effects of radiative and convective heat transfer.

4.4.1 Model geometry

For what concerns the geometry of the numerical model, the dimensions have been resumed from the work previously developed by Manzan et al. [103, 104], in which experimental tests have been conducted at Edilmaster building school in Trieste where, inside a controlled laboratory, a reproduction of a typical massive wall used in historical buildings was realized. The structure was provided with an internal insulation system to replicate a refurbishment activity on an existing building. The setup was composed by two cells maintained at constant different temperatures separated by the studied wall. Electrical resistances warmed up the hot chamber, while a refrigerator unit cooled down the other one. This research started from the aforementioned work in order to continue the study on such

topic through a unique and continuous workflow [105].

The test cell was 4.70 m long, 2.24 m wide and 2.20 m tall; the tested wall had dimensions of (1.90 x 1.93) m for a total area of 3.67 m^2. The specimen consisted in a massive brick wall 51 cm thick with plaster layers on each side. The internal insulation system was composed by an insulating layer and an air gap both 3 cm thick, and 1.25 cm of plasterboard panels as reported in Figure 4.1a. To fix the plasterboard panels to the wall, vertical C-shaped 0.60 mm thick steel studs were placed at a distance of 56 cm between each other as presented in Figure 4.1. The C-shaped (6 x 3) cm metal studs were fixed in place by two metal clamps, 6 cm wide each, fixed to the underneath wall. The stiffness of the structure was obtained through U-shaped (3 x 3) cm metal profiles located at the top and bottom of the tested wall as it can be seen in Figure 4.1b.

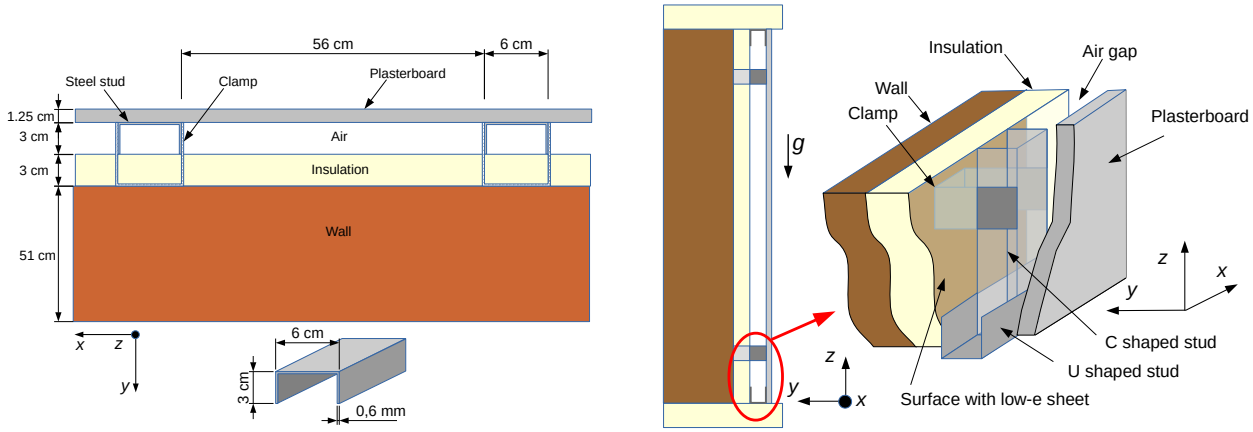

(a) *Layer composition.* (b) *Fixing system detail.*

Figure 4.1: Experimental test characteristics.

Starting from the experimental study dimensions and setup, the geometry for the 3D model was developed. Compared to the sperimental case, the geometry was simplified and modeled as reported in Figure 4.2 in order to speed up the calculation process. This led to the representation of a symmetric portion of the wall considering a width of 1.24 m. 2D thin layers have been used to model the horizontal and vertical metal studs, having a thickness of 0.6 mm, in order to effectively consider the heat conduction. This option allows Fluent to compute heat transfer through these components without generating a true 3D geometry for elements with excessively low thickness. In this way were modeled all the horizontal U-shaped, the vertical C-shaped steel studs present in the air cavity and the clamps that intersect the insulating layer all the way to the brick wall. The insulated structure, from cold to hot side, is composed by the following layers:

- Bricks - 0.51 m;
- Insulation - 0.03-0.08 m;
- Air cavity - 0.03 m;
- Plasterboard - 0.0125 m.

The characteristics of the materials used in the model are reported in Table 4.1.

4.4.2 Numerical model

In the numerical model great attention was posed on the definition of the calculation mesh inside the air cavities formed by the steel studs due to the presence of convective effects caused by the temperature differences. Moreover, Navier-Stokes equations were used in the computation of these spaces and, to properly consider the buoyancy-driven nature of air, the Boussinesq approximation was

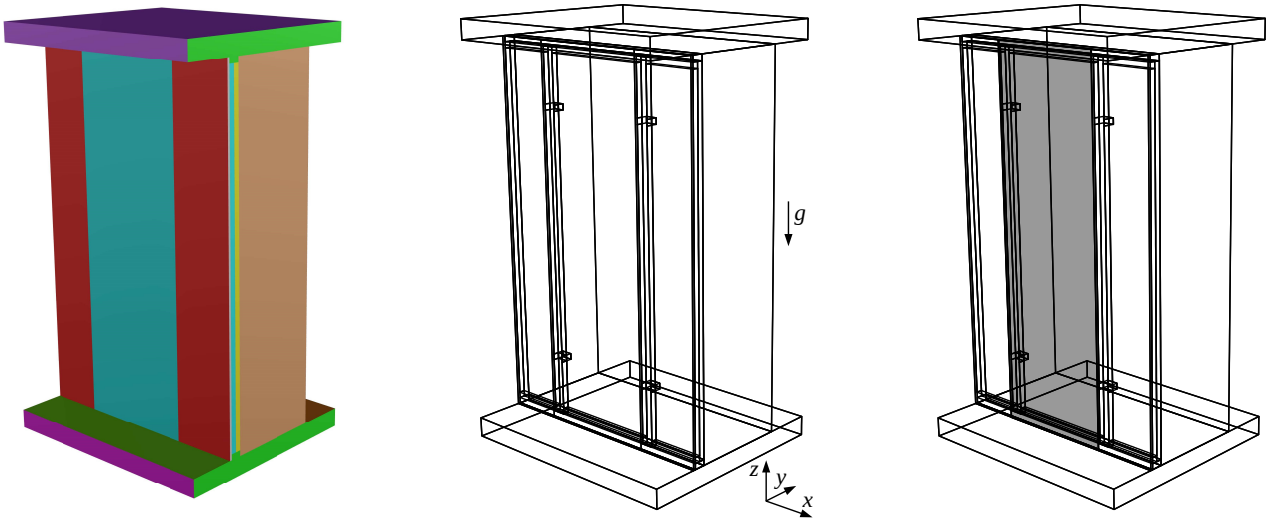

(a) *Model geometry.* (b) *Steel studs positions.* (c) *Plasterboard surface used to compute average output values.*

Figure 4.2: Numerical model characteristics.

Table 4.1: Model material properties.

Material	**Density** [**kg/m^3**]	**Specific heat** [**J/(kg K)**]	**Conductivity** [**W/(m K)**]
Air	1.225	1006.43	0.0242
Brick	1200	840	0.8329
Insulation	30	1450	0.035
Plasterboard	700	1000	0.2
Steel	7800	500	50

used to compute air density inside the cavities. Instead in solid domains steady state energy equations were solved. The simulation was carried on in a steady state condition.
To obtain computation convergence and reliable results, residuals limits of 10^{-5} were set for continuity equation, radiation model and fluid velocity in all directions, while a limit of 10^{-10} was set for the energy equation.

In order to consider the radiative heat transfer process occurring in the air cavities the Surface to Surface (S2S) calculation model was set up in Fluent. This model calculates the radiative heat transfer between the cavity surfaces depending on their size, separation distance, orientation and emissivity. The geometrical part of the model was considered automatically by Fluent through the calculation of the view factors between the surfaces interested by the radiative heat transfer. The emissivity of stud and clamp metal surfaces was set at $\epsilon_{st} = 0.23$ and the plasterboard one at $\epsilon_{pl} = 0.95$. The emissivity of the insulation panel surface facing the air cavity was set at $\epsilon_{ins} = 0.95$ for not treated case and $\epsilon_{ins} = 0.10$ when coated with low-e sheets. The boundary conditions and surface emissivities are reported in Figure 4.3.

As already stated, in order to reduce the computational time, the geometry of the model was simplified. Therefore, only a periodic portion of the wall has been modeled through the use of symmetry boundary conditions applied to the lateral surfaces, showed with dashed lines in Figure 4.3. However, the S2S model does not perform correctly alongside symmetry conditions, since near the boundary the radiative contribution of the not modeled surfaces outside the boundary itself is lost. However, thanks to the reduced thickness of the air cavity, the effect is restricted to a strip located near the lateral open

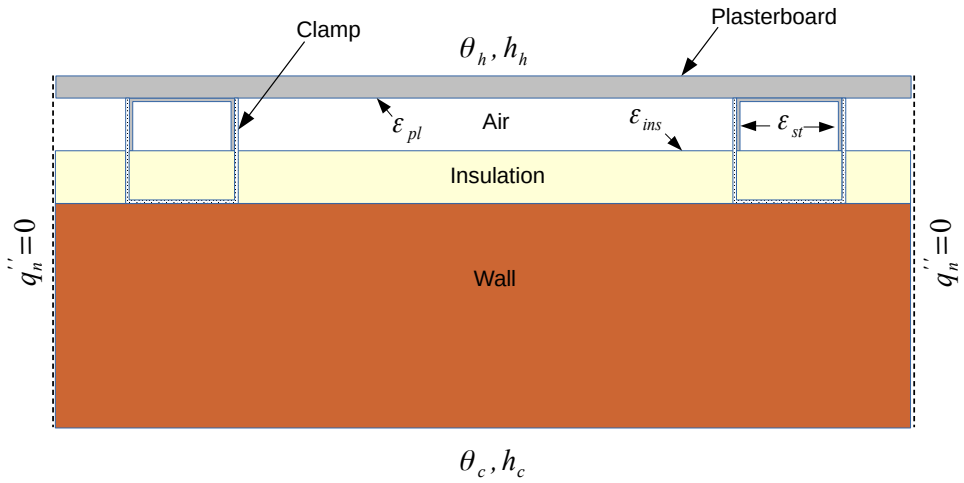

Figure 4.3: Numerical model boundary conditions.

boundary. Because of this issue, two vertical studs were inserted in the model to accurately consider the radiative heat exchange in the central portion of the geometry. Therefore, only the central part of the model, delimited by the two vertical studs, and highlighted in Figure 4.2c, is considered to compute the thermal behavior of the wall.

The presence of hot and cold chambers on the two sides of the wall was modeled through a convective heat transfer wall boundary condition applied to the surfaces as shown in Figure 4.3 . Regarding the hot chamber a temperature of $\theta_h = 26$ °C with a convective heat transfer coefficient of $h_h = 8.546$ $W/(m^2K)$ was chosen. Regarding the cold side instead, it was modeled with a temperature of $\theta_c = 5.01$ °C and convective heat transfer coefficient of $h_c = 14.06$ $W/(m^2K)$. The heat transfer coefficients have been computed using the experimental data obtained by Manzan et al. [103] for temperature and specific heat flux at the center of the insulation board where one dimensional heat flux is expected to occur.

4.4.3 Numerical analysis

In order to assess the reliability of the 3D model, a simplified geometry having 3 cm of insulation without steel studs was first created. This model allowed a direct comparison with the conductance C_{ISO} computable through the procedure reported in the EN ISO 6946:2018 standard [106]. This procedure consisted in an iterative calculation used to evaluate the thermal resistance of an air cavity with various emissivity values and homogeneous stratigraphy. The method proposed by the standard is considered to be very reliable however, as stated by Escudero et al. [107], great attention has to be set on the determination of surfaces emissivity. Escudero considered an emissivity varying from 0.03 to 0.30 for low-e surfaces to determine air cavity thermal resistance and found that little changes of emissivity led to considerable variations of the thermal resistance; this effect also became more important when increasing the air gap thickness.

Calculations conducted through the EN ISO method led to a conductance of the simplified version of the wall of 0.5902 $W/(m^2K)$ for normal emissivity surfaces and of 0.4540 $W/(m^2K)$ for low-e solution. At the same time, the Fluent model of this version of the wall led to conductance values of 0.5320 $W/(m^2K)$ and 0.4467 $W/(m^2K)$ for normal and low-e solutions respectively. It can be noted that the results are quite similar, therefore assessing the reliability of the Fluent model for a homogeneous stratigraphy of the wall system.

To accurately evaluate the combined effects of the steel studs and of air cavity surfaces emissivity variation, different analysis were carried on. In order to generalize the results, configurations with insulating layer thickness varying between 3 and 8 cm with 1 cm steps were considered. For each insulating panel thickness, simulations were carried on considering first high emissivity surfaces only,

i.e. Case 1, and then the configuration with a low-e surface on the insulation panel side of the air cavity, i.e. Case 2. This led to a total of 12 different simulations.

4.5 Results

To properly evaluate the performance of the internal insulation of the wall, the main parameter considered in the results was the conductance calculated in three significant points through Equation 4.1, where q is the heat flux in W/m^2 , θ_h and θ_c are the hot and cold chamber temperatures, h_h and h_c are the hot and cold convective coefficients in $W/(m^2K)$:.

$$C = \left[\left(\frac{q}{\theta_h - \theta_c} \right)^{-1} - \frac{1}{h_h} - \frac{1}{h_c} \right]^{-1} \tag{4.1}$$

The analyzed points are the center of the plasterboard where the steel studs effect is nearly negligible, the center of one of the steel studs themselves, and where the stud connects with the clamp. These three points were chosen to highlight the variation of the conductance along the geometry of the analyzed system. However, the most important output to be analyzed is the difference between the conductance computed through standard formulas, as happens in the technical data sheets provided by the producers of the insulating packages, and the numerical conductance weighted on the domain surface highlighted in Figure 4.2c, including the central part of the plasterboard and one of the steel studs. The analysis performed in this way allowed then to evaluate the difference between the declared values used on the market, which neglect the effect of metal studs, and the correct one that instead considers all the components of the internal insulation system.

Table 4.2 reports the Fluent simulations results for Case 1 and Case 2 with insulating layer thickness, s_{ins}, varying from 3 to 8 cm. The presented values were detected at mid-height of the plasterboard, but in the three different locations described before. In the middle of the plasterboard C_{CW}, identified as a clear wall position, in correspondence of the steel stud C_{st}, and at the connection between the steel stud and the clamp that fixes it to the brick layer C_{cl}.

Table 4.2: Conductance numerical results.

	$\mathbf{C_{cl}}$ [$\mathbf{W/(m^2K)}$]		$\mathbf{C_{st}}$ [$\mathbf{W/(m^2K)}$]		$\mathbf{C_{CW}}$ [$\mathbf{W/(m^2K)}$]	
$\mathbf{s_{ins}}$[cm]	**Case 1**	**Case 2**	**Case 1**	**Case 2**	**Case 1**	**Case 2**
3	1.01	0.97	0.60	0.65	0.57	0.40
4	0.93	0.90	0.51	0.57	0.49	0.35
5	0.86	0.86	0.45	0.52	0.42	0.32
6	0.79	0.79	0.40	0.47	0.37	0.29
7	0.73	0.74	0.36	0.44	0.34	0.27
8	0.69	0.71	0.34	0.47	0.31	0.25

As expected the highest conductance value is detected at the connection between the clamps and the studs, while the lowest on the plasterboard, having an intermediate value on the mid-height point of the steel stud. It can also be highlighted that, as expected, increasing the thickness of the insulation led to an overall reduction of the conductance values.

The inspection of Table 4.2 reveals also that the conductance at clamp position does not significantly change between Case 1 and Case 2. The presence of values higher than the clear wall case can be justified by the presence of a point thermal bridge going from the plasterboard to the underneath cold wall by means of conductance heat transfer along the clamps. Different results are obtained for the conductance computed in correspondence of the vertical studs: Case 1 C_{st} values are always lower than the ones obtained for Case 2, and it is interesting to note how the difference raises with increased insulation layer thickness. As a consequence, it is important to account for the tendency of the conductance to increase in stud, C_{st}, and stud-clamp, C_{cl}, positions when lowering the emissivity

of the insulating surface of the air cavity.

In Figure 4.4 conductance trends are reported along the z-axis of the model. The main characteristic noted is that the trends show disturbances in correspondence of the horizontal studs for both plasterboard and steel stud distributions and at the clamps positions only for the latters. Moreover, it can be noted that the clamps presence has a way greater influence on the system than the horizontal U-shaped supporting frames. This because the clamps create a thermal bridge all the way to the underneath wall, while the horizontal U-shaped studs behave like linear thermal bridges only up to the internal insulation panel surface.

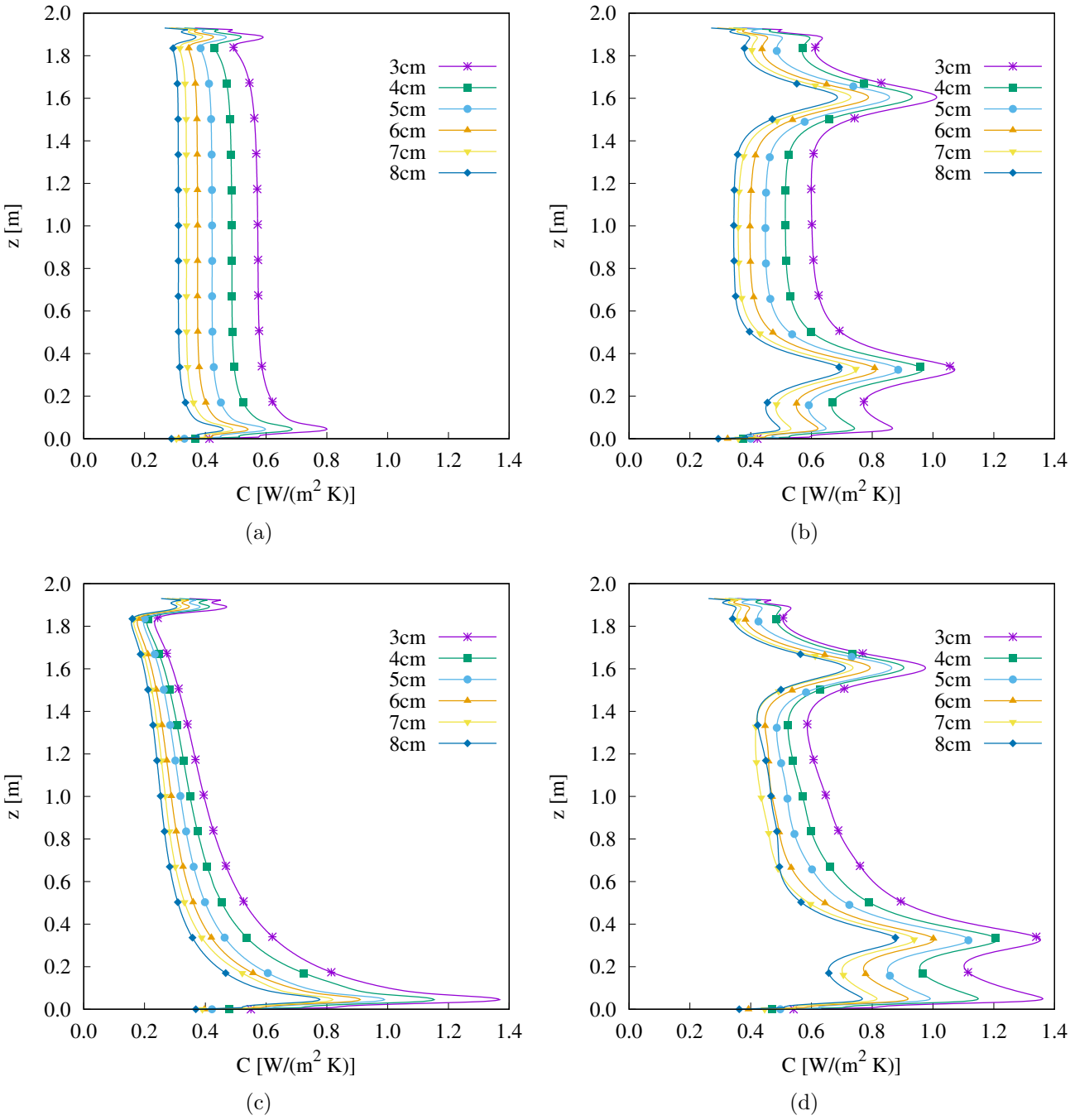

Figure 4.4: Conductance trend along z-axis. On the center of the plasterboard for Case 1 (a) and Case 2 (c) and in correspondence of the stud for Case 1 (b) and Case 2 (d).

The inspection of Figure 4.4 highlights that the presence of low emissivity surfaces increases the disturbance caused by studs and clamps. The high emissivity case shows a more uniform distribution, while in the low-e one it appears tilted, suggesting a different behavior of heat transfer inside the cavity for standard and low-e cases.

Conductance vertical distribution reported in Figure 4.4 suggests the convection phenomenon to be stronger in Case 2 than in Case 1. It is expected that temperature difference between air gap surfaces, i.e. the hot one formed by the plasterboard and the cold one by the insulation panel, generates a circulation flow inside the air gap typical of differentially heated cavities where, the higher the temperature difference, the stronger the air circulation that is generated.

All these results highlight the requirement to include the studs effect in the computation of the overall insulation package performance and the possibility of errors when this effect is discarded using clear wall values only.

The numerical computation of the heat flux through the surface highlighted in Figure 4.2c allows the definition of an average conductance of the wall, C_{AVG}, which correctly considers the presence of the metal studs. Therefore, a result to account for is the comparison between the values obtained applying the international standard method [106] in computing the conductance, C_{ISO}, and the ones obtained considering the average value, C_{AVG}. To evaluate the difference between the results, the error respect the international standard value is introduced with Equation 4.2.

$$E_{ISO} = \frac{C_{ISO} - C_{AVG}}{C_{ISO}} \cdot 100 \tag{4.2}$$

All these outputs are reported in Table 4.3, where the influence of both the steel studs, the surfaces emissivity and their interaction can be appreciated. With normal values of emissivity, i.e. Case 1, the error that occurs disregarding the effect of the steel studs varies in a range between $\approx 0.20\%$ and $\approx 4.00\%$ showing an increasing trend with the insulation thickness.

Considering instead the low-e solution, the error grows consistently reaching a value between $\approx 8.00\%$ and $\approx 16.00\%$. A common behavior is evident: the more the system is insulated, regardless of the insulation method, the more the influence of the steel studs becomes evident and influential.

Table 4.3: Comparison between standard and average numerical conductance values.

	Case 1			**Case 2**		
$\mathbf{s_{ins}}$**[cm]**	$\mathbf{C_{ISO}}$ **[W/(m²K)]**	$\mathbf{C_{AVG}}$	$\mathbf{E_{ISO}}$ **[%]**	$\mathbf{C_{ISO}}$ **[W/(m²K)]**	$\mathbf{C_{AVG}}$	$\mathbf{E_{ISO}}$ **[%]**
3	0.590	0.591	0.23	0.473	0.511	7.97
4	0.505	0.508	0.56	0.414	0.450	8.72
5	0.441	0.443	0.41	0.369	0.403	9.17
6	0.392	0.397	1.22	0.332	0.367	10.61
7	0.353	0.359	1.72	0.302	0.341	12.98
8	0.320	0.333	4.10	0.278	0.322	15.77

However, differences also occur between the results obtained from a numerical computation of a clear wall for the simplified geometry and the average ones, therefore Equation 4.3 presents the error between the average conductance C_{AVG} and the numerical computed clear wall value C_{CW}.

$$E_{CW} = \frac{C_{CW} - C_{AVG}}{C_{CW}} \cdot 100 \tag{4.3}$$

Table 4.4 reports the difference between clear wall and average values obtained using Fluent. This comparison has been done to highlight the different behavior of the two situations if both are computed through numerical simulation. In this manner some simplifications introduced by the standard to represent the heat transfer phenomena are bypassed.

Table 4.4: Comparison between clear wall numerical and average numerical conductance values.

	Case 1			Case 2		
s_{ins}[cm]	C_{CW} [W/(m^{2}K)]	C_{AVG}	E_{CW} [%]	C_{CW} [W/(m^{2}K)]	C_{AVG}	E_{CW} [%]
3	0.573	0.591	3.28	0.399	0.511	28.00
4	0.487	0.508	4.21	0.353	0.450	27.66
5	0.422	0.443	4.88	0.320	0.403	25.79
6	0.374	0.397	6.00	0.290	0.367	26.68
7	0.338	0.359	6.24	0.270	0.341	26.46
8	0.312	0.333	6.88	0.255	0.322	26.41

Results show that in this case differences between clear wall and average values are even greater, ranging from $\approx 3.20\%$ to $\approx 7.00\%$ for Case 1 and from $\approx 25.80\%$ to $\approx 28.00\%$ for Case 2. Table 4.4 inspection then shows that using a numerical method, but disregarding the presence of the steel studs, could lead to a performance evaluation error up to a remarkable 28%.

As a final remark some guidelines for designers can be drawn. In order to reduce heat losses into refurbished buildings internal insulation systems can be applied, but with carefulness. The formation of air gaps in the insulation structure isolates the metal studs from the cold underneath wall reducing the thermal bridge effect in fact, for high emissivity surfaces, the stud effect is rather low with a maximum value of 4.1%.

The adaption of low-e surfaces is a practical and economical way to increase the insulation effect. However, in this case the influence of metal structures cannot be disregarded since the error in computed conductance can be up to 28%. However, even if the effect of metal studs is taken into account, using low-e surfaces is beneficial in decreasing the overall conductance of the wall since the C_{AVG} values for Case 2 are always lower than the ones computed in Case 1 as reported in Tables 4.3 and 4.4.

4.6 Conclusions

The analysis here presented allowed to carry on the correct evaluation of internal insulation systems performances for building refurbishment. This system features an insulating layer positioned on the wall, an air gap, required to accommodate structural metal studs for supporting the finishing layer, and the plasterboard itself. Since the air gap in the structure contributes to the heat exchange with both convection and radiation heat transfer, two cases have been analyzed: the former with high emissivity surfaces and the latter with a low emission layer installed on the cold side of the gap. Different insulation layer thicknesses, ranging from 3 cm to 8 cm, have been analyzed.

A numerical model has been first validated using experimental results obtained using heat flow meter measures in a controlled setup, then used to evaluate the effect of low emission coatings in the air gap and the effect of the interaction of structural metal studs into the air gap layer. The results revealed that for the high emissivity case the impact of the metal studs is negligible, however the use of low emissivity coatings dramatically changes the panorama.

Although the use of low emissivity layers is beneficial, increasing the thermal resistance of the system for clear wall values, the interaction with the metal studs decreases the effectiveness. Taking into account the metal studs the overall thermal conductance shows an increase up to 28.00%. The results show that the use of clear wall values for evaluating the thermal resistance of an internal insulation system may lead to an overestimation of the energy savings for a refurbished building, especially if low emissivity layers are inserted in order to increase the overall thermal resistance.

It is then evident that in an environment like Italy, where this technology is widely exploited due to

the presence of many historical buildings, additional caution should be posed on the determination of the performance level of this insulation technique. Taking for granted the performance values exposed in the producers technical data sheets, without further analyzing the particularities of this technology before applying it to a refurbishment process, could lead to serious design mistakes, thus neglecting or reducing the beneficial effect of the refurbishment practice itself.

Chapter 5

Optimization of a building-plant system refurbishment

5.1 Problem definition

All the analysis described in the previous Chapters have been used for the simulation of a building-plant system, a cornerstone for the development of every adaptation and mitigation policy. Building-plant systems simulation is in fact essential to carry on evaluations about the current buildings energy consumption patterns, how they will change because of climate evolution and how to reduce them to more sustainable levels. It also allows to assess the current and possible future level of thermal comfort perceived by people when using the buildings, therefore giving a wider overview of the interactions between climate and human activities. They also allow to preview the effects of energy refurbishment practices and their results are also the base to perform cost evaluation procedures [108].

Energy simulation techniques are nowadays widespread: in fact, they are fundamental to carry on refurbishment practices on existing buildings or to design new ones. In the common practice these simulations are carried on by considering all parameters as deterministic, however in reality this is not correct. In fact no input parameter can be considered completely known and reliable about its value and behavior. As examples, energy price and investment costs could vary in time, reaching very different values from the ones considered during the design phase. Also material characteristics could be very different than expected. This is particularly true in existing buildings, where often the structural composition of the envelope is hypothesized, and therefore subject to errors and imprecisions. Other unpredictable parameters are the internal heat gains of buildings; these are considered during the design phase and commonly computed basing on predefined people behaviors, despite being very difficult to properly represent the true usage pattern of a building. Finally climate data, a fundamental input for energy analysis, is nearly always considered known, while it is evident that climate changes and can greatly influence the building-plant systems behavior.

All these input uncertainties lead to a great issue: the finished product could not met the fixed objectives or performances because it was designed assuming definite values of the input parameters, without considering their possible variations. This can lead to performances that greatly differs from the expected ones, thus causing unexpected consequences. In the particular case of building-plant systems this could lead to different energy consumption, CO_2 emissions, perceived thermal comfort, and, last but not least, economic performances.

It is then evident that, in order to obtain the best results, a classic approach to the problem is not advisable. Therefore the best method to take into account all the uncertainties influencing the design or retrofit of building-plant systems is the optimization under uncertainties process. In fact optimization models coupled with numerical simulation of buildings proved to be a valuable tool for predicting the behavior of the building taking into account uncertainties [109].

Optimization techniques are currently gaining importance in the engineering practice since they allow

to restrict the possible solutions of a design or a retrofit to an optimal subset, based on specified goals. When dealing with buildings refurbishment, one of the optimization goals usually takes into account the economic return of the intervention, driving the users to select solutions with a convenient trade-off between the energetic and economic perspectives [110].

Usually optimization techniques apply a deterministic approach, using fixed values for some parameters, while changing others during the optimization process. However, it is common to incur in situations where the parameters are not constant and can vary during the time, especially when analyzing the long building's lifetime. In order to consider this aspect into an optimization process, uncertainty in searching optimal designs should be added to the process. This is even more important when optimizing a refurbishment process, for which an investor requires not only a cost analysis, but also an evaluation of the economic risk intrinsic in each investment proposed. While in literature the sensitivity analysis of energy building simulation is a well established research field, the problem of the optimization under uncertainties has gained interest only recently.

A study by Cano et al. [109] applied a stochastic multi-staged optimization algorithm, highlighting the requirement to introduce stochastic variables for risk assessing and decision making.

Also the effect of boundary conditions can affect the results of an optimization. Lu et al. [111] performed an optimization taking into account the uncertainties of the parameters; however the uncertainty was not directly modeled into the optimization loop, but the authors performed a parametric analysis introducing uncertain quantities. An interesting results of this research was that, when the optmimization considered the uncertainties, in some cases it led to optimized solutions performing worse than the starting one.

Various authors pointed out the importance to analyze the effect of uncertain parameters in building simulation. Sun et al. [112] used a probabilistic method for risk assessment in computing the energy requirement and utility cost using a reference commercial building; they computed mean values and standard deviation to identify the risk associated with a project. Another work [113] carried on a stochastic assessment of buildings energy performance considering twelve different regions in Europe and identifying the factors wich more impacted on energy use. Prada [114] analyzed the material properties uncertainty propagation in energy simulations, emphasizing the issue of a correct assessment of physical properties in existing buildings in order to optimize energy refurbishment.

Other studies highlighted the effects of climate data on the optimization loop results for the refurbishment of a social house [115, 116], using as optimization objectives the overall energy consumption and the Net Present Value of the investment. Other researches worked on a sensitivity analysis to identify the main parameters affecting the Life Cycle Cost of a building [117], thus identifying financial factors, inflation, discount rate and energy trend uncertainty as the most influential parameters.

5.2 Analysis scope

In order to provide to the municipalities involved in the Interreg ITA-SLO Secap Project a case study to exploit when developing their mitigation and adaptation policies, an optimization of a refurbishment process for an existing builiding in Trieste was carried on. The aim of the research reported in this Chapter is to highlight the importance of considering all the uncertainties regarding the input parameters used in the classic building-plant analysis. In particular the influence of a stochastic variation of economic parameters in an optimization loop applied to the refurbishment of an existing social housing building is analyzed.

Moreover, in Italy the common habit is to focus on the winter energy performance of buildings, therefore many of the refurbishment interventions aim to heavily insulate the envelope to reduce heating energy usage [31]. The problem of such approach is that the summer performance is commonly disregarged in the analysis, therefore often leading to overheating problems in refurbished buildings [46, 47].

In this research this problem is studied by considering the effects of a winter-centered refurbishment intervention not only on heating energy usage and cost, but also on the indirect effect it could have on the summer performance of the building.

Finally, as stated before, the common practice is to compute the performances of the refurbished or designed buildings referring to the actual climatic data, without considering its possible future evolutions, likely leading to performances that greatly differ from the design phase ones. To highlight the issues that could emerge because of this practice, this research also investigates the effects of data uncertainty on the aforementioned optimization process, focusing on the effects produced by climate change.

5.3 Optimization under uncertainties

The optimization under uncertainties is becoming more and more acknowledged in the design practice; this because most of the human activities are characterized by uncertainties, especially when dealing with long-term projects and designs. Regarding building constructions for example, the manufactured product is generally different from the design one mainly because of assembly imperfections. Also in energy economics issues the parameters are not determinstc, but are characterized by some fluctuations that can change the problem outcome.

As already stated, input uncertainties are transferred to the performance of the system, which cannot therefore be determined with an exact and single value, but can be better described through a statistical distribution. Another frequent design objective is the compliance of constraints and/or limits, which normally should be obtained for a predefined percentage of the performance distribution. Another way to consider this condition is to compute what solutions percentage does not satisfy the limits, i.e. the failure probability, that must be minimized as much as possible to improve the reliability and quality of the product [118]. This approach can be extended to buildings energy optimization, where different solutions must be compared, and where the design parameters can variate with a statistical distribution.

In literature, two main types of optimizations exist for this kind of problems. The first is the Robust Design Optimization [118, 119], which consists in evaluating, for each candidate design proposed by the optimization algorithm, the stochastic distribution of its performances, and in defining objectives based on the mean and standard deviations of the same distribution. For instance, an objective could be the maximization of the mean performances and the minimization of their standard deviations, in order to optimize the results stability under input fluctuations. The strategy is particularly efficient, also because it can take advantage of the Polynomial Chaos Expansion [120], a methodology which exploits proper ortho-normal Polynomials to analytically estimate with high accuracy mean and standard deviation through a reduced number of sampling evaluations. However a limitation of this approach is that it normally requires to double the number of objectives for each performance criteria, having to optimize both the mean performance and to minimize its standard deviation, thus normally producing relevant computational efforts to solve the optimization problem.

The other main approach described in literature is the Reliability-Based Design Optimization, or RBDO, which implements methodologies like the first and second order reliability methods [121], which evaluate the failure probability of any candidate design on the basis of its uncertainties distribution and of the given limits to be respected. The negative side of this methodology is given by the high number of evaluations that may be required by the algorithm to compute the failure probability with accuracy, which often makes practically unfeasible its application to optimization problems of industrial relevance.

In this Chapter, a Reliability-Based Design Optimization (RBDO) approach is proposed. Therefore, the optimization results are obtained by integrating a genetic algorithm with a stochastic output deriving from stochastic inputs related to economic parameters. As a consequence the results are not

reported as a set of optimized solutions, but instead as solutions that can be obtained with a defined probability given the possible values of the stochastic inputs. In particular, the research focused on the refurbishment of an existing building considering also the economic impact of energy conservation measures.

However, since the RBDO presents the computational limitations previously described, in this research an alternative formulation of a reliability-based optimization problem is used, introducing a method which accomplishes good accuracy through a reduced number of evaluations. The methodology takes advantage of the Polynomial Chaos Expansion (PCE) regression model [120, 122], normally applied to robust design problems. The PCE is used to evaluate the complete cumulative distribution function of the performances of the design, from which it is possible to accurately retrieve the percentiles of designs not meeting the goal, i.e. the failure probability, for the predefined objectives/constraints. Through this approach it is possible, for each performance criterion, to define a single objective, i.e. the maximization/minimization of the percentile, instead of two, i.e. mean and standard deviation treatment.

5.3.1 Modeling stochastic parameters: the Polynomial Chaos Expansion

As already stated, in order to describe in a probabilistic way the response of a system subject to uncertainties, one of the most efficient methodologies that can be exploited is the non-intrusive Polynomial Chaos Expansion (PCE) [120]. Through the sampling of the uncertain input parameters accordingly to their probabilistic distribution the PCE regression model, described by Equation 5.1, allows to accurately compute the system performance probabilistic distribution Φ. This is a function of the input variables of the optimization problem, x, and of the distribution ξ of the uncertain variables θ.

$$\Phi(x,\theta) = \sum_{i=0}^{\infty} \phi_i(x) \cdot \psi_i(\xi(\theta)) \tag{5.1}$$

In Equation 5.1, the spectral expansion is given by the combination of the ψ_i Polynomials, function of the uncertain variables θ and which are orthogonal to their corresponding distribution function ξ. In the case of a Normal distribution, the Polynomials are called Hermite Polynomials. For practical reasons, the series is usually truncated to a finite number of terms, which is function of the Polynomial order considered and of the number of uncertain parameters analyzed.

The weight functions, ϕ_i are computed for each design proposed by the optimization algorithm (x being fixed), through the minimization of the Φ function regression error, computed by the sample points, and evaluated accordingly to the distribution ξ of the uncertain variables θ.

The accuracy of the regression model is usually evaluated by performance indexes like Leave-one-out R-square, which consists in iteratively leaving one design out of the training set and evaluating the R-square index by training the regression model with the remaining part of the set, and then averaging the results. It can be proved [123] that the convergence rate to the exact momentum of distributions using polynomial chaos regression is exponential with the number of samples, therefore assuring a high accuracy through a low number of sampling points evaluation.

By applying this evaluation to the baseline version of the building analyzed in this research, it was possible to achieve a Leave-one-out R-square index of over 0.99, with only 40 samples for design and a polynomial degree of the third order.

Through this approach it is then possible to reduce the computational load, being the evaluation of the performance function required only to determine the coefficients of the Polynomial Chaos Expansion, in the sampling phase. Once the coefficients are found, it is possible to express the CDF (Cumulative Distribution Function) of any system response using directly the PCE polynomial, which can be considered as a meta-model of the response, practically free in terms of CPU load. Once the CDF is accurately obtained, the value corresponding to the needed percentile of the distribution can be easily retrieved, to define the objective to be minimized.

5.4 Optimization of a social housing building refurbishment

5.4.1 Building description and numerical modeling

The building analyzed for the refurbishment optimization is an existing one located in Trieste, city included in the Interreg ITA-SLO Secap Project program area. It is a social housing building managed by the Territorial Company for Public Housing of Trieste (ATER Trieste) and it is composed by four adjacent blocks, as it can be seen in Figure 5.1, with apartments adjacent to each other. Every block is formed by four floors with two small flats each. The ground floor apartments consist of a kitchen, a bathroom and a bedroom. Every level above the ground floor features two apartments containing one and two bedrooms respectively, a bathroom and a kitchen.

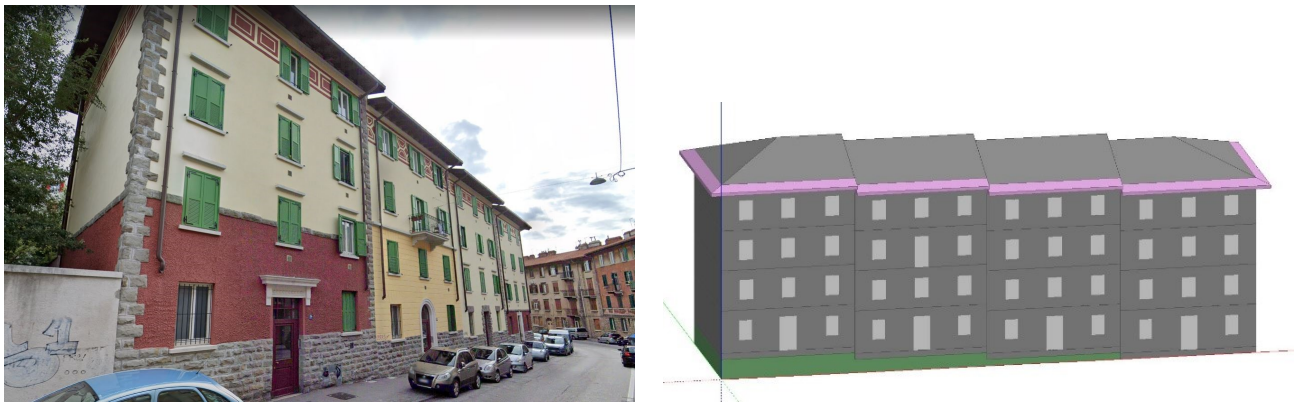

(a) (b)

Figure 5.1: Overview (a) and numerical model (b) of the analyzed building.

The ground level floors and the third level ceilings are adjacent to unheated aerated spaces. The base building is characterized by massive structures without insulation. The external wall is composed by two layers of full-bricks, each 25 cm thick. The ground floor, the roof and the third level ceilings present a concrete structure whose thickness varies from 15 cm to 22 cm. External fenestrations consist of a single-layer glass with high SHGC and thermal transmittance. Two windows sizes are present; the first type presents a surface of 1.65 m^2 and is placed on both north and south walls; the second one, having surface of 0.262 m^2, is present on south wall only. The energy refurbishment has been carried on by windows substitution and by adding insulating layers to the internal vertical and horizontal surfaces in order to preserve the facades, as commonly happens in the Italian area. Windows and opaque surfaces characteristics before and after the refurbishment are reported in Section 5.4.2.

Regarding the internal distribution of spaces, a total of five types of flats have been identified and reported in Table 5.1, presenting the distribution of spaces for each type.

Table 5.1: Spaces distribution for each flat type.

Configuration	**Living Room + Kitchen**	**Other Conditioned Spaces**
Apt 1	34.00%	66.00%
Apt 2	30.00%	70.00%
Apt 3	26.00%	74.00%
Apt 4	28.00%	72.00%
Apt 5	31.00%	69.00%

The base building model was developed using DesignBuilder software, leading to the creation of an *.idf* file describing the building-plant system. This file was then used as input in EnergyPlus software to carry on the energy simulations. During the optimization cycle, this base file was continuously modified according to the refurbished configurations and the calculation phase used EnergyPlus as the simulation engine. The simulation was also allowed to operate in parallel during the optimization

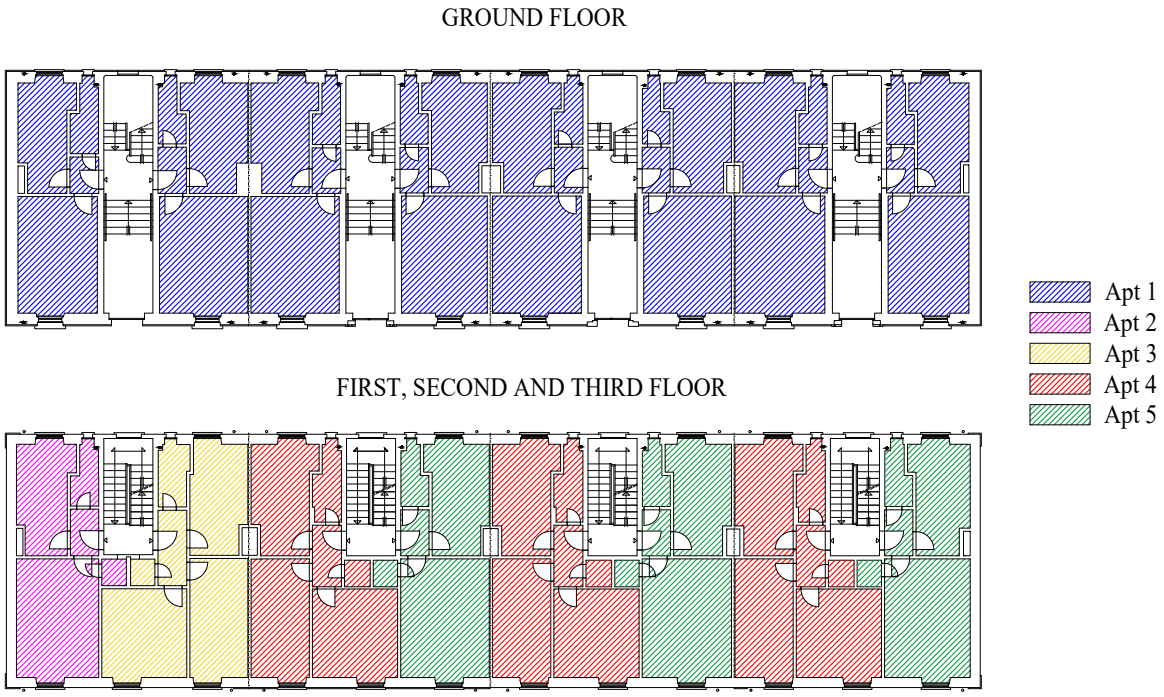

Figure 5.2: Building planimetries and flat types.

runs by exploiting the multicore features of the hardware.

In order to speed up the computation, the partition of interior spaces has been simplified. Every single apartment has been modeled as a unique space while keeping partitions between each other and between apartments and common spaces. However, in order to consider the physical presence of the partitions inside each apartment, equivalent internal masses were added to assure the correct thermal inertia of the system. Internal gains due to people and equipment were computed basing on the pattern for residential buildings of EN ISO 13790 standard [124]. The internal gains defined by the standard were weighted through the areas percentages reported in Table 5.1 to obtain the total internal gain for every type of apartment, presence of people included, as presented in Table 5.2. No gains were modeled for entrances, circulation spaces and bathrooms. Lighting gains are included in internal gains.

Table 5.2: Internal gains patterns.

Day	**Hours**	**Flat Type**				
		1	**2**	**3**	**4**	**5**
		W/m²				
Mon - Fri	07:00-17:00	3.38	3.10	2.82	2.96	3.17
	17:00-23:00	7.46	6.70	5.94	6.32	6.89
	23:00-07:00	4.64	4.80	4.96	4.88	4.76
Sat - Sun	07:00-17:00	4.04	3.8	3.56	3.68	3.86
	17:00-23:00	9.44	8.80	8.16	8.48	8.96
	23:00-07:00	4.64	4.80	4.96	4.88	4.76

Air infiltration has been computed in a simplified manner during winter season, considering an air change rate of 0.50 vol/h for each apartment, while a variable airflow was computed during summertime in order to model the windows opening. This approach aims to better model the occupants behavior during summer period, also highlighting the eventual collateral effects of the envelope insulation level on the thermal comfort of the users. Windows were considered open when the external temperature fell below 2 K than the internal operative temperature. The opening of windows was

scheduled to occur only from May to September and when internal temperatures exceeded 24 °C. The *WindandStackOpenArea* model of EnergyPlus software was used to compute the ventilation phenomenon, considering wind effect only [125].

The building blocks have separate heating plants which were modeled with HVAC systems composed of gas boilers and water radiators as terminals in each flat. Circulation pumps were modeled as variable speed ones. According to Italian regulations for climatic zone E, the boiler availability was set from the 15th of October to April 15. The heating system water temperature was modeled as modulating through an outdoor air temperature sensor. Circulation spaces and entrances were considered as unheated. Heating set-point temperature has been set to 20°C from 7 a.m. to 2 p.m. and from 4 p.m. to 11 p.m., while during the remaining time a setback temperature of 18°C was set. No cooling system was considered, therefore free floating temperatures were present during the summer season. Finally, domestic hot water has not been included into the simulation, therefore energy consumption takes into account heating energy only.

The weather input file was a TRY generated for Trieste using the data recorded between 2001 and 2010, following the procedure described in Section 2.5.

5.4.2 Refurbishment interventions

As previously mentioned, the refurbishing activities focus on the envelope insulation and on windows substitution. Vertical walls were internally treated with different insulation thicknesses considering their different exposition, as well as roof, floors and ceilings that separate the heated areas from crawl spaces. Table 5.3 reports the opaque surfaces thermal transmittances, for base and refurbished configurations. Regarding the latter, Table 5.3 reports the lowest and highest possible values, correlated to the thickness of the insulating layer applied which can be changed with discrete values with 1 cm steps. The insulating material characteristics and costs are reported as well.

Table 5.3: Opaque overall thermal transmittances and insulation layers characteristics and costs.

Opaque constr.	$\mathbf{U_{base}}$ [W/(m²K)]	$\mathbf{U_{ref}}$ [W/(m²K)]		$\mathbf{t_{ins}}$ [cm]		$\mathbf{Cost_{ins}}$ [€/m²]		$\lambda_{\mathbf{ins}}$ [W/(m K)]	$\rho_{\mathbf{ins}}$ [kg/m³]	$\mathbf{c_{ins}}$ [J/(kg K)]
		max	*min*	*min*	*max*	*min*	*max*			
Wall	1.55	0.822	0.215	2	14	9.24	40.60	0.035	25	1,400
Ceiling	14.71	1.565	0.173	2	25	4.93	39.61	0.036	140	1,030
Roof	5.88	1.350	0.170	2	20	13.07	71.15	0.035	25	1,400
Floor	2.89	1.090	0.165	2	20	9.42	53.49	0.035	35	1,400

Regarding glazed surfaces, three different types of new windows have been considered to substitute the low performing existing ones: a double-glass with air gap, a double-glass with Argon filled gap and a triple-glass with Argon filled gaps. The characteristics of existing and new widows are reported in Table 5.4, as well as the costs.

Table 5.4: Windows properties.

Window type	$\mathbf{U_g}$[W/(m²K)]	**SHGC [-]**	**Cost [€]**	
			Small	**Large**
Base	5.7	0.870	-	-
Type 0	1.4	0.660	226.2	417.8
Type 1	1.2	0.425	227.3	423.2
Type 2	0.8	0.398	244.3	500.6

As a consequence of the supposed refurbishment interventions, ten optimization parameters have been considered, each representing a different refurbishment action on building elements; seven are related

to the opaque surfaces and three to the transparent ones. Investment cost are computed taking into account the costs of the material of insulation layers along with the cost of installation. Prices were obtained from the public regional administration price list "Prezzario Regionale dei Lavori Pubblici" [126]. Window prices were instead acquired from real quotes considering transport and installation costs.

5.4.3 Optimization methodology

The optimization was carried out using modeFRONTIER software [127]. Because of some input variables, more precisely the investment cost and the energy price trend, being considered not as fixed values but following a probabilistic distribution, also the outputs of the optimization process have a distribution that can be evaluated by the user. A reliability-based optimization has been performed by considering a stochastic normal distribution for the energy price increasing rate and a normal distribution for the investment costs. However, this two parameters have an effect only on the computation of the economic part of the problem. This suggests a two-step approach for implementing the optimization loop. First the numerical solution with EnergyPlus is performed once per design, then the energy consumption is used to compute the cash flow S_i and, thanks to the Polynomial Chaos Expansion, to generate the NPV distribution from which it is possible to obtain the desired percentiles.

Once the NPV percentiles have been computed, a RBDO can be performed by applying suitable optimization algorithms. modeFRONTIER allows us to operate with nested projects so this capability has been exploited to carry on the optimization: an external project carries on the true optimization step while an inner project performs the Polynomial Chaos Expansion on the economic computation, providing the external one with the NPV 10th percentile value to be used as objective. In Figure 5.3 the optimization workflow is reported.

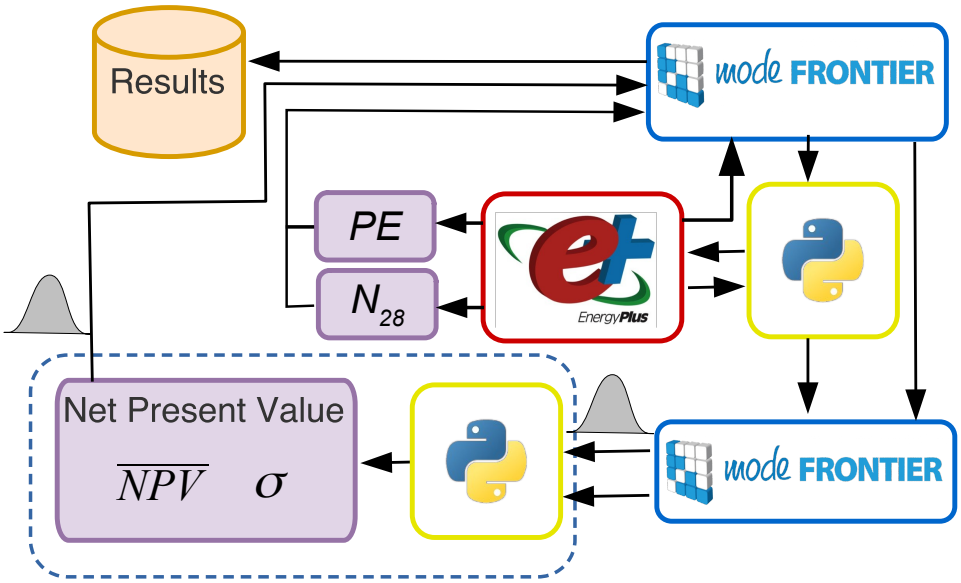

Figure 5.3: RBDO simulation workflow.

As it can be seen, a Python script has been created in order to allow modeFRONTIER to drive the optimization. The Python script implements the "eppy" library [128] using the parameters provided by the optimizer. As described before, it modifies the building model characteristics, creating new *.idf* objects; then the script runs the EnergyPlus simulation, and reads the results of a single run, providing the optimizer with the Primary Energy PE, the number of discomfort hours in summer period N28, and the computed investment cost C_0.

The second modeFRONTIER project is then invoked, where C_0 is changed through a uniform distribution, generated considering a variation of +/-10% of the computed value, and the other economic

parameters are computed. Using the generated input statistical distributions, the NPV output distribution is computed applying what is reported in the following in Section 5.4.3.1, obtaining the objective percentile that is transferred to the outer project. Primary energy, the number of summer discomfort hours, and Net Present Value 10^{th} percentile are used as optimization objectives by modeFRONTIER external project in order to define new designs. In the computation workflow represented in Figure 5.3 the little Gaussian shape identifies the input and output of parameters with stochastic distribution while the part enclosed into the dotted line performs the stochastic simulation. The computation of NPV percentiles has been carried on using the PCE implemented in modeFRONTIER. However, it is worth mentioning that as an alternative solution, a Monte Carlo approach could have been implemented, but with a far slower convergence.

5.4.3.1 Net Present Value computation

The evaluation of the economic performances of the proposed technological solutions was carried out using discounted cash flow (DCF) analysis with reference to the Net Present Value (NPV) of the flow of costs and savings generated by the various solutions, discounted at an appropriate discount rate r. The costs are essentially due to the investment, C_0, necessary to implement the refurbishment, while the savings are computed as the differences S_i between the current operating costs and those of the refurbished solutions. The operating costs usually refer to management, maintenance and energy consumption. However, in this research they refer to energy consumption only. Assuming an evaluation at constant prices, it is necessary to adopt a real discount rate r_r, obtained by removing the effect of inflation r_i from the nominal value r_n, using the following equation:

$$r_r = \frac{r_n - r_i}{1 + r_i} \tag{5.2}$$

The Net Present Value is then computed through Equation 5.3:

$$NPV = -C_0 + \sum_{i=1}^{n} \frac{S_i}{(1 + r_r)^i} \tag{5.3}$$

Moreover, hypothesizing constant savings, S_i, during the analyzed period, Equation 5.3 becomes:

$$NPV = -C_0 + S_i \cdot \frac{(1 + r_r)^n - 1}{r_r \cdot (1 + r_r)^n} \tag{5.4}$$

However this formulation does not take into account the possibility of variation and the future trends of the main components of the operating cost, energy above all. To do this, Equation 5.4 is modified through the insertion of the real annual rate of increase in operating costs, r_e, becoming:

$$NPV = -C_0 + S_i \cdot \frac{\left(\frac{1+r_r}{1+r_e}\right)^n - 1}{\frac{r_r - r_e}{1+r_e} \cdot \left(\frac{1+r_r}{1+r_e}\right)^n} \tag{5.5}$$

That can be rearranged as:

$$NPV = -C_0 + S_i \cdot \frac{1 + r_e}{r_r - r_e} \cdot \left[1 - \left(\frac{1 + r_e}{1 + r_r}\right)^n\right] \tag{5.6}$$

The simulation of the economic performances of the refurbished solutions was carried out assuming the economic values reported in Table 5.5. Most of the economic parameters have been assumed constant and equal to the average of the values recorded in the last ten years. However, in order to investigate the influence of stochastic variables, the future trend in the energy price r_e and the investment cost C_0 were supposed to variate following a stochastic normal distribution and a normal distribution respectively. The investement cost should be known in advance however, as stated by Di Giuseppe et al. [117], prices often change between the time of the design and the final construction. The introduction of stochastic input variables obviously leads a stochastic output. This implies the definition of a "decision rule" to use when dealing with the uncertainty induced by the stochastic variables on the computed NPV.

Table 5.5: Economic parameters used in the optimization. *(*) Mean of the last 10 years prices for household consumers, all taxes and levies included. (**) Mean of the last 10 years.*

Parameter	Value	Unit	Source
Gas*	0.899	€/m^3	Eurostat
Electricity*	0.255	€/kWh	Eurostat
Inflation rate r_i**	1.173	%	Worldwide Inflation Data; www.inflation.eu
Discount rate r_n	4.090	%	Bank of Italy
Energy price trend r_e	1.59 (s.d. 1.40)	%	Energy Information Administration

There are various ways to introduce the effect of uncertainty in a DCF analysis [129]:

- Computing a deterministic DCF where the inputs are fixed, the risk is represented by the incremental risk premium on the risk free discount rate and the output is a fixed NPV;
- Computing a deterministic DCF where the inputs are fixed and valued at "certainty equivalent", the discount rate is risk free and the output is a fixed NPV [130];
- Computing a probabilistic DCF where the inputs are distributions, the discount rate is risk free and the output is a NPV distribution.

In this research, the optimization process was carried on by implementing the third approach, therefore aiming at the identification of a confidence limit to be associated with the stochastic objective to be optimized, in this case the NPV. Assuming a risk-neutral decision maker and a stochastic distribution of the NPV, the value to be optimized is the average or modal one. Normally, the decision maker is risk-adverse and therefore optimizes a value with a probability to be overcame more than 50%. Unfortunately, to our knowledge, there are no studies that have examined this aspect with reference to the energy requalification choices. Therefore, a very cautious attitude was assumed, hypothesizing a reference NPV with a 90% probability of being exceeded.

5.4.3.2 Optimization settings and objectives

Two optimization runs were performed with two and three objectives, respectively. The first run took into account the economic and environmental impact of refurbishment activities by maximizing the tenth percentile of the Net Present Value (NPV) of the investment and by minimizing the building Primary Energy (PE) consumption. The second optimization considered an additional objective inherent to the minimization of the maximum number of hours during which the operative temperature of each apartment is higher than 28 °C, named N28. This objective takes into account the possibility of overheating problems during summer season as a consequence of the major enevolpe insulation implemented through the refurbishment activities. Overheating was chosen instead of the cooling demand as a defining parameter because usually this kind of building does not present centralized cooling plants. The three optimization objectives can then be summarized as follows:

- The minimization of the building primary energy consumption;
- The maximization of the 10^{th} percentile of the NPV;
- The minimization of the summer discomfort hours.

Regarding the first objective, conversion factors to Primary Energy were set to 3.167 and 1.084 for electricity and natural gas respectively. Standard cubic meters of natural gas were calculated considering the lower heating value of natural gas equal to 9.94 kWh/sm^3. Moreover, it is worth noting that the NPV objective is a statistical one, with the meaning that 90% of the solution are expected to have a value greater than the objective one. As already pointed out, the choice has been made in order to replicate the decisions of an investor with a low-risk attitude.

The optimization process has been performed using the NSGA II optimization algorithm, starting with an initial Design of Experiments of 24 individuals. The genetic optimization has been performed for 50 generations. Since the numerical computation with EnergyPlus and the stochastic optimization have been decoupled the genetic algorithm has been the straightforward choice. However, if the stochastic approach would be extended to parameters affecting directly the simulation with EnergyPlus, other algorithms, such as response factors or the modeFRONTIER FAST algorithm [131] would be more appropriate in order to obtain solutions in reasonable time.

5.4.4 Results

Optimizations results are reported using bubble plots to present up to four variables. The bubble diameters are proportional to the external walls thermal conductance, whose maximum and minimum values are graphically and numerically reported in the charts for clarity. Bubble colors represent window types that is, grey is Type 0, magenta is Type 1 and turquoise is Type 2. The 10^{th} percentile of the NPV and the Primary Energy are the axes of the plot. Since the abscissa is the 10^{th} percentile of NPV, it is worth noting that the reported value means that the 90% of the possible solutions will show higher values of economic return, depending on the real behavior displayed by the stochastic parameters.

Figure 5.4 presents the comparison between the Pareto fronts of the solutions related to the North and South facades for the two-objective optimization: the figure shows how the optimization selects opaque walls transmittance and drives window selection. Window Type 1 is seldom selected and never for solutions pertaining to the Pareto front. For the South wall facade, the solution for windows is always the Type 0, with the highest value of transmittance. On the other hand, on the North wall windows, Type 2 are selected for the low energy case, while Type 0 is the one selected for the high NPV case.

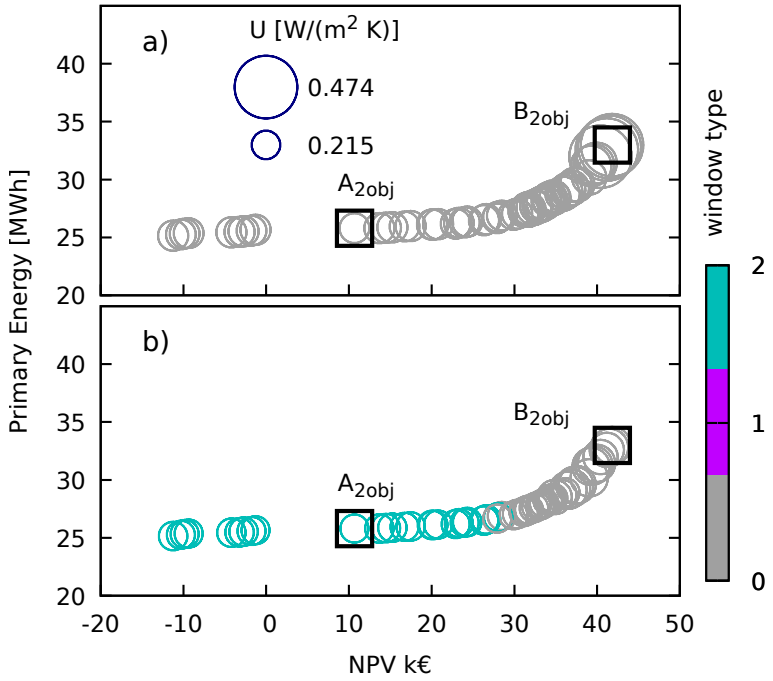

Figure 5.4: Two-objective optimization Pareto fronts for South (a) and North (b) facades.

Finally, two designs from the Pareto front are compared for each case, representing the solutions that grant the minimum NPV greater than zero, A_{2obj} and the maximum NPV, B_{2obj}. The chosen designs are highlighted by squares in Figure 5.4. It can be noted that design B_{2obj} grants the maximum NPV but with a greater energy consumption than A_{2obj}. This is due to the fact that B_{2obj} uses low levels of insulation for the South wall and less performant windows for the North one, leading to an increased energy consumption but less expensive refurbishment solutions. The shape of the Pareto fronts shows

as a conflict emerges between the minimization of Primary Energy consumption and NPV maximization. However, Figure 5.4 shows that a significant increase in NPV with small increases in Primary Energy consumption is achievable. Only when the NPV increases above 30 k€ also the Primary Energy consumption increases significantly. In other words, it is possible to identify technological solutions which at the same time have low energy consumption and good economic performances.

Figures 5.5 and 5.6 present the Pareto fronts for the three-objective optimization for South and North facades respectively. As already stated, the additional objective is represented by the minimization of the maximum number of hours over 28 °C, namely N28, for each apartment of the building. In order to highlight the correlation between the parameters and the number of exceeding hours, in both figures the designs are categorized as the ones with N28 over 480 h (a), between 380 and 480 (b), and under 380 h (c). As before, the results are reported through bubble plots representation: as before, the circle diameter is proportional to wall conductance, while the color identifies the window type.

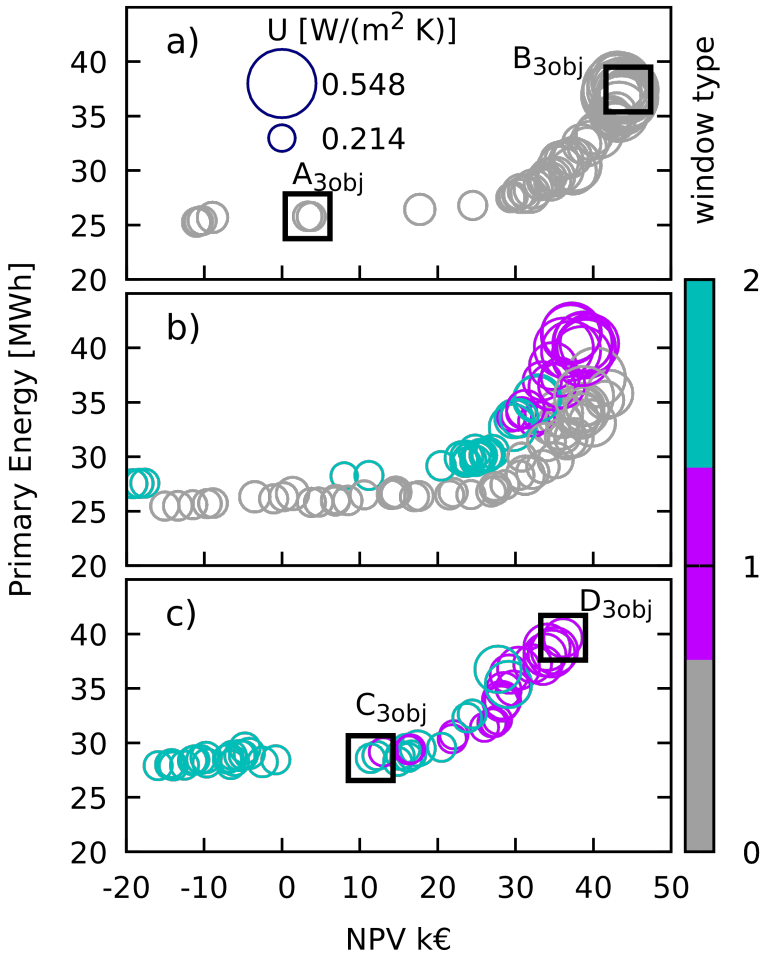

Figure 5.5: Three-objective optimization Pareto fronts for South oriented wall with different number of N28: greater than 480 (a); between 380 and 480 (b); less than 380 (c).

It is worth comparing the results with the ones obtained with two objective optimization and reported in Figure 5.4. For instance, the Pareto front of Figures 5.5a and 5.6a are quite similar to the results presented in Figure 5.4a and b respectively, instead the results of Figures 5.5c and 5.6c show completely different patterns. In order to obtain results with low values of N28 the optimization selects solutions with low conductance value for both North and South walls and, above all, windows Type 1 and Type 2 for the South-oriented windows. As a side effect, the energy consumption during the winter heating period increases due to the lower solar heat gain from the windows on the south wall with low SHGC.

For completeness it has to be pointed out that the results reported for the two-objective optimization, not considering the minimization of the summer discomfort hours, nearly always fall into the higher

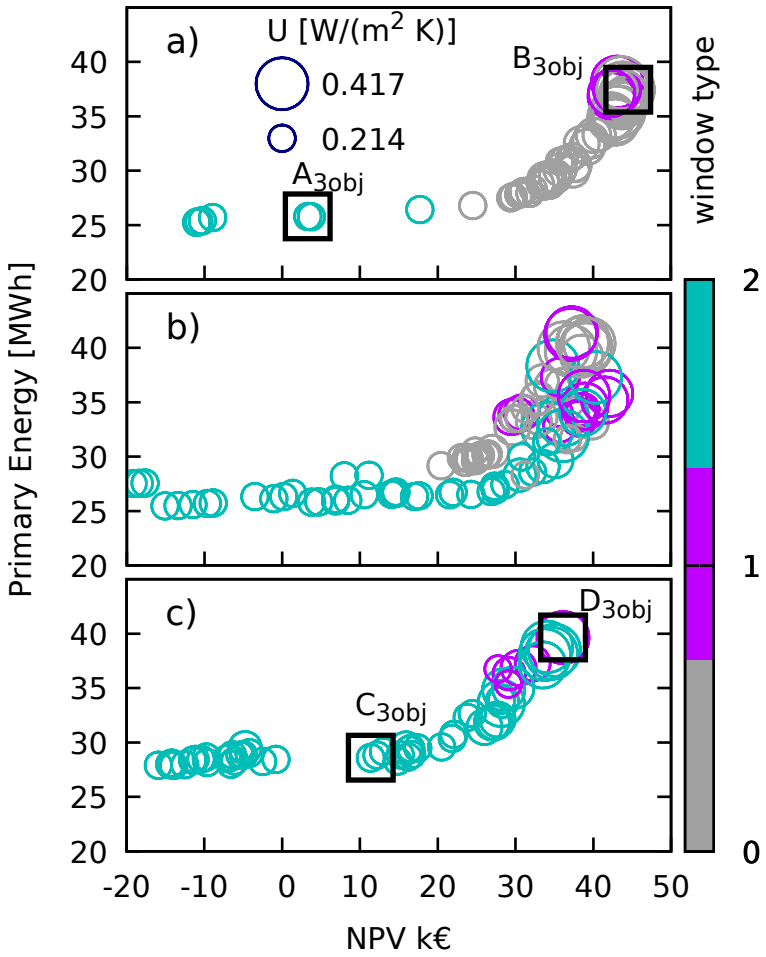

Figure 5.6: Three-objective optimization Pareto fronts for North oriented wall with different number of N28: greater than 480 (a); between 380 and 480 (b); less than 380 (c).

range of N28, further assessing the aforementioned similarities with case (a) of Figures 5.5 and 5.6.

It is clear that, if it is deemed important to improve the summer internal conditions, reducing the N28 objective during summer season, the preferred solutions are the ones less performant regarding the NPV and the PE objectives. Therefore, it is very important to correctly weight the importance of each objective of the optimization in order to obtain reliable and efficient performances.

In order to understand the different behavior of the designs and how they are influenced by the insertion of the summer performance objective, Table 5.6 reports six different designs, their performances in terms of PE and NPV and the features of the parameters applied. The corresponding solutions are graphically reported in Figures 5.4, 5.5 and 5.6. Two designs, A_{2obj} and B_{2obj}, have been selected for the two objective optimization and four designs have been selected for the three objective optimization: two for low PE and with high (A_{3obj}) and low (C_{3obj}) N28 value, other two with the highest NPV, again with high (B_{3obj}) and low (D_{3obj}) N28 value.

By analyzing Table 5.6, it can be noted that the solutions of the two-objective analysis, A_{2obj} and B_{2obj}, are similar to those of the three-objective one with high values of N28 A_{3obj} and B_{3obj}. Instead the selected designs with low N28 values, namely C_{3obj} and D_{3obj}, are characterized by lower levels of insulation on opaque walls but with more performing windows applied, namely Type 1 and 2. It is then evident the purpose to reduce the overheating problem by limiting the envelope insulation and decreasing the solar heat gains through the usage of low SHGC windows.
The results highlighted three different approaches a decision maker can have regarding the problem of building refurbishment. The energy-aware approach implies that the solutions with the higher insulation and higher cost are chosen; for instance, this means applying the triple glazing windows and

Table 5.6: Selected designs.

Parameter		$\mathbf{A_{2obj}}$	$\mathbf{B_{2obj}}$	$\mathbf{A_{3obj}}$	$\mathbf{B_{3obj}}$	$\mathbf{C_{3obj}}$	$\mathbf{D_{3obj}}$
$U_{wall,S}$	[W/(m2 K)]	0.23	0.47	0.23	0.47	0.23	0.31
$U_{wall,N}$	[W/(m2 K)]	0.21	0.28	0.21	0.42	0.21	0.42
$U_{wall,E}$	[W/(m2 K)]	0.24	0.28	0.28	0.28	0.24	0.28
$U_{wall,W}$	[W/(m2 K)]	0.21	0.42	0.21	0.42	0.23	0.37
$U_{ceiling}$	[W/(m2 K)]	0.15	0.2	0.14	0.39	0.14	0.39
U_{roof}	[W/(m2 K)]	0.41	1.35	0.33	1.35	0.76	1.35
U_{floor}	[W/(m2 K)]	0.19	0.49	0.15	0.49	0.23	0.49
$Window_{1,N}$		Type2	Type0	Type2	Type0	Type2	Type1
$Window_{1,S}$		Type0	Type0	Type0	Type0	Type2	Type1
$Window_{2,S}$		Type0	Type0	Type0	Type0	Type2	Type1
PE	[MWh]	25.8	32.98	25.8	37.45	28.6	39.64
NPV	[k€]	10.69	41.83	3.29	44.54	11.38	36.11
N28	[hours]	466	528	481	519	353	377

higher insulation thicknesses. However, in this case, the return of the investment can be poor and, in some cases, depending on the economic stochastic parameters, there is a risk to obtain negative NPV, so the energy savings are not sufficient to compensate the initial costs. The solutions identified as A_{2obj} and A_{3obj} follow this pattern.

Another approach aims at having the highest NPV possible, so the reduction in energy consumption is less important; this means that the less expensive solutions are the preferred ones, so designs such as B_{2obj} and B_{3obj} are selected. However, the results may be excluded due to the regulation requirements which fix minimum threshold values for energy performance. In this case, the limits can be incorporated into the optimization process by introducing suitable constraints.

A different approach can also take into account the effect of insulation on summer conditions, which leads to a change in preferred designs, since a lower value of overheating hours drives the solutions towards higher energy consumption, such as C_{3obj} or a lower NPV, as the D_{3obj} case.

However, irrespective of the preferred solution, a decision maker using the presented approach has the feeling of the economic risk involved in carrying out the refurbishment. For each design, there is a high probability to have an economic return of the invested money, for instance the optimization could have used higher values of NPV percentiles (less risk-adverse decision maker) resulting in higher expected returns but with a lower chance. In fact, the convenience of an energy saving investment depends on climate, economic and technological uncertainties. It follows that the choice of an investment affects both the expected NPV and the probability of reaching it. In this work, a high risk-adverse decision-maker has been hypothesized and therefore the proposed efficient solutions are very prudent in economic terms.

5.5 Climate change influence on the optimization process

As previously stated, one of the research objectives is to assess the influence of climate change on the optimization of the refurbishment process of an existing building. The possible evolution in climate conditions introduces an additional uncertainty that can influence energy savings, but that can also indirectly influence the economic and comfort aspects of the problem.

Ascione et al. [110] considered in a simple way the effect of increasing temperatures in the future, highlighting the necessity to perform a robust optimization in order to obtain resilient solutions. Shen et al. [132] analyzed the impact of the future climate scenarios in a retrofit analysis, realizing that the changing climate scenarios increase the complexity of decision-making models for building refur-

bishment. Moazami et al. [59] analyzed the effects of climate change on various building typologies highlighting considerable variations in primary energy, especially regarding the cooling component.

In this research the climatic variability was considered through the use of six different climatic situations, analyzed to evaluate the influence of various boundary conditions on the optimization process. The analyzed climatic sets were the TRY generated for Trieste using the data collected between 1995 and 2019, whose creation process is reported in Chapter 2, and its projections into the future whose generation is reported in Chapter 3.

As it can be noted, the actual TRY refers to a different timeframe than the one used in the previous optimization runs, referring to the 2001-2010 period. This has been done to also highlight how choosing different data source periods to generate the actual TRY could influence the simulation results.

Regarding the projected TRYs, as already stated in Chapter 3, they represent the 2021-2050 period, splitted in two to better assess climate evolution in the near future. Each TRY couple has been used to represent a possible evolution of climate in the next 30 years.The choice of using TRYs to represent such a long future period, 30 years, is due to the computational burden of the optimization process. This would have made troublesome to perform the optimizations if the models projections were used to run year-by-year simulations for the considered timeframe. However, the TRYs have widely demonstrated to be able to well represent the overall behavior and the main characteristics of climate for the timeframes they represent. The six climatic sets used in this optimization process can then be summarized as:

1. Historical TRY (1995-2019);
2. Projected TRYs (2021-2035 + 2036-2050) using HadGEM2-ES_RACMO22E model applied to RCP8.5 scenario;
3. Projected TRYs (2021-2035 + 2036-2050) using MPI-ESM-LR_REMO2009 model applied to RCP8.5 scenario;
4. Projected TRYs (2021-2035 + 2036-2050) using EC-EARTH_CCLM4-8-17 model applied to RCP8.5 scenario;
5. Projected TRYs (2021-2035 + 2036-2050) using EC-EARTH_RACMO22E model applied to RCP8.5 scenario;
6. Projected TRYs (2021-2035 + 2036-2050) using EC-EARTH_RCA4 model applied to RCP8.5 scenario.

Six distinct optimizations were carried on for every climatic dataset used in this work in order to highlight the effects of different climates on the whole optimization process. The optimization approach remained almost totally unchanged, with only some upgrades needed to consider the presence of two TRYs for the future scenarios.

5.5.1 Methodology modifications

First of all, the energy simulation carried on by EnergyPlus for the future climates has been performed twice because of the two timeframes, 2021-2035 and 2036-2050, considered in this work. Therefore, the Primary Energy consumption takes into account the changes between these two periods and the values reported in the results refer to a whole period of 30 years. Regarding the actual climate instead, the original TRY was applied to the whole 30 years timeframe.

In this way, it was possible to consider different climates for the next 30 years, supposing that no changes will happen respect to the actual situation, i.e. climatic set 1, or that various evolutions could happen, discretized in two timeframes of 15 years, i.e. climatic sets 2-6. The possible different evolutions are then represented by the distinct climate models used to project the TRY, giving different

results for the same period.

Because of the energy analysis being split in two periods as stated above, also the NPV computation had to be divided in two terms. Defining m and n as the duration in years of the first part and the total time of calculation respectively, the Net Present Value is then given by:

$$NPV = -C_0 + \sum_{i=1}^{m} \frac{S_i}{(1+r)^i} + \frac{1}{(1+r)^m} \cdot \sum_{i=m+1}^{n} \frac{S_i}{(1+r)^i} \tag{5.7}$$

Where the remaining parameters were already defined in Section 5.4.3.1. As already stated in that Section, in order to properly evaluate the NPV the discount rate had to be corrected removing the effects of inflation from the nominal value, obtaining the real discount rate. This was done using Equation 5.2.

As before, the computation must also take into account the future variability of the main components of operating costs. Assuming again equal to r_e the real annual rate of increase in operating costs, considering the correction of the discount rate and hypothesizing S_i constant from 1 to m (S_a) and from m+1 to n (S_b), Equation 5.7 can be rearranged as:

$$NPV = -C_0 + S_a \cdot \frac{1+r_e}{r_r - r_e} \cdot \left[1 - \left(\frac{1+r_e}{1+r_r}\right)^m\right] + S_b \cdot \frac{1+r_e}{r_r - r_e} \cdot \left[1 - \left(\frac{1+r_e}{1+r_r}\right)^{n-m}\right] \cdot \frac{1}{\left(\frac{1+r_r}{1+r_e}\right)^m} \tag{5.8}$$

The evaluation of the economic performances of the refurbished solutions considered the values of the parameters reported in Table 5.5.

The optimization process was still performed using the NSGA II optimization algorithm, starting with an initial design of experiments of 24 individuals and performing the optimization for 40 generations.

5.5.2 Results

Optimizations results are again reported using bubble-plots to present up to four variables. However, because of the great amount of information to be reported, the results are not divided by wall orientation but regards the behavior of all the building. As a consequence, in this case the bubble diameters are no more proportional to the external walls thermal conductance, but to the overall mean heat transfer coefficient of the building H'_t, whose maximum and minimum values are graphically and numerically reported in the charts for clarity. The H'_t coefficient has been calculated for every output design using Equation 5.9:

$$H'_t = \frac{\sum_{j=1}^{P} A_j \cdot U_j + \sum_{k=1}^{Q} A_k \cdot U_k \cdot b_k}{\sum_{j=1}^{P} A_j} \tag{5.9}$$

Where P is the total number of surfaces facing the outside, both opaque and windowed, A_j, U_j are the area and transmittance of the j-th surface respectively. Q is the number of surfaces facing unheated spaces or the ground and b_k is the correction factor for the transmittance accounting for the presence of unheated spaces or of the ground, depending on the case as defined in the UNI-TS 11300-1 standard [133].

Also bubble colors have a different meaning in this case, representing four ranges of N28 value that is, the blue is range 650-1150, green 1150-1300, orange 1300-1450 and red is range 1450-1550. As before, the 10^{th} percentile of NPV and Primary Energy consumed over 30 years are the axes of the plot.

Figure 5.7 shows the Pareto fronts resulting from the optimizations carried on with the original TRY (a) and the five climate models (b-f) for the 30 years timeframe. The most evident, and most expected, feature synthetized by Figure 5.7 is the great difference between the case with actual TRY (a) and the other cases computed with the climate models (b-f).

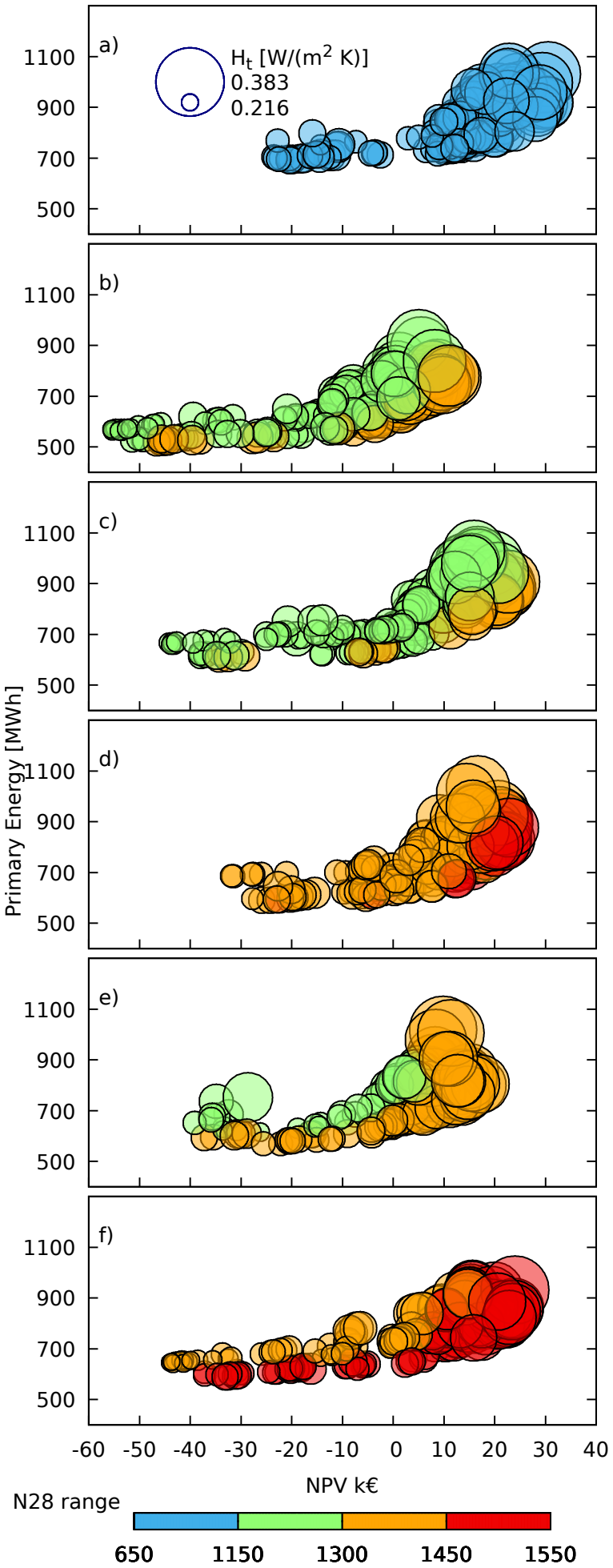

Figure 5.7: Pareto fronts for original TRY (a) and for future TRYs generated with climate models (b-f).

Great differences can be detected in all the three objectives of the optimization: the Primary Energy consumption is notably higher in case (a) because of the climate analyzed being colder than the others. Despite the greater energy consumption, the optimization solutions perform better than in the other cases, showing significantly higher NPV values for all the designs.

Also the hours of discomfort detected during summer season, N28, display significantly lower values than the other situations, being this case the only one with N28 values falling in the lowest range. Also in the cases were climate models were used, from (b) to (f), the optimizations results show very different behaviors depending on the climatic model used. In fact, the simulations performed with HadGEM2-ES_RACMO22E (b), MPI-ESM-LR_REMO2009 (c) and EC-EARTH_RACMO22E (e) display N28 values falling in lower ranges (green and orange), than the ones performed with the models EC-EARTH_CCLM4-8-17 (d) and EC-EARTH_RCA4 (e) showing N28 values falling in higher ranges (orange and red). It is also very interesting to note that the two models having the higher values of N28 are also the colder ones within the five projections, as if the optimization underestimated the summer comfort objective. The real explanation is the choice of less performant windows in these two cases in order to exploit the solar heat gains to reduce winter heating energy consumption. As it can be seen in Figure 5.7, this choice also had beneficial effects on the NPV because of these windows being cheaper, but obviously it reduced the performance during summer season.

The Primary Energy is the output that is least affected by the different climatic conditions. This proves that the optimization often succeeds at finding solutions that are reliable through different boundary conditions in terms of energy consumed, confirming the resilience of energy measures to climatic conditions. On the other hand, the NPV and N28 objectives are much more influenced by the climate model used in the optimization. About the former, it performs in very different manners, showing minimum and maximum values that vary in a range of about 25 k€ and 13 k€ respectively.

Another relevant output is that the results obtained through the actual TRY generated using climate data from 1995-2019 period (Figure 5.7a), are quite different from the ones computed in Section 5.4 with the TRY obtained through 2001-2010 historical data. Primary Energy consumption over 30 years is lower, leading also to lower NPV values. Moreover, if with the 2001-2010 TRY the summer discomfort hours reached values of at most 530, by using the 1995-2019 TRY, N28 values ranged between 650 and 1150. It is then evident how using various historical data timeframes to create the TRY leads to very different results in the simulation of building-plant systems, therefore highlighting the importance to carefully choose wich period consider when creating the weather input file for energy simulations, even if climate change is not involved.

Finally, an interesting feature can be detected in all the six optimization results: there are cases of more insulated solutions that have higher PE consumption than less insulated ones, while falling in the meantime in a lower range of N28. The higher-insulated designs feature high quality windows in their refurbished configuration; because of the characteristics of these windows, the solar gains are consistently reduced throughout the year. This implies less solar heat gains in both winter and summer seasons, thus leading to greater heating energy consumption and less number of discomfort hours (N28) during summer season.

To further highlight this feature, a correlation matrix is reported in Figure 5.8, representing the relationships between the reported variables that are primary energy (PE), Net Present Value (NPV), wall insulation (insN) and windows performance (winN) of the North facade, wall insulation (insS) and windows performance (winS) of the South facade.

In Figure 5.8a are reported the minimum values of the Pearson correlation coefficients among the six optimizations, while Figure 5.8b reports the maximum ones. It can be noted that, generally, there is a relevant difference between the minimum and maximum values of almost all the correlation coefficients, highlighting then different reciprocal influences between the parameters depending on the climate chosen for the simulation.

	N28	PE	NPV	insN	insS	winN
PE	0.034					
NPV	0.287	0.509				
insN	-0.646	-0.787	-0.608			
insS	-0.504	-0.787	-0.674	0.236		
winN	-0.680	-0.549	-0.598	0.083	-0.106	
winS	-0.655	0.011	-0.389	0.051	-0.316	-0.035

(a)

	N28	PE	NPV	insN	insS	winN
PE	0.484					
NPV	0.634	0.656				
insN	-0.309	-0.611	-0.436			
insS	-0.009	-0.641	-0.382	0.549		
winN	-0.500	0.120	-0.076	0.495	0.689	
winS	-0.547	0.310	-0.131	0.261	0.136	0.233

(b)

Figure 5.8: Parameters correlation matrix, minimum (a) and maximum (b) correlation values among the six optimizations.

The correlation matrix provides also a clearer explanation for the aforementioned phenomenon of higher-insulated solutions having greater PE consumption and lower N28 values than less insulated ones. In fact, by analyzing the correlation between winS, N28 and PE, a negative correlation coefficient is detected in all cases between the first two. It is then evident that as winS increase, i.e. as more efficient windows are selected, N28 decreases. Instead, the correlation coefficient between winS and PE is always positive, therefore more efficient windows lead to major energy consumption. It is also interesting to note that the absolute value of the first coefficient is way greater than the second one. Therefore, as it can be deducted also by the bubble charts inspection, the benefic effect of a more efficient window on N28 is way greater than the penalizing effect that it has on the PE consumption.

5.6 Conclusions

In order to provide the municipalities an applicative example to exploit when drafting their mitigation and adaptation policies, a Reliability-Based Design Optimization for a social housing building energy refurbishment has been carried out. The choice fell on a social housing building because of this typology being the most probable to be included in refurbishment initiatives and not being provided with centralized cooling plants.

Data uncertainty was taken into account for economic parameters and climatic data. About the formers, the uncertainty was considered through the assumption of a stochastic distribution of the investment cost and of the increase in energy prices during the building lifetime. Regarding the latter, seven different climatic inputs were used for different optimization runs: of these inputs, two referred to the actual climatic situation and have been obtained through the data detected during 2001-2010 and 1995-2019 timeframes respectively. The other five inputs were obtained through the projection of the 1995-2019 dataset by using five different climate models applied to the RCP8.5 scenario. The objectives of the optimization reflected the stochastic nature of the problem by maximizing the NPV with a probability of being exceeded by 90% in order to model the choices of a prudential decision-maker.

Two first optimization runs have been performed using as input the TRY obtained through the 2001-2010 historical data. The former used two objectives related to Primary Energy consumption and Net Present Value, the latter added a third objective in order to search solutions able to minimize overheating problems during summer season, identified as the number of hours in which the operative temperature of the apartments was greater than 28 °C. The optimizations led toward solutions with different choices between North and South facades, thus highlighting how important is to consider the orientation of the envelope when dealing with refurbishment practices. Moreover, the introduction of an additional objective in the second optimization gave rise to a set of solutions quite different from the ones obtained with only energy and economical objectives, leading to the use of more performant windows, irrespective of the wall orientation. This represents an important outcome, since economic or energy-related objectives are usually not sufficient parameters to be taken into account when dealing with building refurbishment. This also highlights the importance of considering the building performance during the whole year, even when dealing with seasonal-centered refurbishment interventions. In fact, as seen in this research, the characteristics of the winter-centered refurbishments greatly influenced the perceived thermal comfort during summer season.

After that, six more optimization runs, considering all three objectives, have been carried on using the TRY obtained through the 1995-2019 historical data and its future projections computed through five different climate models applied to the RCP8.5 scenario. The results showed important differences for the three objectives behavior due to the various climatic datasets used. In particular great differences are highlighted between the optimization carried on with the historical TRY and the ones exploiting its projections, leading to very different performances for all three objectives. Moreover, notable discrepancies are detected also between the optimizations developed with the 2001-2010 and 1995-2019 historical data, thus highlighting the importance of carefully choosing the climatic input data of the energy simulations even when dealing with actual climate. Finally, the implementation of some refurbishment interventions led to unexpected counterintuitive results in terms of energy consumption, with more performing refurbishment solutions leading to higher energy consumption.

Summarizing what emerges from this research, it is evident the necessity of carefully weighting which objectives pursue when dealing with buildings refurbishment, because of the capacity of said objectives to greatly influence the final design solutions. Moreover, it is of the uttermost importance choosing the correct climatic boundary condition to set for the simulation, let this be an actual or future situation. Furthermore, it is highlighted that it should not be taken for granted that more performing refurbishment solutions necessarily lead to better performances for the refurbished building. Finally, this work also emphasizes the importance of considering the performances all over the year, even when dealing with a seasonal-centered refurbishment design.

As a footnote, the results also show that the designs can be variegated and depend on the level of acceptable risk. In this research, a 10% risk has been selected, meaning 90% of the solutions may give NPV values greater than the ones computed. However, other values can be chosen depending on the amount of risk a possible investor could accept. The use of Polynomial Chaos Expansion in evaluating the stochastic functions allows, with few computations for each design, to determine the percentiles to be used in the optimization, allowing an easy extension to problems which are more demanding in terms of computational resources.

Chapter 6

Conclusions and future developments

The research described in this thesis is placed within the Seap-Secap transition process. Starting from the needs of the municipalities that have joined the project or are willing to do so, a methodology that could be exploited when drafting climate mitigation and adaptation policies was developed. Moreover, some applicative samples were carried on for Trieste location, included in the Interreg ITA-SLO Secap Project program area.

Being the creation of policies to tackle climate change the principal aim of the Secap project, it is evident that the starting point for the municipalities when joining such process is to properly analyze actual climate and its evolution. To do so, a well defined and reliable methodology should be used in the process and was developed in this research, starting with a quality check of the Italian historical climatic data, leading to an evaluation of which ones can be used for energy simulations.

The quality check highlighted different behaviors across the analyzed Italian meteorological stations, however assessing a fairly good overall climatic data quality, proving the data to be exploitable for energy simulations in most of the cases. Some issues were assessed regarding the amount of detected material, not reaching the 10 years recommended amount in almost half of cases. The major part of the stations having few data were placed in South Italy, therefore highlighting the delay affecting this part of the nation in developing a climatic database. Regarding the instruments capacity, some issues were assessed in the detection of relative humidity and wind speed. However, the locations where these issues emerged were mostly placed in hilly or mountain environments, thus suggesting a connection between the orography of the territory and the functioning issues of the instruments.

Given the growing importance of buildings cooling performance, the research then focused on the review of the European EN ISO standard method to select Cooling Design Days (CDD) from climatic data. The review highlighted that input parameters choice had great effects on the CDDs selection results, therefore pointing out that designers should be careful when using this selection method. Moreover, a case study was developed to assess how the standard method performs when applied to a building, highlighting that in many cases the selected CDDs would give design powers not respecting the target risk levels, often giving counterintuitive results. Additionally, the EN ISO method proved to be difficult to understand and to implement, therefore a formal upgrade was carried on, leaving untouched the theoretical principles, leading to a new formal approach, easier to automate and to modify.

After having assessed the current climatic situation and its effects on human activities, the next step for municipalities when drafting adaptation and mitigation measures is to study the climate change and how it will affect the aforementioned activities. To do so, climate models are fundamental, however they often present issues regarding their capacity of properly represent the future evolution of climate. In this research the performance of five different climate models in representing climate evolution for Trieste has been evaluated, highlighting some discrepancies when comparing their projections with measured data for a common timeframe. This led to the necessity of correcting the models by using the quantile correction method through which models performances were greatly improved.

The corrected models were then exploited to carry on analysis on future climate, in particular focusing on the evolution of thermal extreme events like heat waves and cold spells. A methodology to define both events was developed and applied to the Trieste location to study the actual and future behaviors of such phenomena. The results showed a steadily future increase in heat waves frequency and intensity if compared to the actual situation, therefore highlighting the necessity for the municipality to take into account this phenomenon for its social and health policies. Regarding the cold spells, both actual and future behaviors showed no significant events. By exploiting this analysis, a methodology to compile the Risk & Vulnerability Assessment of the Secap Projects was developed to give municipalities a quick procedure to follow.

Performing energy simulations on building-plant systems in order to assess the current state of the building stock and how to improve it, is a fundamental task to develop mitigation policies. To be able to perform such analysis, a climatic input is obviously required; commonly this input has the form of a Test Reference Year (TRY), being it a valuable way to represent climate during a selected timeframe. In this research a TRY for the location of Trieste was generated through the Finkelstein-Schafer statistic applied to data detected between 1995 and 2019. However, in order to perform energy analysis also for future climate, another climatic input must be used. To provide the municipalities with a process to perform energy simulations for future climate, a projection method of the actual TRY was developed. The calibrated climate models, applied to the RCP8.5 scenario, were used to project the current TRY of Trieste in the future through the mathematical Morphing Process. The projection carried on through the five models gave notable different outputs, despite all aiming towards warmer climates, thus highlighting how choosing different climate models to carry on future climate forecasts have a notable influence on the expected outputs.

Being Italy characterized by a huge amount of historical buildings, often the best solution to improve their energy performance is the application of internal insulation systems. It is then important to correctly evaluate the behavior of such technique when applying it in refurbishment processes. With this aim CFD analysis were carried out to study the behavior of internal insulation systems for walls. The study considered the effect of the steel studs commonly used to sustain the package and their interaction with low-e sheets usually included in the insulating system to improve its performance. The results showed that neglecting the effect of the supporting studs, as it is commonly done in design practice, leads to significant errors, up to 28%, in the evaluation of system performance.

To this point the research underlined an important aspect: many factors included in refurbishment practices, like climate data or insulating packages performances, are not deterministic. In the common pratice this aspect is often neglected, however this could lead to design errors with consequent performance flaws. The final topic pursued in this research was then the optimization of a refurbishment process subject to uncertainties applied to a social housing building. This typology of building was chosen because of its diffusion in Italy and of it being the most probable target of municipalities refurbishment policies. The optimization aimed to maximize the performances of the studied building in terms of energy consumption, economic aspect and thermal comfort. The undertainty was introduced in the process by assigning stochastic distributions to economic parameters and by considering different climatic conditions, both actual and future. The results highlighted that, depending on the objectives pursued and on the boundary conditions applied, the possible refurbishment solutions and their performances greatly varied, sometimes even leading to unespected results, like more expensive refurbishment solutions having worse energy and comfort performances than cheaper ones.

This research then constitutes a complete workflow that municipalities could exploit to tackle some of the most important topics when developing their climate mitigation and adaptation policies, starting from the raw actual climate data, following with the analysis of climate change and of insulating systems performances, finally exploited to optimize the refurbishment practice of the social housing building sector.

Further developments will be carried on for this researchfor improving and extending it to obtain more complete and valuable results by overcoming the limitations affecting the presented analysis.

For what concerns climatic data treatment, the approach proposed by Nik et al. to represent climate by using three distinct TRYs rather than only one will be implemented for both actual and future climates. Regarding the latter, more projections techniques will be explored and their results compared to assess their reliability, and climate projections will be extended to year 2100 to cover all the timeframe considered by the predicting models. Moreover the TRY generation for both present and future climate will be extended to several location included in the program area of the Interreg ITA-SLO Secap Project to aid more municipalities in their SECAPs drafting process. With this in mind, also the focus on the cooling plants sizing, and therefore on the Cooling Design Day selection procedure, will be further developed. In order to consider more systems tipologies in the analysis, studies on the reliability of the output sizing powers for several combination of building-plant systems presenting different characteristics.

Having proved the importance of a correct evaluation of internal insulating packages performances, this analysis will be extended by conducting a parametric study to properly consider the influence of every package configuration on the discrepancy between declared and real performance. This will be done in order to define a corrective formula to compute the exact conductance of the package starting from the official one reported in the data sheets.

Finally, for what concerns the optimization of the refurbishment process of buildings, cross correlation between parameters and variables will be introduced in the models to better assess the reciprocal influence of the various actors included in the process and uncertainty regarding insulating packages will be introduced as well. Moreover, the models will be implemented to speed up the computation and allowing to run optimizations through the use of more TRYs to represent future climates, to better discretize climatic evolution in the future.

Bibliography

[1] International Energy Agency. Global Energy and CO2 Status Report - The latest trends in energy and emissions in 2017. 2018. https://www.iea.org/reports/global-energy-co2-status-report-2017.

[2] International Energy Agency. Global Energy Review 2021 - Assessing the effects of economic recoveries on global energy demand and co2 emissions in 2021. 2021. https://www.iea.org/reports/global-energy-review-2021.

[3] Y. Cui, D. Yan, T. Hong, C. Xiao, X. Luo, and Q. Zhang. Comparison of typical year and multiyear building simulations using a 55-year actual weather data set from China. *Applied Energy*, 195:890–904, March 2017. https://doi.org/10.1016/j.apenergy.2017.03.113.

[4] T. Hong, W. Chang, and H. Lin. A sensitivity study of building performance using 30-year actual weather data. *Proceedings of BS 2013: 13th Conference of the International Building Performance Simulation Association*, pages 1398–1405, August 2013. http://www.ibpsa.org/proceedings/BS2013/p_1059.pdf.

[5] G. Sorrentino, G. Scaccianoce, M. Morale, and V. Franzitta. The importance of reliable climatic data in the energy evaluation. *Energy*, 48:74–79, December 2012. https://doi.org/10.1016/j.energy.2012.04.015.

[6] Eurostat. Energy data - 2020 edition. 2020. doi:10.2785/68334.

[7] D. Borozan. Decomposing the changes in european final energy consumption. *Energy Strategy Reviews*, 22:26–36, November 2018. https://doi.org/10.1016/j.esr.2018.08.002.

[8] Eurostat. Eurostat Manual for air emission accounts - 2015 edition. 2015. doi:10.2785/527552.

[9] Directorate-General for Energy. EU energy in figures - Statistical pocketbook 2019. 2019. doi:10.2833/197947.

[10] D.B. Crawley. Estimating the impacts of climate change and urbanization on building performance. *Journal of Building Performance Simulation*, 1:91–115, June 2008. https://doi.org/10.1080/19401490802182079.

[11] D. Claridge, M. Liu, Y. Zhu, M. Abbas, A. Athar, and J. Haberl. Implementation of Continuous Commissioning in the Texas LoanSTAR Program: "Can You Achieve 150% of Estimated Retrofit Savings" Revisited. *ACEEE 1996 Summer Study on Energy Efficiency in Buildings Proceedings*, 4:59–67, 1996. https://www.aceee.org/files/proceedings/1996/data/papers/SS96_Panel4_Paper06.pdf.

[12] H. Yoshino, T. Hong, and N. Nord. IEA EBC annex 53: Total energy use in buildings - Analysis and evaluation methods. *Energy and Buildings*, 152:124–136, October 2017. https://doi.org/10.1016/j.enbuild.2017.07.038.

[13] J. Clark. Energy Simulation in Building Design. November 2007. https://doi.org/10.4324/9780080505640.

[14] J.L. Hensen. Simulation of building energy and indoor environmental quality - some weather data issues. *Proceedings of the International Workshop on Climate Data and their Applications in Engineering*, pages 1–15, October 1999. https://www.researchgate.net/publication/302988276_Simulation_of_building_energy_and_indoor_environmental_quality_-_some_weather_data_issues.

[15] T. Hong, S.K. Chou, and T.Y. Bong. Building simulation: An overview of developments and information sources. *Building and Environment*, 35:347–361, May 2000. https://doi.org/10.1016/S0360-1323(99)00023-2.

[16] H. Wang and Q. Chen. Impact of climate change heating and cooling energy use in buildings in the United States. *Energy and Buildings*, 82:428–436, October 2014. https://doi.org/10.1016/j.enbuild.2014.07.034.

[17] World Meteorological Organization (WMO). International meteorological vocabulary. *WMO*, 182, 1992. https://library.wmo.int/index.php?lvl=notice_display&id=220#.YUw2jWJBxPZ.

[18] World Meteorological Organization (WMO). Guide to instruments and methods of observation. *WMO*, 8, 2018. https://library.wmo.int/index.php?id=12407&lvl=notice_display#.YUxenGJBxPY.

[19] D.R. Myers. Solar radiation modeling and measurements for renewable energy applications: data and model quality. *Energy*, 30:1517–1531, July 2005. https://doi.org/10.1016/j.energy.2004.04.034.

[20] P. Blanc, B. Espinar, N. Geuder, C. Gueymard, R. Meyer, R. Pitz-Paal, B. Reinhardt, D. Renné, M. Sengupta, L. Wald, and S. Wilbert. Direct normal irradiance related definitions and applications: The circumsolar issue. *Solar Energy*, 110:561–577, December 2014. https://doi.org/10.1016/j.solener.2014.10.001.

[21] Refrigerating American Society of Heating and Inc. Air-Conditioning Engineers. 2021 ASHRAE Handbook: Fundamentals. 2021.

[22] J. Cook, N. Oreskes, P.T. Doran, W. Anderegg, B. Verheggen, E. Maibach, J.S. Carlton, S. Lewandowsky, A. Skuce, S. Green, D. Nuccitelli, P. Jacobs, M. Richardson, B. Winkler, R. Painting, and K. Rice. Consensus on consensus: A synthesis of consensus estimates on human-caused global warming. *Environmental Research Letters*, 11, April 2016. http://dx.doi.org/10.1088/1748-9326/11/4/048002.

[23] K.K.W. Wan, D.H.W. Li, W. Pan, and J.C. Lam. Impact of climate change on building energy use in different climate zones and mitigation and adaptation implications. *Applied Energy*, 97:274–282, September 2012. https://doi.org/10.1016/j.apenergy.2011.11.048.

[24] T.N.T. Lam, K.K.W. Wan, S.L. Wong, and J.C. Lam. Impact of climate change on commercial sector air conditioning energy consumption in subtropical hong kong. *Applied Energy*, 87:2321–2327, July 2010. https://doi.org/10.1016/j.apenergy.2009.11.003.

[25] H. Radhi. Evaluating the potential impact of global warming on the UAE residential buildings – A contribution to reduce the CO2 emissions. *Building and Environment*, 44:2451–2462, December 2009. https://doi.org/10.1016/j.buildenv.2009.04.006.

[26] M.F. Jentsch, A. Bahaj, and P.A.B. James. Climate change future proofing of buildings—generation and assessment of building simulation weather files. *Energy and Buildings*, 40:2148–2168, 2008. https://doi.org/10.1016/j.enbuild.2008.06.005.

[27] A. Robert and M. Kummert. Designing net-zero energy buildings for the future climate, not for the past. *Building and Environment*, 55:150–158, September 2012. https://doi.org/10.1016/j.buildenv.2011.12.014.

[28] D.J. Sailor. Relating residential and commercial sector electricity loads to climate—evaluating state level sensitivities and vulnerabilities. *Energy*, 26:645–657, July 2001. https://doi.org/10.1016/S0360-5442(01)00023-8.

[29] T. Wilbanks, V. Bhatt, D. Bilello, S. Bull, J. Ekmann, W. Horak, Y.J. Huang, M. Levine, M.J. Sale, D. Schmalzer, and M. Scott. Effects of climate change on energy production and use in the united states. *US Department of Energy Publications*, February 2008.

[30] IPCC. Climate change 2014: Synthesis report. contribution of working groups i, ii and iii to the fifth assessment report of the intergovernmental panel on climate change. 2014.

[31] V. Corrado and I. Ballarini. Refurbishment trends of the residential building stock: Analysis of a regional pilot case in italy. *Energy and Buildings*, 132:91–106, November 2016. https://doi.org/10.1016/j.enbuild.2016.06.022.

[32] Paris Agreement. https://ec.europa.eu/clima/policies/international/negotiations/paris_en.

[33] Covenant of Mayors: Objectives & Scope. https://www.eumayors.eu/about/covenant-initiative/objectives-and-scope.html.

[34] Interreg ITA-SLO Secap Project. https://www.ita-slo.eu/en/secap.

[35] *EN ISO 15927-2:2009. Hygrothermal performance of buildings – Calculation and presentation of climatic data – Part 2: Hourly data for design cooling load*, 2009.

[36] T. Hong, W. Chang, and Lin H. A fresh look at weather impact on peak electricity demand and energy use of buildings using 30-year actual weather data. *Applied Energy*, 111:333–350, November 2013. https://doi.org/10.1016/j.apenergy.2013.05.019.

[37] W. Gang, S. Wang, K. Shan, and D. Gao. Impacts of cooling load calculation uncertainties on the design optimization of building cooling systems. *Energy and Buildings*, 94:1–9, May 2015. https://doi.org/10.1016/j.enbuild.2015.02.032.

[38] G. Murano, V. Corrado, and D. Dirutigliano. The new Italian Climatic Data and their Effect in the Calculation of the Energy Performance of Buildings. *Energy Procedia*, 101:153–160, November 2016. https://doi.org/10.1016/j.egypro.2016.11.020.

[39] Italian Organization for Standardization (UNI). UNI 10349:1994, Heating and cooling of buildings - Climatic data. 1994.

[40] S. Petrarca, F. Spinelli, E. Cogliani, and M. Mancini. Profilo climatico dell'Italia. *Edizioni ENEA*, 1999.

[41] https://energyplus.net/weather/sources, Last access: March 2021.

[42] G. Cannistraro, C. Giaconia, M. Pietrafesa, and G. Rizzo. Reduced weather data for building climatization and application to 29 European locations. *Energy*, 20:637–646, July 1995. https://doi.org/10.1016/0360-5442(94)00100-H.

[43] D. Erbs, S. Klein, and W. Beckmann. Estimation of degree-days and ambient temperature bin data from monthly-average temperatures. *ASHRAE Journal*, 25:60–65, 1983.

[44] Y. Yang, L.T. Wilson, and J. Wang. Development of an automated climatic data scraping, filtering and display system. *Computer and Electronics in Agriculture*, 71:77–87, April 2010. https://doi.org/10.1016/j.compag.2009.12.006.

[45] D.J. Thevenard and R.G. Humphries. The calculation of climatic design conditions in the 2005 ashrae handbook-fundamentals. *ASHRAE Transactions*, 11:457–466, 2005.

[46] M. Vellei, A.P. Ramallo-Gonzalez, D. Kaleli, J. Lee, and S. Natarajan. Investigating the overheating risk in refurbished social housing. *Proceedings of the 9th Windsor Conference: Making Comfort Relevant*, April 2016. https://www.researchgate.net/publication/301182192_Investigating_the_overheating_risk_in_refurbished_social_housing.

[47] M. Manzan, G. Lupato, A. Pezzi, P. Rosato, and A. Clarich. Reliability-Based Optimization for Energy Refurbishment of a Social Housing Building. *Energies*, 2020, 13, May 2020. https://doi.org/10.3390/en13092310.

[48] Italian Thermotechnical Committee Energy and Environment - CTI. https://energyplus.net/weather/sources, Last access: November 2020.

[49] Italian Organization for Standardization (UNI). *Technical report UNI/TR 10349-2:2016. Heating and cooling of buildings - Climatic data - Part 2: Data for design load*, 2016.

[50] ISTAT. http://dati-censimentopopolazione.istat.it/, Last access: November 2020.

[51] Tabula Project Webtool. https://webtool.building-typology.eu/, Last access: November 2020.

[52] G. Pernigotto, A. Prada, P. Baggio, A. Gasparella, and A. Mahdavi. Solar irradiance modelling and uncertainty on building hourly profiles of heating and cooling energy needs. *Proceedings of the IV High Performance Buildings Conference*, July 2016. https://www.researchgate.net/publication/305387865_Solar_irradiance_modelling_and_uncertainty_on_building_hourly_profiles_of_heating_and_cooling_energy_needs.

[53] G. Lupato, M. Manzan, and S. Cirilli. Comparison of direct radiation split algorithms for energy simulation of buildings. *Proceedings of Building Simulation Applications BSA 2017*, February 2018. http://hdl.handle.net/11368/2926193.

[54] E. Keeble. Availability of UK Climatic Data for Use in Simulation. *BEPAC Technical Note 90/1, Building Research Establishment*, October 1990.

[55] G. Pernigotto, A. Prada, D. Cóstola, A. Gasparella, and J.L. Hensen. Multi-year and reference year weather data for building energy labelling in north italy climates. *Energy and Buildings*, 72:62–72, April 2014. http://dx.doi.org/10.1016/j.enbuild.2013.12.012.

[56] L. Yang, C. Lok, J. Liu, and C.L. Tsang. Building energy simulation using multi-years and typical meteorological years in different climates. *Energy Conversion and Management*, 49:113–124, January 2008. http://dx.doi.org/10.1016/j.enconman.2007.05.004.

[57] T. Kershaw, M. Eames, and D. Coley. Comparison of multi-year and reference year building simulations. *Building Services Engineering Research and Technology*, 31:357–369, October 2010. http://dx.doi.org/10.1177/0143624410374689.

[58] V. Nik. Making energy simulation easier for future climate – Synthesizing typical and extreme weather data sets out of regional climate models (RCMs). *Applied Energy*, 177, September 2016. http://dx.doi.org/10.1016/j.apenergy.2016.05.107.

[59] A. Moazami, V.M. Nik, S. Carlucci, and S. Geving. Impacts of future weather data typology on building energy performance - Investigating long-term patterns of climate change and extreme weather conditions. *Applied Energy*, 238:696–720, March 2019. https://doi.org/10.1016/j.apenergy.2019.01.085.

[60] C.S. Barnaby and U.B. Crawley. Weather data for building performance simulation. *Chapter of Building Performance Simulation for Design and Operation*, pages 37–55, 2011. https://doi.org/10.4324/9780203891612.

[61] D.B. Crawley. Which Weather Data Should You Use for Energy Simulations of Commercial Buildings? *ASHRAE Transactions*, 104:498–515, June 1998. https://www.researchgate.net/publication/268390615_Which_Weather_Data_Should_You_Use_for_Energy_Simulations_of_Commercial_Buildings.

[62] J.C. Baltazar and D. Claridge. Study of Cubic Splines and Fourier Series as Interpolation Techniques for Filling in Short Periods of Missing Building Energy Use and Weather Data. *Journal of Solar Energy Engineering*, 128, January 2002. http://dx.doi.org/10.1115/SED2002-1031.

[63] K. Skeiker. Comparison of methodologies for TMY generation using 10 years data for Damascus, Syria. *Energy Conversion and Management*, 48:2090–2102, July 2007. http://dx.doi.org/10.1016/j.enconman.2006.12.014.

[64] *EN ISO 15927-4:2005. Hygrothermal performance of buildings – Calculation and presentation of climatic data – Part 4: Hourly data for assessing the annual energy use for heating and cooling*, 2005.

[65] J. Bilbao, A.H. De Miguel, J.A. Franco, and A. Ayuso. Test reference year generation and evaluation methods in the continental mediterranean area. *Journal of Applied Meteorology*, 43:390–400, February 2004. http://dx.doi.org/10.1175/1520-0450(2004)043%3C0390:TRYGAE%3E2.0.CO;2.

[66] A. Argiriou, S. Lykoudis, S. Kontoyiannidis, C.A. Balaras, M. Asimakopoulos, M. Petrakis, and P. Kassomenos. Comparison of methodologies for tmy generation using 20 years data for Athens, Greece. *Solar Energy*, 66:33–45, May 1999. https://doi.org/10.1016/S0038-092X(99)00012-2.

[67] L. Wang, P. Mathew, and X. Pang. Uncertainties in energy consumption introduced by building operations and weather for a medium-size office building. *Energy and Buildings*, 53:152–158, October 2012. https://doi.org/10.1016/j.enbuild.2012.06.017.

[68] M. Bhandari, S. Shrestha, and J. New. Evaluation of weather datasets for building energy simulation. *Energy and Buildings*, 49:109–118, June 2012. https://doi.org/10.1016/j.enbuild.2012.01.033.

[69] J.C. Lam, K.K.W. Wan, S.L. Wong, and T.N.T. Lam. Principal component analysis and long-term building energy simulation correlation. *Energy Conversion and Management*, 51:135–139, January 2010. https://doi.org/10.1016/j.enconman.2009.09.004.

[70] J.M. Finkelstein and R.E. Schafer. Improved goodness-of-fit tests. *Biometrika*, 58:641–645, December 1971. https://doi.org/10.2307/2334400.

[71] H. Lund. The design reference year users manual. 1995.

[72] R. Festa and C.F. Ratto. Proposal of a numerical procedure to select reference years. *Solar Energy*, 50:9–17, January 1993. https://doi.org/10.1016/0038-092X(93)90003-7.

[73] Ente per le Nuove tecnologie l'Energia e l'Ambiente (ENEA). Metodologia per l'elaborazione dei dati climatici necessari per la progettazione degli impianti per il riscaldamento degli edifici. 2009.

[74] IPCC. Climate change 2021: The physical science basis. contribution of working group i to the sixth assessment report of the intergovernmental panel on climate change. 2021.

[75] Intergovernmental Panel on Climate Change. What is a gcm? https://www.ipcc-data.org/guidelines/pages/gcm_guide.html.

[76] M. Hamdy, S. Carlucci, P.J. Hoes, and J.L.M. Hensen. The impact of climate change on the overheating risk in dwellings - A Dutch case study. *Building and Environment*, 122, June 2017. http://dx.doi.org/10.1016/j.buildenv.2017.06.031.

[77] N. Holodkov, A. Pezzi, Č. Kurnik, M. Pizzato, F. Flapp, V. Gallina, S. Alessandrini, F. Tomasi, F. Morea, M. Grmek, and I. Kacafura. Preliminary Context Analysis. July 2020. https://www.ita-slo.eu/sites/default/files/allegati/SECAP-D1-ATT7_EN.pdf.

[78] Agenzia Regionale per la Protezione dell'Ambiente del Friuli Venezia Giulia (ARPA FVG). Studio conoscitivo dei cambiamenti climatici e di alcuni loro impatti in Friuli Venezia Giulia. March 2018. https://www.meteo.fvg.it/clima/clima_fvg/03_cambiamenti_climatici/01_REPORT_cambiamenti_climatici_e_impatti_per_il_FVG/impattiCCinFVG_marzo2018.pdf.

[79] H. Hoffmann and T. Rath. Meteorologically consistent bias correction of climate time series for agricultural models. *Theoretical and Applied Climatology*, 110:129–141, March 2012. https://doi.org/10.1007/s00704-012-0618-x.

[80] P. Grenier. Two Types of Physical Inconsistency to Avoid with Univariate Quantile Mapping: A Case Study over North America Concerning Relative Humidity and Its Parent Variables. *Journal of Applied Meteorology and Climatology*, 57:347–364, February 2018. https://doi.org/10.1175/JAMC-D-17-0177.1.

[81] B.L. Thrasher, E.P. Maurer, C. McKellar, and P.B. Duffy. Technical Note: Bias correcting climate model simulated daily temperature extremes with quantile mapping. *Hydrology and Earth System Sciences Discussions*, 9:5515–5529, April 2012. https://doi:10.5194/hessd-9-5515-2012.

[82] A.J. Cannon, S.R. Sobie, and T.Q. Murdock. Bias Correction of GCM Precipitation by Quantile Mapping: How Well Do Methods Preserve Changes in Quantiles and Extremes? *Journal of Climate*, 28:6938–6959, September 2015. https://doi.org/10.1175/JCLI-D-14-00754.1.

[83] B. Casati, A. Yagouti, and D. Chaumont. Regional Climate Projections of Extreme Heat Events in Nine Pilot Canadian Communities for Public Health Planning. *Journal of Applied Meteorology and Climatology*, 52:2669–2698, December 2013. http://dx.doi.org/10.1175/JAMC-D-12-0341.1.

[84] P.J. Robinson. On the Definition of a Heat Wave. *Journal of Applied Meteorology*, 40:762–775, April 2001. http://dx.doi.org/10.1175/1520-0450(2001)040%3C0762:OTDOAH%3E2.0.CO;2.

[85] Covenant of Mayors & Mayors Adapt Offices. The Covenant of Mayors for Climate and Energy Reporting Guidelines. 2016. https://www.covenantofmayors.eu/IMG/pdf/Covenant_ReportingGuidelines.pdf.

[86] K.H. Hamed and A. Rao. A modified Mann-Kendall trend test for autocorrelated data. *Journal of Hydrology*, 204:182–196, January 1998. https://doi.org/10.1016/S0022-1694(97)00125-X.

[87] H.B. Mann. Nonparametric Tests Against Trend. *Econometrica*, 13:245–259, July 1945. https://doi.org/10.2307/1907187.

[88] M. Kendall. Rank correlation measures. *Charles Griffin, London*, 1975.

[89] M.P. Tootkaboni, I. Ballarini, M. Zinzi, and V. Corrado. A Comparative Analysis of Different Future Weather Data for Building Energy Performance Simulation. *Climate*, 9, February 2021. https://doi.org/10.3390/cli9020037.

[90] S. Belcher, J. Hacker, and D. Powell. Constructing design weather data for future climates. *Building Services Engineering Research and Technology*, 26:49–61, February 2005. https://doi.org/10.1191%2F0143624405bt112oa.

[91] M. Cellura, F. Guarino, S. Longo, and G. Tumminia. Climate change and the building sector: Modelling and energy implications to an office building in southern Europe. *Energy for Sustainable Development*, 45:46–65, August 2018. https://doi.org/10.1016/j.esd.2018.05.001.

[92] V. Palermo, P. Bertoldi, M. Apostolou, A. Kona, and S. Rivas. Assessment of climate change mitigation policies in 315 cities in the Covenant of Mayors initiative. *Sustainable Cities and Society*, 60, 2020. https://doi.org/10.1016/j.scs.2020.102258.

[93] L. de Santoli. Guidelines on energy efficiency of cultural heritage. *Energy and Buildings*, 86:534–540, January 2015. https://doi.org/10.1016/j.enbuild.2014.10.050.

[94] J. Kosny, D. Yarbrough, P. Childs, and S.A. Mohiuddin. How the Same Wall Can Have Several Different R-Values: Relations Between Amount of Framing and Overall Thermal Performance in Wood and Steel-Framed Wall. *Thermal Performance of the Exterior Envelopes of Buildings X, proceedings of ASHRAE THERM X*, 2007.

[95] P. Johansson, S. Geving, C. Hagentoft, B. Petter Jelle, E. Rognvik, A. Sasic Kalagasidis, and B. Time. Interior insulation retrofit of a historical brick wall using vacuum insulation panels: Hygrothermal numerical simulations andlaboratory investigations. *Building and Environment*, 79:31–45, 2014. http://dx.doi.org/10.1016/j.buildenv.2014.04.014.

[96] M.A. Eben Saleh. Impact of thermal insulation location on buildings in hot dry climates. *Solar and Wind Technology*, 7:393–406, 1990.

[97] A. Galatioto, G. Ciulla, and R. Ricciu. An overview of energy retrofit actions feasibility on Italian historical buildings. *Energy*, 137:991–1000, 2017. http://dx.doi.org/10.1016/j.energy.2016.12.103.

[98] M. Ibrahim, L. Bianco, O. Ibrahim, and E. Wurtz. Low-emissivity coating coupled with aerogel-based plaster for walls' internal surface application in buildings: Energy saving potential based on thermal comfort assessment. *Journal of Building Engineering*, 18:454–466, July 2018. https://doi.org/10.1016/j.jobe.2018.04.008.

[99] H.H. Saber. Investigation of thermal performance of reflective insulations for different applications. *Building and Environment*, 52:32–44, June 2012. https://doi.org/10.1016/j.buildenv.2011.12.010.

[100] J. Kosny and J.E. Christian. Thermal evaluation of several configurations of insulation and structural materials for some metal stud walls. *Energy and Buildings*, 22:157–163, 1995. https://doi.org/10.1016/0378-7788(94)00913-5.

[101] E. de Angelis and E. Serra. Light Steel-frame Walls: Thermal Insulation Performances and Thermal Bridges. *Energy Procedia*, 45:362–371, 2014. https://doi.org/10.1016/j.egypro.2014.01.039.

[102] N. Soares, P. Santos, H. Gervásio, J.J. Costa, and L. Simões da Silva. Energy efficiency and thermal performance of lightweight steel-framed (LSF) construction: A review. *Renewable and Sustainable Energy Reviews*, 78:194–209, October 2017. https://doi.org/10.1016/j.rser.2017.04.066.

[103] M. Manzan, E. Zandegiacomo De Zorzi, and W. Lorenzi. Experimental and Numerical Comparison of Internal Insulation Systems for Building Refurbishment. *Energy Procedia*, 82:493–498, December 2015. https://doi.org/10.1016/j.egypro.2015.11.853.

[104] M. Manzan, E. Zandegiacomo De Zorzi, and W. Lorenzi. Numerical simulation and sensitivity analysis of a steel framed internal insulation system. *Energy and Buildings*, 158:1703–1710, January 2018. https://doi.org/10.1016/j.enbuild.2017.11.069.

[105] M. Manzan, A. Pezzi, and Giandegiacomo De Zorzi. Analysis of the coupled effect of steel studs and surface emissivity on internal insulation systems performance. *Energy and Buildings*, 204, December 2019. https://doi.org/10.1016/j.enbuild.2019.109520.

[106] *UNI EN ISO 6946:2018. Componenti ed elementi per edilizia - Resistenza termica e trasmittanza termica - Metodi di calcolo*, 2018.

[107] C. Escudero, K. Martin, A. Erkoreka, I. Flores, and J.M. Sala. Experimental thermal characterization of radiant barriers for building insulation. *Energy and Buildings*, 59:62–72, April 2013. https://doi.org/10.1016/j.enbuild.2012.12.043.

[108] G. Desogus, L. Di Pilla, S. Mura, G. Pisano, and R. Ricciu. Economic efficiency of social housing thermal upgrade in Mediterranean climate. *Energy and Buildings*, 57:354–360, February 2013. http://localhost/var/www/apps/conversion/tmp/scratch_7/dx.doi.org/10.1016/j.enbuild.2012.11.016.

[109] E.L. Cano, J.M. Moguerza, and A. Alonso-Ayuso. A multi-stage stochastic optimization model for energy systems planning and risk management. *Energy and Buildings*, 110:49–56, January 2016. https://doi.org/10.1016/j.enbuild.2015.10.020.

[110] F. Ascione, N. Bianco, R.F. De Masi, G.M. Mauro, and G.P. Vanoli. Energy retrofit of educational buildings: Transient energy simulations, model calibration and multi-objective optimization towards nearly zero-energy performance. *Energy and Buildings*, 144:303–319, June 2017. http://dx.doi.org/10.1016/j.enbuild.2017.03.056.

[111] S. Lu, J. Li, and B. Lin. Reliability analysis of an energy-based form optimization of office buildings under uncertainties in envelope and occupant parameters. *Energy and Buildings*, 209, February 2020. https://doi.org/10.1016/j.enbuild.2019.109707.

[112] S. Sun, K. Kensek, D. Noble, and M. Schiler. A Method of Probabilistic Risk Assessment for Energy Performance and Cost Using Building Energy Simulation. *Energy and Buildings*, 110, October 2015. http://dx.doi.org/10.1016/j.enbuild.2015.09.070.

[113] A. Chari, S. Xanthos, and S. Christodoulou. Stochastic assessment of the energy performance of buildings. *Energy Efficiency*, 10, December 2017. https://link.springer.com/article/10.1007/s12053-017-9545-0.

[114] A. Prada, G. Pernigotto, P. Baggio, and A. Gasparella. Uncertainty propagation of material properties in energy simulation of existing residential buildings: The role of buildings features. *Building Simulation*, 11:449–464, June 2018. http://dx.doi.org/10.1007/s12273-017-0418-4.

[115] G. Lupato, M. Manzan, and A. Pezzi. The Effect of Climatic Data on Building Performance Optimization. *Proceedings of BSO 2018 Conference*, 2018.

[116] M. Manzan, R. Rossi, E. Zandegiacomo De Zorzi, and G. Lupato. Genetic Optimization for Economic Feasibility of Refurbishment in Buildings. *Energy Procedia*, 101:145–152, November 2016. http://dx.doi.org/10.1016/j.egypro.2016.11.019.

[117] E. Di Giuseppe, A. Massia, and M. D'Orazio. Probabilistic Life Cycle Cost analysis of building energy efficiency measures: selection and characterization of the stochastic inputs through a case study. *Procedia Engineering*, pages 491–501, 2017.

[118] A. Clarich and V. Pediroda. Robust Design Applications with modeFRONTIER, Applying NODESIM-CFD Tools. *NODESIM-CFD Workshop on Quantification of CFD Uncertainties*, 2009.

[119] M. Kalsi, K. Hacke, and K. Lewis. A Comprehensive Robust Design Approach for Decision Trade-Offs in Complex Systems Design. *Journal of Mechanical Design*, 123:1–10, April 2001. http://dx.doi.org/10.1115/1.1334596.

[120] G.J.A. Loeven, J.A.S. Witteveen, and H. Bijl. Probabilistic Collocation: An Efficient Non-Intrusive Approach for Arbitrarily Distributed Parametric Uncertainties. *Conference: 45th AIAA Aerospace Sciences Meeting and Exhibit*, January 2007. http://dx.doi.org/10.2514/6.2007-317.

[121] A. Kiureghian. Engineering Design Reliability Handbook. *CRC Press*, 2005.

[122] P. Westermann and R. Evins. Surrogate modelling for sustainable building design - A review. *Energy and Buildings*, 198:170–186, September 2019. https://doi.org/10.1016/j.enbuild.2019.05.057.

[123] O.G. Ernst, A. Mugler, H.J. Starkloff, and E. Ullmann. On the convergence of generalized polynomial chaos expansions. *ESAIM Mathematical Modelling and Numerical Analysis*, 46:317–339, March 2012. http://dx.doi.org/10.1051/m2an/2011045.

[124] *EN ISO 13790:2008. Energy performance of buildings - Calculation of energy use for space heating and cooling*, 2008.

[125] G.V. Fracastoro, G. Mutani, and M. Perino. Experimental and theoretical analysis of natural ventilation by windows opening. *Energy and Buildings*, 34:817–827, September 2002. https://doi.org/10.1016/S0378-7788(02)00099-3.

[126] Friuli Venezia Giulia region. Prezzario regionale dei lavori pubblici. 2017. https://www.regione.fvg.it/rafvg/cms/RAFVG/infrastrutture-lavori-pubblici/lavori-pubblici/FOGLIA7/.

[127] ESTECO. modefrontier 2020r3. 2020. https://www.esteco.com/.

[128] eppy v0.5.56. 2021. https://pypi.org/project/eppy/.

[129] D. Vose. Risk Analysis: A Quantitative Guide. *John Wiley & Sons*, 2008.

[130] G. Brown. A Certainty Equivalent Expectation Model for Estimating the Systematic Risk of Property Investments. *Journal of Valuation*, 6:17–41, 1988. https://doi.org/10.1108/eb008020.

[131] M. Manzan and A. Clarich. FAST energy and daylight optimization of an office with fixed and movable shading devices. *Building and Environment*, 113:175–184, February 2017. https://doi.org/10.1016/j.buildenv.2016.09.035.

[132] P. Shen, W.W. Braham, and Y.K. Yi. The feasibility and importance of considering climate change impacts in building retrofit analysis. *Applied Energy*, 233, October 2018. http://dx.doi.org/10.1016/j.apenergy.2018.10.041.

[133] *UNI/TS 11300-1:2014. Energy performance of buildings Part 1: Evaluation of energy need for space heating and cooling*, 2014.